LITHOS

Ages, geochemistry and Sr-Nd-Pb isotopes of alkaline potassic volcanic rocks from the Arasbaran region (NW Iran): evidence for progressive evolution of mantle sources during the Neotethyan subduction system

--Manuscript Draft--

Manuscript Number:	
Article Type:	Regular Article
Keywords:	Arasbaran volcanism; Neotethys subduction; ultrapotassic volcanic rocks; , geochronology; geochemistry; Sr-Nd-Pb isotopes

Corresponding Author:	Claudio Natali, Prof. University of Florence Department of Earth Sciences Florence, ITALY
First Author:	Claudio Natali, Prof.
Order of Authors:	Claudio Natali, Prof.
	Mehraj Aghazadeh, Prof.
	Eleonora Braschi, Dr.
	Riccardo Avanzinelli, Prof.
	Zahra Badrazdeh, Dr.
	Gianluca Bianchini, Prof.
	Martina Casalini, Dr.
	Samuele Agostini, Dr.
	Massimo Mattei, Prof.
	Sandro Conticelli, Prof.

Abstract:	The volcanism of the Arasbaran region, northwest Iran is characterized by multiple magmatic pulses from Cretaceous to Quaternary related to the consumption of the Neotethys oceanic basin and the subsequent continental collision between the Arabia and the Eurasian plates. This work deals with the Eocene volcanic products. They show wide compositional variations, ranging from shoshonite to tephrite and phonolite. They may be further grouped into leucite (analcime)-bearing and leucite-free rock types on the basis of their mineralogy. Leucite-bearing and leucite-free Eocene rocks are geographically distinct outcropping in the WNW and ESE part of the Arasbaran area, respectively. K-Ar dating show leucite-bearing rocks (39.4-39.6 +/- 1.0 Ma) being slightly younger with respect to leucite-free rocks (41.0-41.9 +/- 1.0 Ma). The two rock types are differentiated by each other by different silica saturation degrees but display similar incompatible trace elements distributions, typical of subduction-related volcanic rocks, with clear depletions in HFSE (e.g., Nb, Ta, Ti, Zr) and enrichments in LILE (e.g., Ba, K) and Pb. The leucite-bearing volcanic rocks are strongly SiO2-undersaturated (ca. -35) and show higher LILE/HFSE, LILE/REE Ba/La (30- 90) and Ba/Th (up to 520) values with respect to leucite-free rocks (q from 0 to -15; Ba/La up to 30). The two rock types also show distinct Sr-Nd-Pb isotopic composition, with leucite-bearing rocks characterized by less radiogenic Sr (87Sr/86Sr 0.704424-0.704634) and Pb (206Pb/204Pb 18.58-18.65, 207Pb/204Pb 15.57-15.60, 208Pb/204Pb 38.63-38.71) and more radiogenic Nd (143Nd/144Nd 0.512695-0.512791), with respect to leucite-bearing rocks (87Sr/86Sr 0.704481-0.705669; 206Pb/204Pb 18.65-18.75, 207Pb/204Pb 15.61-15.64, 208Pb/204Pb 38.65-38.87; 143Nd/144Nd 0.512572-0.512623). The geochemical and isotopic composition, coupled with the strong SiO2-undersaturated character, of leucite bearing-rocks suggest in their mantle source the involvement of metasomatizing partial melts from subducted altered oceanic crust and subordinate carbonate-bearing sediments. On the other hand, the composition of leucite-free magmas is compatible with the involvement of a relatively higher contribution of partial melts from terrigenous (carbonate-poor) subducted sediments. The close spatial association and the relative geographical/stratigraphic position of

	these products indicate diachronous metasomatic events in the mantle wedge underlying the Arasbaran area that could have been originated by the late arrival of carbonate-rich sediments at depth during slab steepening and incipient roll-back preceding the continental collision. K-Ar dating indicates that the Arasbaran magmatism was triggered by a late geodynamic event, during middle Eocene, plausibly consisting of re-adjusting of isotherms that heated the veined mantle wedge following the slab migration after roll-back. The slightly younger age of leucite-bearing rocks with respect to leucite-free rocks, coupled with the lower melting degree of the former may suggest an evolution of the local thermal regime with the progressive involvement of portions of the mantle wedge closer to the subducted plate.
Suggested Reviewers:	Yildirim Dilek, Prof. Prof., Miami University dileky@MiamiOH.edu He's an expert of the volcanism in the studied area
	Dejan Prelevic, Prof. Prof., University of Belgrade Faculty of Mining And Geology dejan.prelevic@rgf.bg.ac.rs He's an expert of subduction related magmatism
	Leone Melluso, Prof. Prof., University of Naples Federico II Department of Earth Sciences Environment and Resources leone.melluso@unina.it He's an expert of igneous petrology in different geodynamic settings
Opposed Reviewers:	

Ages, geochemistry and Sr-Nd-Pb isotopes of alkaline potassic volcanic rocks from the Arasbaran region (NW Iran): evidence for progressive evolution of mantle sources during the Neotethyan subduction system

Natali C.[1,*,$], Aghazadeh M.[2,*,$], Braschi E.[3,*], Avanzinelli R. [1,3], Badrzadeh Z.[2], Bianchini G.[4], Casalini M.[1], Agostini S.[5], Mattei M.[6], Conticelli S.[1,7]

[1] Dipartimento di Scienze della Terra, Università degli studi di Firenze, Via Giorgio La Pira, 4, I-50121, Firenze, Italy
[2] Department of Geology, Payame Noor University, Iran
[3] CNR - Istituto di Geoscienze e Georisorse, Unità di Firenze, Via Giorgio La Pira, 4, I-50121, Firenze, Italy
[4] Dipartimento di Fisica e Scienze della Terra, Università degli studi di Ferrara, Via Giuseppe Saragat, 1, 44124, Ferrara, Italy
[5] CNR - Istituto di Geoscienze e Georisorse, Unità di Pisa, Area Territoriale di Ricerca di Pisa, Via G. Moruzzi, 1, I-56124, Pisa, Italia
[6] Dipartimento di Scienze, Università degli studi di Roma III, Largo San Leonardo Murialdo, 1, I-00146, Roma, Italia
[7] CNR - Istituto di Geologia Ambientale e Geoingegneria, Unità di Montelibretti, Area Territoriale di Ricerca di Roma 1, Strada Provinciale 35d, 9, I-00010, Montelibretti (RM), Italia

[*] These authors contributed equally to this research
[$]Corresponding authors: claudio.natali@unifi.it, mehrajaghazadeh@yahoo.com

Dear Editor,

we are submitting the manuscript titled "**Ages, geochemistry and Sr-Nd-Pb isotopes of alkaline potassic volcanic rocks from the Arasbaran region (NW Iran): evidence for progressive evolution of mantle sources during the Neotethyan subduction system"** to be published on Lithos. The manuscript provides a comprehensive petrological study of igneous rocks characterizing the Eocene magmatic phase of the Ahar-Arasbaran sector of the Alpine-Himalayan belt in NW Iran. In this study, the transition from leucite-free to leucite bearing magma production has been dated and the magmatic evolution of magmas and related mantle sources modelled by the use of petrographic, geochemical and isotopic data. A notable outcome of this work regards the similarity of the Arasbaran volcanism with that of the Neapolitan district of the Roman magmatic province, in particular the magmatic affinity of the ultrapotassic rocks. This suggest that analogous subduction systems formed along with the diachronous closure of the Tethys ocean in the Alpine-Himalayan realm.

We hope that the submitted manuscript could fit the requirements and standards of Lithos

We confirm that neither the manuscript nor any parts of its content are currently under consideration or published in another journal.

All authors have approved the manuscript and agree with its submission to Lithos

Best Regards,

Claudio Natali and co-Authors

Abstract

The volcanism of the Arasbaran region, northwest Iran is characterized by multiple magmatic pulses from Cretaceous to Quaternary related to the consumption of the Neotethys oceanic basin and the subsequent continental collision between the Arabia and the Eurasian plates. This work deals with the Eocene volcanic products. They show wide compositional variations, ranging from shoshonite to tephrite and phonolite. They may be further grouped into leucite (analcime)-bearing and leucite-free rock types on the basis of their mineralogy. Leucite-bearing and leucite-free Eocene rocks are geographically distinct outcropping in the WNW and ESE part of the Arasbaran area, respectively. K-Ar dating show leucite-bearing rocks (39.4-39.6 +/- 1.0 Ma) being slightly younger with respect to leucite-free rocks (41.0-41.9 +/- 1.0 Ma). The two rock types are differentiated by each other by different silica saturation degrees but display similar incompatible trace elements distributions, typical of subduction-related volcanic rocks, with clear depletions in HFSE (e.g., Nb, Ta, Ti, Zr) and enrichments in LILE (e.g., Ba, K) and Pb. The leucite-bearing volcanic rocks are strongly SiO_2-undersaturated (Δq ca. -35) and show higher LILE/HFSE, LILE/REE Ba/La (30- 90) and Ba/Th (up to 520) values with respect to leucite-free rocks (Δq from 0 to -15; Ba/La up to 30). The two rock types also show distinct Sr-Nd-Pb isotopic composition, with leucite-bearing rocks characterized by less radiogenic Sr ($^{87}Sr/^{86}Sr$ 0.704424-0.704634) and Pb ($^{206}Pb/^{204}Pb$ 18.58-18.65, $^{207}Pb/^{204}Pb$ 15.57-15.60, $^{208}Pb/^{204}Pb$ 38.63-38.71) and more radiogenic Nd ($^{143}Nd/^{144}Nd$ 0.512695-0.512791), with respect to leucite-bearing rocks ($^{87}Sr/^{86}Sr$ 0.704481-0.705669; $^{206}Pb/^{204}Pb$ 18.65-18.75, $^{207}Pb/^{204}Pb$ 15.61-15.64, $^{208}Pb/^{204}Pb$ 38.65-38.87; $^{143}Nd/^{144}Nd$ 0.512572-0.512623). The geochemical and isotopic composition, coupled with the strong SiO_2-undersaturated character, of leucite bearing-rocks suggest in their mantle source the involvement of metasomatizing partial melts from subducted altered oceanic crust and subordinate carbonate-bearing sediments. On the other hand, the composition of leucite-free magmas is compatible with the involvement of a relatively higher contribution of partial melts from terrigenous (carbonate-poor) subducted sediments. The close spatial association and the relative geographical/stratigraphic position of these products indicate diachronous metasomatic events in the mantle wedge underlying the Arasbaran area that could have been originated by the late arrival of carbonate-rich sediments at depth during slab steepening and incipient roll-back preceding the continental collision. K-Ar dating indicates that the Arasbaran magmatism was triggered by a late geodynamic event, during middle Eocene, plausibly consisting of re-adjusting of isotherms that heated the veined mantle wedge following the slab migration after roll-back. The slightly younger age of leucite-bearing rocks with respect to leucite-free rocks, coupled with the lower melting degree of the former may suggest an evolution of the local thermal regime with the progressive involvement of portions of the mantle wedge closer to the subducted plate.

Research Highlights:

- A subduction-related magmatic pulse occurred in NW Iran at ca. 40 Ma
- Shoshonite leucite-free slightly preceded UK leucite-bearing volcanism
- Leucite-free magma source was metasomatised by dominant LC-sediment melts
- Leucite-bearing magmas was metasomatised by dominant HC-sediment melts
- Leucite-bearing rocks share similarities with Neapolitan Roman-type UK rocks

Ages, geochemistry and Sr-Nd-Pb isotopes of alkaline potassic volcanic rocks from the Arasbaran region (NW Iran): evidence for progressive evolution of mantle sources during the Neotethyan subduction system

Natali C.[1,*,$], Aghazadeh M.[2,*,$], Braschi E.[3,*], Avanzinelli R.[1,3], Badrzadeh Z.[2], Bianchini G.[4], Casalini M.[1], Agostini S.[5], Mattei M.[6], Conticelli S.[1,7]

[1] Dipartimento di Scienze della Terra, Università degli studi di Firenze, Via Giorgio La Pira, 4, I-50121, Firenze, Italy

[2] Department of Geology, Payame Noor University, Iran

[3] CNR - Istituto di Geoscienze e Georisorse, Unità di Firenze, Via Giorgio La Pira, 4, I-50121, Firenze, Italy

[4] Dipartimento di Fisica e Scienze della Terra, Università degli studi di Ferrara, Via Giuseppe Saragat, 1, 44124, Ferrara, Italy

[5] CNR - Istituto di Geoscienze e Georisorse, Unità di Pisa, Area Territoriale di Ricerca di Pisa, Via G. Moruzzi, 1, I-56124, Pisa, Italia

[6] Dipartimento di Scienze, Università degli studi di Roma III, Largo San Leonardo Murialdo, 1, I-00146, Roma, Italia

[7] CNR - Istituto di Geologia Ambientale e Geoingegneria, Unità di Montelibretti, Area Territoriale di Ricerca di Roma 1, Strada Provinciale 35d, 9, I-00010, Montelibretti (RM), Italia

[*] These authors contributed equally to this research

[$] Corresponding authors: claudio.natali@unifi.it, mehrajaghazadeh@yahoo.com

Abstract

The volcanism of the Arasbaran region, northwest Iran is characterized by multiple magmatic pulses from Cretaceous to Quaternary related to the consumption of the Neotethys oceanic basin and the subsequent continental collision between the Arabia and the Eurasian plates. This work deals with the Eocene volcanic products. They show wide compositional variations, ranging from shoshonite to tephrite and phonolite. They may be further grouped into leucite (analcime)-bearing and leucite-free rock types on the basis of their mineralogy. Leucite-bearing and leucite-free Eocene rocks are geographically distinct outcropping in the WNW and ESE part of the Arasbaran area, respectively. K-Ar dating show leucite-bearing rocks (39.4-39.6 +/- 1.0 Ma) being slightly younger with respect to leucite-free rocks (41.0-41.9 +/- 1.0 Ma). The two rock types are differentiated by each other by different silica saturation degrees but display similar incompatible trace elements distributions, typical of subduction-related volcanic rocks, with clear depletions in HFSE (e.g., Nb, Ta, Ti, Zr) and enrichments in LILE (e.g., Ba, K) and Pb. The leucite-bearing volcanic rocks are strongly SiO_2-undersaturated (Δq ca. -35) and show higher LILE/HFSE, LILE/REE Ba/La (30- 90) and Ba/Th (up to 520) values with respect to leucite-free rocks (Δq from 0 to -15; Ba/La up to 30). The two rock types also show distinct Sr-Nd-Pb isotopic composition, with leucite-bearing rocks characterized by less radiogenic Sr ($^{87}Sr/^{86}Sr$ 0.704424-0.704634) and Pb ($^{206}Pb/^{204}Pb$ 18.58-18.65, $^{207}Pb/^{204}Pb$ 15.57-15.60, $^{208}Pb/^{204}Pb$ 38.63-38.71) and more radiogenic Nd ($^{143}Nd/^{144}Nd$ 0.512695-0.512791), with respect to leucite-bearing rocks ($^{87}Sr/^{86}Sr$ 0.704481-0.705669; $^{206}Pb/^{204}Pb$ 18.65-18.75, $^{207}Pb/^{204}Pb$ 15.61-15.64, $^{208}Pb/^{204}Pb$ 38.65-38.87; $^{143}Nd/^{144}Nd$ 0.512572-0.512623). The geochemical and isotopic composition, coupled with the strong SiO_2-undersaturated character, of leucite bearing-rocks suggest in their mantle source the involvement of metasomatizing partial melts from subducted altered oceanic crust and subordinate carbonate-bearing sediments. On the other hand, the composition of leucite-free magmas is compatible with the involvement of a relatively higher contribution of partial melts from terrigenous (carbonate-poor) subducted sediments. The close spatial association and the relative geographical/stratigraphic position of these products indicate diachronous metasomatic events in the mantle wedge underlying the Arasbaran area that could have been originated by the late arrival of carbonate-rich sediments at depth during slab steepening and incipient roll-back preceding the continental collision. K-Ar dating indicates that the Arasbaran magmatism was triggered by a late geodynamic event, during middle Eocene, plausibly consisting of re-adjusting of isotherms that heated the veined mantle wedge following the slab migration after roll-back. The slightly younger age of leucite-bearing rocks with respect to leucite-free rocks, coupled with the lower melting degree of the former may suggest an evolution of the local thermal regime with the progressive involvement of portions of the mantle wedge closer to the subducted plate.

Keywords: Arasbaran volcanism; Neotethys subduction, ultrapotassic volcanic rocks, geochronology, geochemistry, Sr-Nd-Pb isotopes

1. Introduction

K-rich igneous rocks (shoshonitic and ultrapotassic) are common magmatic products of destructive plate margins and can occur from the subduction to syn and post-collisional stages of orogenic geodynamic settings (e.g., Lustrino and Wilson, 2007, Conticelli et al., 2009, 2015; Prelević et al., 2008, 2010). The origin of these magmas has been attributed to the partial melting of a mantle source variably metasomatised by the addition of fluids/melts during the subduction of oceanic lithosphere under the continental margin (e.g., Chase, 1981; Hofmann and White, 1982; Palacz and Saunder, 1986; Hart, 1988; Nakamura and Tatsumoto, 1988; Barling and Goldstein, 1990; Weaver, 1991; Chauvel et al., 1992; Foley, 1992; Stolz et al., 1996; Elliott, 2003; Avanzinelli et al., 2009). The coexistence of K-rich magmas with various alkalinity degree has been interpreted because of the involvement of a sedimentary component to the mantle source, coupled with a steepening and roll-back of the subducted plate in the late stage of convergence or in post-collisional settings (e.g., Wilson and Bianchini, 1999; Conticelli et al., 2002; Beccaluva et al., 2005). In a generalized model of the evolution of the Mesozoic Tethyan realm and development of the western sector of the Alpine-Himalayan belt, ultrapotassic and shoshonitic rocks were interpreted as the product of increasing partial melting degree of a metasomatised mantle source progressively involving the residual highest temperature liquidus domains (e.g., Foley, 1992; Conticelli et al., 2007; Avanzinelli et al., 2009, 2020; Tommasini et al., 2011; Dallai et al., 2019, 2022). In the Cenozoic magmatic evolution of western Mediterranean, many authors have constrained this general hypothesis by petrographic, geochemical and isotopic data, providing comprehensive explanation for the genesis and the evolution of the magmatism in this very complex natural laboratory. In these studies, a particular attention has been devoted to potassic-rich rocks (shoshonitic and ultrapotassic) and the genesis of leucite-bearing and leucite-free magmas (e.g., Peccerillo et al., 1988; Conticelli and Peccerillo, 1992; Beccaluva et al., 2005; Prelević et al., 2005; Prelević and Foley, 2007; Conticelli et al., 2010, 2015). The genesis of K-rich magmas has generally been ascribed to various contribution of continental terrigenous and carbonate-bearing sediment/lithologies to the metasomatic agents in their mantle sources (Avanzinelli et al., 2008, 2009; Conticelli et al., 2015). Experimental studies indicate that mantle peridotite including hydrous, incompatible element-rich net veins derived from subducted sediments is a viable source for the generation of K-rich alkaline magmas (e.g., Foley, 1992; Mitchell, 1995; Bianchini et al., 2015; Avanzinelli et al., 2020). Moreover, Thomsen and Schmidt (2008) demonstrated the capability to generate potassic granite or phonolite melts from carbonated pelites in the T-P range 950-1070 °C 2.4-5.0 GPa, suggesting that the involvement of a carbonate component in the mantle source could be responsible for the generation of SiO_2-undersaturated magmas. In particular, strongly silica-undersaturated ultrapotassic leucite-bearing magmas are thought to be derived from a metasomatised upper mantle by partial melting of a phlogopite-bearing lherzolite or wehrlite characterized by a CO_2 excess with respect to H_2O, then high XCO_2 (e.g., Lloyd et al., 1985 and references therein), recalling the presence of a carbonate-bearing component in the metasomatized mantle sources (Conticelli et al., 2002; 2010; 2015; Avanzinelli et al., 2008, 2009; 2018; Boari et al., 2009; Bragagni et al., 2022). On the other hand, the generation of high silica leucite-free ultrapotassic magmas is compatible with the partial melting of a phlogopite-bearing harzburgite produced by metasomatism by sediment melts under high XH_2O (Avanzinelli et al., 2009; Conticelli et al, 2009; Prelevic et al., 2008; 2010; Casalini et al., 2022). Neogene to Quaternary ultrapotassic rocks of kamafugitic (SiO_2-poor) and lamproitic (SiO_2-rich) affinities also occur in the central-eastern Mediterranean sector of the Alpine-Himalayan belt, from the Balkans (Prelević et al., 2005) to western Anatolia (Francalanci et al., 2000; Doglioni et al., 2002; Innocenti et al., 2005; Çoban and Flower, 2006, 2007; Akal, 2008; Dilek and Altunkaynak, 2010; Prelević et al., 2008; 2012; 2015; Di Giuseppe et al., 2018, 2021; Casalini et al., 2022) and have been generally interpreted as the counterpart of western Mediterranean ultrapotassic rocks.

In the eastern sector of the Alpine-Himalayan belt, extending from the Pontide Arc in Central-Eastern Anatolia to the Alborz mountain range in Iran, widespread Late Cretaceous to Quaternary subduction-related magmatism, including K-rich rocks, occurred in response to the diachronous (mainly Cenozoic) closure of Tethyan oceanic branches and subsequent continental collision of the Arabia-Eurasian plates (e.g., Dilek et al., 2010). In this sector, several occurrences of leucite-bearing and leucite-free ultrapotassic (often associated to shoshonitic) volcanic rocks have been reported in the literature. This rock association is commonly recognized from Central (Gülmez et al., 2016) and Eastern Pontides, where plagioleucitites (Altherr et al., 2008) and shoshonitic leucite-free and ultrapotassic leucite-bearing rocks of Maastrichtian-early Paleocene age (Eyuboglu, 2010; Eyuboglu et al., 2011) outcrop, as well as in NW Iran. In particular the Iranian area display a heterogenous and complex rock assemblage and spatial distribution, with shoshonitic, leucite-free and ultrapotassic leucite-bearing rocks of Late Miocene age outcropping in the Eslamy Peninsula, (Moayyed et al., 2008; Shafaii Moghadam et al., 2014a); high-K leucite-bearing and leucite-free rocks of Eocene age (Shafaii Moghadam et al., 2018, Soltanmohammadi et al., 2018; 2021) exposed in Lahrud area and Salavat range in the Ardabil province; leucite-bearing rocks of Eocene age in Moghan area (Amraee et al., 2019), Alborz Mountains (Aghazadeh et al., 2011) and Lesser Caucasus (Lustrino et al., 2019; Dilek et al., 2010). The numerous, different interpretations regarding the genesis of the different K-rich igneous rocks characterizing this complex area, mainly arisen from the lack of systematic differences in their geochemical and isotopic features, with respect to their analogues in western Mediterranean. In fact, the relatively limited variability, especially in the isotopic composition, exhibited by leucite-free and leucite-bearing rocks from this sector poses several problems in the precise identification of the nature of the metasomatic agents affecting their mantle sources.

In this paper, we report new petrographic, geochemical, and isotopic composition, as well as new K-Ar age determination, of K-rich leucite-bearing and -free igneous rocks from the Ahar-Arasbaran area (NW Iran). This region is a key area in between the other localities we listed above, thus assessing the genesis of the coexisting leucite-bearing and leucite-free magmas can help improving the knowledge of the subduction-related Cenozoic volcanism of this sector of the Alpine-Himalayan belt, and better define the processes that characterized the diachronous closure of the Tethian Realm.

2. Geological Outline

The Ahar–Arasbaran region is located in the hinterland of the Arabia–Eurasia collision zone, in the broad Alpine–Himalayan orogenic belt (Fig. 1a). The area is part of the Turkish Iranian Plateau (TIP), consisting of several pre-Mesozoic micro-continents accreted to the Eurasia margin as a result of the opening and closing of different branches of the Tethyan ocean (Soltanmohammadi et al., 2018). While the subduction of the

Paleo-Tethys was active, from 360 to 210 Ma, along the Greater Caucasus and northern Iran (Stampfli, 2000; Zanchetta et al., 2013), the successive subduction system of the Neo-Tethys migrated southward from the Pontides arc and southwest Zagros, due the multiple arc-microcontinent collisions that prolonged up to the Cenozoic (Dilek et al., 2010 and references therein). Sengor and Yilmaz (1981) suggested a northward subduction of the Neo-Tethyan ocean from the Upper Cretaceous until the end of the Eocene, which ended with the continental collision between Arabian and Eurasian plates (McQuarrie and van Hinsbergen, 2013). The partial subduction of the Eastern Tauride-South Armenian microcontinent caused slab break-off and opening of asthenospheric window, which, in turn, generated an increase in the heat-flow that triggered melting of the overlying subduction-metasomatised lithospheric mantle (Grosjean et al., 2023 and references therein). The related Eocene calc-alkaline to K-alkaline magmatism developed along a curvilinear belt from Eastern Pontides to peri-Caspian region in northwestern Iran, including the Arasbaran area (Fig. 1a (Dilek et al., 2010). The Geology of the Arasbaran region is mainly composed of Upper Cretaceous-Eocene volcano-sedimentary rocks. Plutonic and volcanic rocks were emplaced starting from the Upper Cretaceous time and continued during the Paleogene until the Quaternary time (Aghazadeh et al., 2011). The Upper Cretaceous–Paleocene marine volcanism includes mafic to intermediate lava flows and pyroclastic rocks with calc-alkaline to high-K calc-alkaline affinities. This period of intense volcanic activity is also associated with deep-sea marine sediments. In this time span two main Cenozoic volcanic periods are recognized: i) an Eocene volcanic sequence, consisting of potassic trachybasalts, shoshonites, latites, and trachytes, straddling the boundary with more alkali-rich rocks ranging basanites/tephrites, phonolitic tephrites, and phonolites (e.g., Alberti et al., 1980; Dilek et al., 2010; Soltanmohammadi et al., 2018; 2021), which represent the precise focus of this paper; ii) an Upper Miocene-Quaternary sequence having a within-plate geochemical signature, including both basic rocks and differentiated products, that will not be investigated in this paper. Cenozoic plutonic rocks with shoshonitic to ultrapotassic affinity (Aghazadeh et al., 2010; 2011) are also widespread throughout the Arasbaran zone and the western sector of the Alborz magmatic belt (Castro et al., 2013).

3. Materials and methods

Mafic to intermediate potassic rocks with basaltic to tephritic composition, emplaced in the form of lava flows, pillows, dikes, and pyroclastic units, widely outcrop in the Arasbaran region. These K-alkaline igneous products are mainly emplaced into deep to shallow level submarine environment, shifting to a subaerial environment along the sequence during the late magmatic stage. The oldest outcrops of potassic igneous rocks in the Arasbaran region are made of pyroclastic units with different thickness, interlayered with silico-clastic sedimentary rocks.

Leucite-bearing volcanic rocks are found in the *Majid Abad, Gheshlagh*, and *Moshiran* areas, whereas leucite- (and foid) free rocks occur in the neighbors of *Moradlu*, *Tullun*, *Marallu* and south of the *Moshiran* villages (Fig. 1b; modified from Geological Survey of Iran-GSI, Geological map 1:100,000). The leucite-bearing lava flows overlie Eocene conglomerates, sandstones and tuffs and are sometimes interlayered with pyrolclastic rocks that are widespread in the *Majid Abad* and *Moshiran* area. Tephritic lava layers (Supplementary Fig. 1a, e) have megaporphyritic to porphyritic texture with centimetric analcime (leucite) phenocrysts. Mafic to intermediate lavas with pillow and columnar jointing structures outcrop in the *Gheshlagh* area (Supplementary Fig. 1c). According to geological maps published by GSI these pillow lavas have andesitic to basaltic composition. The leucite-free rocks outcrop in the form of basaltic and tephritic lava flows interbedded with pyroclastic rocks in the *Tullun* and *south Moshiran* (Supplementary Fig. 1b), and *Marallu* sections (Supplementary Fig. 1f). Trachytic and basaltic dykes, generally with NE-SW direction, outcrop in the *Moradlu* area (Supplementary Fig. 1d).

56 igneous rock samples were collected in order to investigate in extreme detail the volcanic sequence of magmatism of the Ahar-Arasbaran volcanic belt related with the Neo-Tethian subduction and collision. Samples were representative of the overall occurrences in the area, and their sampling locations are reported in Fig. 1b. The samples were collected with care to avoid weathered ones although, further care was taken during preparation. Specimens were cut in order to remove altered portions and fresh sample aliquots were used to obtain thin sections for petrographic analysis and powders (after grinding in an agate mill) for geochemical analyses.

Major and selected trace elements (Ni, Co, Cr, V, and Ba) were analyzed by X-ray fluorescence (XRF) on powder pellets, using a wavelength dispersive automated ARL Advant'X spectrometer at the Dipartimento di Fisica e Scienze della Terra of the University of Ferrara. Accuracy and precision for major elements are estimated as better than 3% for Si, Ti, Fe, Ca, and K, and 7% for Mg, Al, Mn, Na; for trace elements (above 10 ppm) they are better than 10%.

REE, Rb, Sr, Y, Zr, Hf, Nb, Th, and U were analyzed, after acid digestion, by inductively coupled mass spectrometry (ICP-MS) at the Dipartimento di Fisica e Scienze della Terra of the University of Ferrara, using a Thermo-Scientific X-Series. Accuracy and precision, based on the replicated analyses of samples and standards, are estimated as better than 10% for all elements, well above the detection limit.

Analyses of radiogenic isotopes were carried out on rock powders preliminarily treated with 2.5M HCl for 4 hours and then rinsed three times with Milli-Q water, as leaching generally minimize isotopic variation - induced by supergene processes – that may overprint the magmatic signature (Nobre Silva et al., 2010 and references therein). After acid digestion by a mixture of HF and HNO_3, Sr, Nd and Pb were separated by cation-exchange chromatography and then Sr-Nd isotopic ratios were determined using thermal ionization mass spectrometry (Thermo-Fisher Scientific Triton™ Plus) at the Dipartimento di Scienze della Terra of the University of Florence, with the methods described by (Avanzinelli et al., 2005). The normalizing factors used to correct the isotopic fractionation of Sr and Nd were $^{86}Sr/^{88}Sr$ = 0.1194, $^{146}Nd/^{144}Nd$ = 0.7219 and 0.001% per atomic mass unit, respectively. The NIST 987, La Jolla and NIST981 standard solutions yield values of $^{87}Sr/^{86}Sr$ = 0.710279 ± 28 (2σ), $^{143}Nd/^{144}Nd$ = 0.511851 ± 13 (2σ). Pb radiogenic isotopic analyses were performed using a Thermo Fisher Neptune Plus MC-ICP-MS at the CNR - Istituto di Geoscienze e Georisorse in Pisa (Italy) in 2% HNO_3 solution containing 20-50 ng*g-1 of analyte. The correction for mass bias fractionation of Pb isotope ratios was performed adding an in-house Tl standard to the samples, and isobaric interferences of 204Hg to 204Pb was also corrected. Results were normalized to values recommended by (Todt et al., 1996), respectively 16.9356, 15.4891 and 36.7006 for the $^{206}Pb/^{204}Pb$, $^{207}Pb/^{204}Pb$ and $^{208}Pb/^{204}Pb$ isotope ratios. Full analytical details in (Agostini et al., 2022).

K–Ar dating was performed by ActLabs and Geochronex (Ontario, Canada). For Ar analysis, an aliquot of bulk rock powder was weighed, loaded into the sample system of extraction, degassed at ca 100 °C for 2 days to remove the surface gases. Argon was extracted from a double vacuum furnace at 1700 °C and its concentration determined using isotope dilution with ^{38}Ar spike, which is introduced to the sample system prior to each extraction. The extracted gases are cleaned up in a two steps purification process. Then pure Ar is introduced into a magnetic sector mass spectrometer (Reynolds type). Ar isotope ratios were corrected for mass-discrimination and then atmospheric argon was corrected assuming that ^{36}Ar is only from the air. The concentration of radiogenic ^{40}Ar was calculated by using the ^{38}Ar spike concentration. K analysis was performed by ICP.

4. Results

4.1. Petrography

Arasbaran volcanic rocks were divided in two groups on the basis of the occurrence of leucite, or analcite after leucite, into leucite-bearing and leucite-free, respectively.

4.1.1. Leucite-bearing volcanic rocks

The *Majid Abad* lavas show medium grained, porphyritic to mega porphyritic textures with centimetric leucite, variously transformed in analcite (Fig. 2a), clinopyroxene, plagioclase, and rare sanidine phenocrysts, set in a microcrystalline groundmass composed of the same mineral assemblage plus apatite, opaque minerals and rare glass (Fig. 2b). The *Gheshlagh* pillow lavas show medium grained porphyrytic textures with plagioclase, clinopyroxene, leucite (analcime) and minor iddingsitized olivine as phenoscrysts, in a microcrystalline groundmass of plagioclase, Ti-magnetite, apatite, k-feldspar, foids, other than devitrified glass (Fig 2c). The columnar jointing lavas have similar petrographic features, but a coarser grained groundmass with respect to that observed in the pillow lavas. Few samples are characterized by abundant olivine and clinopyroxene phenocrysts in a glassy matrix with abundant clinopyroxene microcrystals, recalling the petrographic features of ankaramites (Fig. 2d). The *Moshiran* rocks show petrographic features very similar to the *Majid Abad* lavas, varying from leucite (analcime) porphyry– to –megaporphyritic textures (Fig. 2e) except for the common presence of olivine (altered to iddingsite) and plagioclase as phenocryst phases (Fig. 2f). Most of the leucite-bearing rocks show clear petrographic evidence of cumulus analcime (leucite), except for a couple of columnar jointing lava samples characterized by cumulus clinopyroxene.

4.1.2. Leucite-free rocks

The *Marallu* lavas show medium grained porphyritic texture with clinopyroxene (and rare plagioclase) phenocrysts in a microcrystalline (sometimes glassy) matrix with k-feldspar, plagioclase, clinopyroxene, apatite, biotite and horneblende (Fig. 3a). Clinopyroxene and plagioclase phenocrysts often show sieve textures (Fig. 3b) that, together with replacement of plagioclase and olivine by potassium feldspar and clinopyroxene, suggest that these rocks underwent magma mixing processes. One sample (M-09) shows rare leucite phenocrysts. The *south Moshiran* and *Tullun* lavas show similar petrographic features and are characterized by medium-grained porphyritic textures with olivine, plagioclase and clinopyroxene phenocrysts (Fig. 3c) in an intergranular to intersertal microcrystalline (sometimes containing glass, Fig. 3d) matrix including the same minerals plus apatite and Ti-magnetite. Olivine crystals are often replaced by serpentine and iddingsite, whereas plagioclase and clinopyroxene show sieve texture and zoning. The *Moradlu* hypabyssal rocks show two distinct petrographic features, on the basis of their degree of differentiation. The more mafic rocks are characterized by porphyritic texture with olivine, clinopyroxene and plagioclase phenocrysts in a fine-grained matrix of the same minerals and glass (Fig. 3e). They show petrographic features similar to those of the *south Moshiran* and *Tullun* rocks. The felsic rocks show porphyritic texture with sanidine (and rare plagioclase) phenocrysts in the fine to medium grained matrix composed of feldspar, biotite, apatite, opaque minerals, and rare nepheline (Fig. 3f).

4.2 Major and trace element composition

The major and trace element composition of Arasbaran igneous rocks is reported in Tables 1 and 2. The major element budget conforms to that of basic to acid igneous rocks, with SiO_2 varying between 51.5 and 61.7 wt%, and MgO between 7.9 and 0.1 wt%. In the Total Alkali Silica (TAS) diagram (Fig. 4a? Fig. 5a; Le Maitre et al., 2002), the Arasbaran magmatic rocks span from transitional to alkaline series. The leucite-free rocks generally include less differentiated products and are characterized by both transitional and alkaline affinities, whereas the leucite-bearing rocks include exclusively alkaline rocks (with the exception of 2 ankaramitic samples).

Among the leucite-bearing rocks the *Majid Abad* section is characterized by shoshonite, latite, tephritic phonolite to phonolite compositions (SiO_2 53.7-58.0 wt %, K_2O 3.5-8.2 wt%), the *Gheshlagh* section by high-K basaltic andesite (2 ankaramitic samples) to shoshonite, latite and tephritic phonolite (SiO_2 52.4-54.2 wt %, K_2O 2.3-6.6 wt%), and the *Moshiran* section varies from latite to tephritic phonolite (SiO_2 54.8-55.2 wt %, K_2O 1.3-5.1 wt%).

Among the leucite-free rocks, samples from the *Marallu* section plot at the boundary between shoshonite latite, phonolitc tephrite and tephritic phonolite fields (SiO_2 53.2-54.3 wt %, K_2O 4.5-7.2 wt%), whereas those from the *Tullun* and *south Moshiran* sections in the shoshonite field (SiO_2 51.9-54.0 wt %, K_2O 3.0-4.9 wt%). Mafic and felsic dikes outcropping westward from *Moradlu* are shoshonitic (SiO_2 51.5-53.7 wt %, K_2O 4.2-6.3 wt%) to trachytic (SiO_2 61.5-61.7 wt %, K_2O 6.3 wt%) in composition.

Despite of the above cited differences between the two lithotypes, according to the K_2O *vs* SiO_2 classification diagram (Peccerillo and Taylor, 1976; Fig. 4b) all the studied Arasbaran igneous rocks display shoshonitic affinity except for the ankaramitic samples. However, the normative composition reveals that leucite-bearing rocks are more SiO_2-undersaturated than leucite-free ones (Fig. 5).

The Arasbaran rocks are characterized by a variable Loss on Ignition (LOI) values, ranging between 0.6 and 6.7 wt% and displaying a broad inverse correlation with CaO; leucite-bearing rocks show relatively high LOI values due to the presence of low-temperature secondary phases (e.g., analcime from leucite, calcite). In any case, the restricted compositional range observed for an element scarcely mobile during weathering processes such as TiO_2, and the lack of clear relationships between LOI and major oxides (with the exception of CaO) suggest that the bulk rock major element composition (recalculated on anhydrous basis) still preserves information on the magmatic signature.

The variation diagrams of Figure 6 show that MgO is inversely correlated with SiO_2, Al_2O_3, alkalis (Na_2O and K_2O, not shown), and directly correlated with Fe_2O_3 and TiO_2, suggesting that the various rocks could reflect different degrees of fractional crystallization. All of the investigated volcanic products depict a common distribution, with the exception of the *Gheshlagh* pillow lavas, which are characterized by invariably lower TiO_2, Fe_2O_3, CaO, higher alkalis and Al_2O_3 contents at comparable MgO. The main difference in the liquid lines of descent (LLD) of leucite-bearing and leucite-free rocks is represented by the variation of CaO and Al_2O_3 of least differentiated products, with the former characterized by a higher clinopyroxene fractionation with respect to the latter (Supplementary figure 2). Leucite-bearing *Gheshlagh* pillow lavas show the lowest compatible trace elements content, coupled with a distinctive enrichment in the most incompatible Large

Ion Lithophile Element (LILE) such as Ba (Fig. 6g). On the other hand, the leucite-free rocks (*South Moshiran, Tullun* lavas and *Moradlu* dykes) show a relative enrichment in High-Field Strength Elements (HFSE), as demonstrated by the distribution of Zr and Nb (Fig. 6f and h).

Primordial Mantle (PM)-normalized incompatible element distribution (Fig. 7) of Arasbaran igneous rocks show the typical features of subduction-related magmatism, with troughs in HFSE (Nb, Ta, Ti, Zr) and spikes in LILE (Ba, K; Condie, 2001) and Pb. Coherently, in the Ce/Yb vs Ta/Yb and diagram (Fig. 8a) proposed by Pearce (1982) Arasbaran rocks plot in the shoshonite field. This affinity, certainly attributable to a convergent plate setting, is confirmed by the use of recent tectonomagmatic diagrams (Fig. 8b and c) such as those proposed by Hastie et al. (2007) and Saccani (2015).

Notably, leucite-bearing rocks are generally characterized by a higher LILE/HFSE ratio, with respect to the leucite-free rocks. In particular, samples from *Majid Abad*, *Quarah Su* and *Moshiran* occurrences show average Ba/Nb ratio of 157, 242 and 106, respectively. On the other hand, samples from *South Moshiran, Tullun* and *Marallu* generally show lower average Ba/Nb ratio (43, 63 and 98, respectively). Similar distribution concerns the LILE/REE ratio, which shows distinct ranges for leucite-bearing rocks (Ba/La 30-117) and leucite-free rocks (Ba/La 10-32). These geochemical features are also observed in other Late-Cretaceous-Eocene leucite-bearing and leucite-free rocks from NW Iran (Lahrud, Shafaii Moghadam et al., 2018; Moghan, Amraee et al., 2019), Central (Gülmez et al., 2016) and Eastern Pontides (Altherr et al., 2008; Eyuboglu et al., 2011). Leucite-free and leucite-bearing rocks are characterized by overlapping REE patterns, with La_N/Yb_N varying from 6.3 to 17.8, which is inversely correlated with MgO (wt%), probably as a result of fractional crystallization of clinopyroxene in the most evolved products. Striking differences are also observed in the Eu/Eu* values, which are systematically higher in the leucite-bearing rocks (1.05-1.15) with respect to leucite-free rocks (0.82-0.88).

The Sr and Nd isotopic compositions of the Arasbaran rocks plot between the depleted MORB mantle (DM) and enriched mantle (EM) components (Fig. 9). On the whole, the $^{87}Sr/^{86}Sr_{(i)}$ varies between 0.704407 and 0.705669, whereas $^{143}Nd/^{144}Nd_{(i)}$ values range from 0.512572 to 0.512791 (Table 3). Notably, leucite-bearing rocks are characterized by the lowest Sr and the highest Nd radiogenic values plotting above the Bulk Silicate Earth (BSE). In particular, the pillow and columnar jointing basalts from *Gheshlagh* river show a composition similar to that of slightly Altered Oceanic Crust (AOC) defined by (Hauff et al., 2003) thus trending toward the composition of an hypothetical Depleted Mantle (DM) geochemical component (Zindler and Hart, 1986). On the other hand, leucite-free rocks show the highest Sr and the lowest Nd radiogenic values, plotting in the Enriched Mantle (EM) quadrant of the diagram. Among them, the *Moradlu* mafic and felsic dykes show the highest Sr radiogenic values, the latter plotting toward the Global Oceanic Subducted Sediments (GLOSS) end-member defined by Plank and Langmuir (1998). The lead isotopic composition of the Arasbaran igneous rocks is reported in (Fig. 10a). All samples are characterized by lead isotope values well above the Northern Hemisphere Reference Line (NHRL - Hart, 1984) on $^{207}Pb/^{204}Pb$ vs $^{206}Pb/^{204}Pb$ and $^{208}Pb/^{204}Pb$ vs $^{206}Pb/^{204}Pb$ (not shown). They vary from 18.60 to 18.75 for $^{206}Pb/^{204}Pb$, from 15.58 to 15.64 for $^{207}Pb/^{204}Pb$ and from 38.69 to 38.87 for $^{208}Pb/^{204}Pb$. It is noteworthy that the leucite-bearing rocks are characterized by the lowest Pb radiogenic values ($^{206}Pb/^{204}Pb$ 18.58-18.65, $^{207}Pb/^{204}Pb$ 15.57-15.60, $^{208}Pb/^{204}Pb$ 38.63-38.71), whereas the leucite-free rocks the highest Pb radiogenic composition ($^{206}Pb/^{204}Pb$ 18.65-18.75, $^{207}Pb/^{204}Pb$ 15.61-15.64, $^{208}Pb/^{204}Pb$ 38.65-38.87), thus defining distinct Pb compositional features

4.3 K-Ar dating

K-Ar radiometric ages have been carried out on 6 samples representative of the various leucite-free and leucite-bearing Arasbaran igneous rocks (Table 3). Although K-Ar datings indicates that all the investigated samples are nearly coeval and of Middle Eocene in age (Lutetian-Bartonian), slight but significant differences can be observed. Leucite-free rocks were mainly emplaced from 41.9 +/- 1.1 Ma at *South Moshiran* to 40.0 +/- 1.1 Ma at *Marallu*, whereas leucite-bearing lavas are slightly younger and were erupted in a short time interval from 39.6 +/- 1.0 at *Majid Abad* to 39.4 +/- 1.0 Ma at *Gheshlagh*.

5. Discussion

The main petrographic, geochemical and isotopic features of the Arasbaran igneous rocks are discussed below in order to define the magmatic affinities, the space-time distribution of the different magma types and the nature of the metasomatic agents affecting their mantle sources, in turn related the subduction geodynamic framework in this sector of the Alpine-Himalayan belt.

5.1 Magmatic affinity and differentiation processes of the Arasbaran volcanic rocks

The observed mineralogical parageneses and the related geochemical features of the Arasbaran igneous products are important markers indicating that the relative magma was basically mafic and potassic, i.e., features observed in many Cenozoic “orogenic” (subduction-related) volcanic rock associations of the circum-Mediterranean area (Beccaluva et al., 2011, 2013; Bianchini et al., 2008; Conte et al., 2016; Conticelli et al., 2009; Wilson and Bianchini, 1999). Petrographic observation allows distinguishing two different rock-types zonally arranged in adjacent sectors of the study area: leucite (analcime)-bearing rocks at *Majid Abad, Gheshlagh* and *Moshiran* (WNW) and leucite (analcime)-free rocks occurring at *South Moshiran, Marallu, Tullun* and *Moradlu* (ESE). The genesis of analcime in silica-undersaturated rocks is highly debated, since it can occur either as primary magmatic crystallizing phase or by secondary post-magmatic/hydrothermal substitution over leucite (e.g., Luhr & Kyser, 1989). Despite the primary genesis of analcime bearing rocks in this sector of the Alpine-Himalayan belt has been proposed by some authors (Didon and Gemain, 1976;

Soltanmohammadi et al., 2021), most interpretations favor a secondary origin (Comin-Chiaramonti et al., 1979; Altherr et al., 2008; Eyuboglu, 2010; Amraee et al., 2019). The primary analcime should be characterized by low K and high Fe contents. Considering the analcime compositions for NW Iran rocks with low Fe contents (Soltanmohammadi et al., 2021), coupled with the absence of magmatic hydrous minerals such as amphibole or mica in the rock we suggest that the observed analcime is a product of leucite transformation during secondary processes.

Noteworthy, the observed petrographic differences reflect different water content and degrees of SiO_2-undersaturation of the two lithotypes, with the leucite-bearing rocks being generally water-free and characterized by lower silica saturation index (Δq = CIPW normative q − [lc + ne + kal + ol]) and K_2O/Na_2O, with respect to leucite-free rocks (Fig. 5). The observed trend in the Δq *vs.* K_2O/Na_2O binary diagram is probably related to the effect of alteration, with the preferential loss of K_2O over Na_2O. As reported by Prelević et al. (2004), analcimization and alteration mainly induce loss of K_2O and Rb, suggesting that the protolith of leucite-bearing rocks were highly potassic. The same interpretation was provided by Altherr et al., (2008) for plagioleucitites from Pontides, who suggested an ultrapotassic affinity for these rocks.

Among leucite-bearing rocks *Gheshlagh* lavas include the most mafic end-members (mg# 0.57-0.70) and do not show petrographic evidence of olivine accumulation, thus representing the most suitable candidates as parental melts of this magma type. These rocks are, however, characterized by variable Na_2O/K_2O, high Al_2O_3 and LOI confirming the petrographic evidence of leucite accumulation and analcime substitution. Moreover, their low CaO (and Sc) at relatively high MgO and Al_2O_3 contents indicate that they suffered significant clinopyroxene fractionation. All these evidence pose several problems in reconstructing the pristine geochemical composition of leucite-bearing magmas both in terms of petrologic and geochemical affinities. For those reasons only the most mafic and potassic samples (samples M31, M36, M39) were selected for classification and modelling of the leucite-bearing rocks. Following a backward correction of the geochemical composition for the pseudomorphic substitution of analcime (from 10 to 25 vol%) over leucite (mineral chemistry from Comin-Chiaramonti et al., 2009) and fractionation (addition of 10-20% clinopyroxene, mineral chemistry from Conticelli et al., 1997) basing on the petrographic observation, the samples composition reconcile with the geochemical features required by the classification criteria defined by Foley et al. (1987) for ultrapotassic rocks (MgO and K_2O >3 wt%, K_2O/Na_2O>2). The backward corrected parental leucite-bearing magmas share geochemical features with the leucitites and plagioleucitites of the Roman province (data compilation from Conticelli et al., 2015) and with Central and Eastern Pontides leucitites and plagioleucitites (Altherr et al., 2008; Gülmez et al., 2016) in the Foley's classification diagrams for ultrapotassic rocks (Supplementary Fig. 3).

Contrarily, the petrographic and geochemical features of the *South Moshiran*, *Moradlu* and *Tullun* leucite-free rocks do not match those of ultrapotassic rocks, and their low K_2O/Na_2O ratio (< 1.5) confirmed their shoshonitic affinity. On the other hand, the *Marallu* lavas show intermediate geochemical features between leucite-bearing and leucite-free rocks (K_2O/Na_2O between 1.0 and 4.0).

In order to test the possible occurrence of magmatic relationships among the Arasbaran rocks suites the thermodynamically based Magma Chamber Simulator model (MSC, Bohrson et al., 2020; Heinonen et al., 2020) for fractional crystallization processes (FC) has been applied to leucite-bearing and leucite-free magma types. Leucite-bearing rocks type are characterized by a wide spectrum of volcanic products at growing differentiation degree from the *Gheshlagh* pillow and columnar jointing lavas (mg# up to 0.7) to the *Majid Abad* lavas (mg# down to 0.1). The observed small, but consistent differences in the isotopic composition would also suggest a distinct mantle source for the mafic and intermediate/felsic leucite-bearing products. However, these products share petrographic and geochemical similarities, suggesting that they are nearly comagmatic. We thus tested if the most differentiated leucite-bearing products can be achieved through a simple FC model. Starting from the backward corrected composition of the *Gheshlagh* mafic lavas, the FC trend of the leucite-bearing rocks (FC1) correctly reproduce the observed major elements distribution of the more differentiated products, confirming their common magmatic affinity (Supplementary Fig. 2). Results show that the most differentiated leucite-bearing products are compatible with fractionation of 10-16% Ol, 20-40% Pl, 10-20% Cpx, 5-15% Leu, 2-10% Af and 4-5% Fe-Ti oxides, from the relative calculated parental magmas, at the pressure of 1 Kb, oxygen fugacity on QFM buffer with low (0.5-1.0 wt%) initial water content. The liquid fraction corresponding to the most differentiated leucite-bearing product vary from 20 to 25% of the original parental melt at the temperature of 850 °C. The fractionated mineralogy and the crystallization order is consistent with that observed by petrographic analysis of the most differentiated leucite-bearing samples. In particular, the occurrence of leucite on the liquidus after clinopyroxene and plagioclase and its rapid growth predicted by the model is compatible with what observed in megaporphyritic samples showing big leucite crystals including the above cited mineral phases having higher crystallization temperature. The selected initial water content of parental magma is an important variable (at isobaric conditions) for reproducing the observed crystallization order and mineral proportions of the leucite-bearing melts. Indeed, at low (ca. 0.5 wt% H_2O) initial water content the model predicts an early appearance of leucite on the liquidus following olivine in the crystallization sequence, whereas at higher water magma initial content (> 1.0 wt% H_2O) leucite is not present in the fractionated solid assemblage and potassium is mainly hosted by alkali feldspar and minor biotite. The low water content of the parental leucite-bearing rocks was also inferred for Central Pontides (Gülmez et al., 2016) and for the Roman (Avanzinelli et al., 2009, Conticelli et al., 2015) rocks, and it is in agreement with the favored conditions for leucite crystallization in low P_{H2O}

conditions (Freda et al., 1997, Gaeta et al., 2000). Therefore, model results suggested that the physico-chemical conditions of differentiation for the leucite-bearing magma that best fit the petrographic features and the LLD of this suite include a FC process at low (1.0 Kb) pressure and a low water content of the parental magma ranging from 0.5 to 1.0 wt%

The same FC modelling has been applied to leucite-free samples, using the most mafic samples (M58, M56 and M17 for the *South Moshiran, Tullun* and *Moradlu* series, respectively – black asterisk symbols in Supplementary Fig. 2) as parental melts. The composition of the most differentiated products, identified by the *Moradlu* trachytic dikes, of the leucite-free rocks can be successfully matched by the FC crystallization trends (FC2) of the related parental melts with 1.0-1.5 wt% water content at the pressure of 1 Kb and at QFM oxygen fugacity buffer (Supplementary Fig. 2). In particular, the fractionation of 9-13% Ol, 12-17% Cpx, 23-33% Pl, 5-6% Fe-Ti oxides and 0.5% Ap from the most mafic leucite-free melts allow reproducing the composition of the most differentiated products, which correspond to a liquid fraction of ca. 40% of the parental melt at ca. 1000 °C. The higher volatile content of the leucite-free rocks is confirmed by the significant presence of biotite in the mineral paragenesis, which is also predicted by the model. The *Marallu* series, although lacking petrographic evidence of leucite in its mineral assemblage, often plot in between the FC1 and FC2 differentiation trends, suggesting a possible derivation by a mixing of the two main magma types of the Arasbaran area. This is corroborated by the pervasive sieved textures observed in their phenocrysts (Fig. 4), by the intermediate isotopic composition (Fig. 9), as well as by the geographic position in between of the leucite-bearing and leucite-free occurrences (Fig. 1b).

5.2 Magma genesis, metasomatic agents and mantle sources of the Arasbaran rocks

The geochemical features of both leucite-free and leucite-bearing rocks conform to those of magma series typically occurring in convergent plate margins in connection with the occurrence of subduction processes (e.g., Conticelli and Peccerillo 1992 Beccaluva et al., 2013 and references therein; Bianchini et al., 2008; Conticelli et al., 2009; Mattioli et al., 2012). In fact, the incompatible element distribution of all the Arasbaran igneous rocks show the typical features of subduction-related magmatism, with troughs in Nb–Ta-Ti-Zr (HFSE) and spikes in Ba-K (LILE) and Pb (Condie, 2001). However, leucite-bearing rocks are characterized by higher LILE/HFSE (e.g., Ba/Nb), LILE/LREE (e.g., Ba/La) as well as Ba/Th ratios with respect to leucite-free rocks. The pronounced enrichment in some LILE (and Pb) was commonly attributed to the addition of these water-soluble elements by fluids derived from the dehydration of the subducted slab (e.g., Tatsumi et al., 1986), while depletion of the generally fluid-immobile HFSE is thought to reflect a preexisting depletion within the mantle wedge (e.g., Elliott, 2003; McCulloch and Gamble, 1991; Woodhead et al., 1993). Therefore, the relative contribution of slab-derived fluids and slab-melt to the mantle sources of subduction-related magmas is usually represented by the ratios between fluid-mobile (Ba, Pb) and fluid-immobile (e.g., Th, REE) elements. Subduction-related magmas having a geochemical signature characterized by Ba/Th > 1000 coupled with low $(La/Sm)_N$ values (around 1), as well as a consistent Sr isotope ratio, has been traditionally related to a magma source mainly metasomatised by a 'fluid' phase from subducted altered MORB oceanic crust (e.g., Tonga, Izu–Bonin, some Mariana islands) whereas the contribution of sediment-derived melt will produce magmas characterized by higher trace element content, radiogenic Sr, low Ba/Th and high La/Sm ratios (Elliot et al., 2003). In this framework, leucite-bearing lavas share some geochemical similarities with the first source type, being characterized by high Ba/Th (170-520) and relatively low $^{87}Sr/^{86}Sr_i$ (0.70439-0.70464) values, whereas leucite-free lavas mainly conform to the latter, showing systematically lower Ba/Th (12-170) and higher $^{87}Sr/^{86}Sr_i$ (0.70481-0.70567) values (Fig. 11a). Recent experimental studies (Carter et al., 2015) demonstrated that also epidote-bearing Altered Oceanic Crust (AOC) experimental hydrous melts at 800-850°C are characterized by high Ba/Th values because of phengite (releasing Ba) but not epidote (retaining Th) melting in this narrow supra-solidus temperature range. The persistence of epidote in the melting residue of non-anomalously hot slab conditions, could also be responsible for the observed low La/Sm ratios of these AOC supercritical fluids/melts. In this regard, all the Arasbaran rocks (including leucite-bearing lavas) are characterized by high La/Sm ratios (2.7-5.7), incompatible with those originated from either AOC fluids or melts metasomatizing agents (Fig. 11b).

Similar results were obtained by the experimental study of Skora et al. (2015) that tested the melting of undoped marly sediments in T-P conditions typical of subduction environments (3GPa and 800-1100°C). These authors highlighted that high-carbonate (HC) sediments produce partial melts enriched in 'fluid-mobile' elements such Cs, Ba, Rb, K and Sr showing geochemical similarities with fluids conventionally ascribed to altered oceanic crust. On the other hand, HFSE such as Ti, Nb, and Ta are depleted, due to retention in residual rutile at temperature < 1000° C, as well as Y, and HREE due to their compatibility in residual garnet or carbonate. Moreover, partial melts produced by HC sediments in the presence of residual epidote are characterized by higher Ba/Th than those produced by carbonate-poor (LC) epidote-free lithologies. It follows that the presence of a residual phase in the subducted lithologies that selectively acts as sink for trace elements, such as epidote, is plausibly the reason of the observed Ba/Th ratios, irrespective of their nature. On the other hand, both LC and HC partial melts obtained at T>900°C produce high $(La/Sm)_N$ values (4.0-7.0) that may originate from the relative stabilities of epidote and garnet (Skora et al., 2015). These values conform with those observed in both leucite-bearing and leucite-free, suggesting that both magma types require a sedimentary input in their metasomatized mantle sources. Leucite-bearing rocks show different geochemical trends with respect to that defined by arc magmas (data from Elliot et al., 1997), pointing to unusually high Ba/Th and La/Sm values that conform with those of experimental partial melts of epidote-bearing HC sediments at T>=900°C. The involvement of a sedimentary component in the magma source of leucite-bearing rocks is also evident by the comparison with Marianas arc lavas that show higher Ba/Th coupled with systematically lower La/Sm values, as a result of the exclusive contribution of AOC component to their mantle source. On the other hand, leucite-free rocks show systematically lower Ba/Th but similar La/Sm with respect to leucite-bearing rocks, which are compatible with those of partial melts from epidote-poor or -free LC lithologies in the same temperature interval. This geochemical composition is also comparable to that of the Roman (Neapolitan district) volcanic province, for which a significant sedimentary (carbonate) contribution to the mantle source has been invoked (Avanzinelli et al., 2009; 2018; Conticelli et al., 2015; Fig. 11).

Sr-Nd-Pb isotopes provide further evidence that support the involvement of sedimentary partial melts, rather than AOC supercritical melts/fluids as a metasomatizing agents of the Arasbaran mantle section. Although the Sr isotopic composition of leucite-bearing rocks (among the least radiogenic values of the whole TIP) is compatible with those of the neighboring Neotethyan Mesozoic ophiolites, representing the local subducted AOC, their low $^{143}Nd/^{144}Nd$ and high $^{207}Pb/^{204}Pb$ are not consistent with fluids/melts from the basaltic oceanic crust, instead requiring partial melts derived from continental crustal (i.e. sedimentary) material.

The application of the genetic model to the generation of the Arasbaran igneous rocks is reported in Fig. 9 and Fig. 10. In this model, we report the partial melting of a mantle wedge enriched by metasomatic agents consisting of supercritical liquids and/or partial melt components deriving from the subducted AOC and by the associated sediments. The composition of the pre-metasomatised mantle wedge and of AOC can be carried out by the least metasomatised/altered mantle rocks and mafic rocks from Neyriz (Shafaii Moghadam et al., 2014b) and Kermanshash (Saccani et al., 2013) ophiolites, respectively, since they represent remnants of the Neotethyan mantle and oceanic crust involved in this subduction system. The sedimentary metasomatic agents could be instead represented by carbonate-rich (HC) and carbonate-poor (LC) marly sediments (e.g., Avanzinelli et al., 2018). The least differentiated volcanics (Mg# > 0.60, SiO_2 < 55 wt%) from leucite-bearing (samples M36, M38; M45) and leucite-free (M54, M56, M58, M60), were chosen to be the target compositions of the genetic model since they reasonably represent the most suitable parental magma types of the area. The results of elemental and isotopic based mass balance calculations, together with those of the non-modal melting model (Shaw, 1970) highlight that both igneous and sedimentary metasomatic components need to be added to the mantle wedge to reproduce the source of leucite-bearing and leucite-free magmas of the Arasbaran area.

In particular, we infer that the geochemical signature of the mantle source is achieved through a two-steps process concerning a first enrichment event of the local mantle wedge involving metasomatic supercritical liquids/melts, followed by a second one involving different proportions and quality of a sedimentary components.

In our model, the addition of 5-6% of AOC component (represented by the average Zagros MORB ophiolites) to the pre-subduction local mantle wedge can be inferred as an ubiquitous enrichment stage that characterized the whole mantle section source (S1) of the Arasbaran magmas. The composition of the slab derived metasomatic supercritical liquids/melts was obtained by the application of experimental results of (Carter et al., 2015) at 3 GPa and temperature between 900 and 1000 °C to the average local MORB-type ophiolites. The second enrichment stage, was instead distinct in terms of nature and proportions of the sedimentary component, differentiating the mantle sources of the leucite-bearing (S2) and leucite-free (S3) magma types. In particular, the addition of a small amount (3-4 %) of a HC-dominated (80-90%) sediment partial melts to the enriched mantle wedge successfully reproduces the isotopic composition of the most undersaturated leucite-bearing lavas, whereas higher proportions (4-8 %) of LC-dominated (60-80 %) sediment melts are needed to reproduce the isotopic features of the less undersaturated leucite-free lavas (Fig. 9). The two distinct isotopic trends defined by the second enrichment stage originated from the different isotopic and elemental budget of the HC and LC sediment partial melts, which are characterized by a Sr/Nd ratio higher (Sr/Nd > 100) and lower (Sr/Nd < 20), respectively, with respect to the S1 source (Sr/Nd ca. 70). The composition of sediment partial melts was obtained by the application of the experimental results of (Skora et al., 2015) performed at 3 GPa pressure and 900-1000°C temperature to the HC and LC Mediterranean marly sediments reported in Avanzinelli et al. (2018).

Similar results were obtained by the magma genesis melting model depicted in Fig. 12 that corroborate our interpretation. The observed incompatible elements distribution of the leucite-bearing and leucite-free magmas can be indeed reproduced by different partial melting degree of their relative mantle sources as defined by the previous model. The best fit for leucite-bearing magma-type is obtained by low melting degree (F around 4 %) of the S2 mantle source (Ol_{54}, Opx_{25}, Cpx_{12}, Sp_2, Gt_3, $Amph_2$, Phl_1), whereas a higher melting degree (F around 10 %) of the S3 source (Ol_{54}, Opx_{25}, Cpx_9, Sp_3, Gt_3, $Amph_2$, Phl_4) is required to fit the distribution of the leucite-free magmas (Fig. 12). The difference in the composition and partial melting degree of these two mantle sources is corroborated by the incompatible element distribution of leucite-free magmas, which is very similar to that of the LC-dominated sedimentary component. In this model, the composition of the High-Carbonate and Low-Carbonate sediment partial melts at temperatures between 900 and 1000°C were tested as the sedimentary metasomatic agents, since they are the main carrier of REE (especially LREE). The results of our genetic model clearly indicate that, although AOC fluids/melts can imprint some geochemical features typical of Arasbaran magmas (high K, Sr, Ba/Th), they cannot provide the proper LREE budget to the mantle sources. As indicated by recent studies (e.g., Rustioni et al., 2021) REE mobilization from the oceanic slab could be achieved also through the interaction with saline fluids. However, the application of these experimental results to the genetic model of Arasbaran magma fails to reproduce some geochemical features, such as Ba/Th and Th/LREE ratios. Moreover, as reported in Li et al. (2022), the addition of 2-3% of such saline fluids to the mantle source would produce a high H_2O content (>10 wt%) magma, which is inconsistent with the absence of hydrous phases in leucite-bearing lavas. Therefore, the addition of the AOC component alone to the depleted mantle wedge cannot explain the observed isotopic features of the Arasbaran lavas, which need a metasomatically overprinted source by a sedimentary component.

The different incompatible element budget provided by the two sedimentary components is reflected by the distinct geochemical composition of the S2 and S3 modelled mantle source. The S2 source is generally less enriched than S3 source and this is reflected by their modal metasomatism, with the former characterized by a lower content of hydrous accessory phases (phlogopite+amphibole = 3) with respect to the latter (phlogopite+amphibole = 6). Moreover, the S2 source displayed distinctly higher Ba/Th, Sr/Nd and Sr/Y ratio with respect to S3 source, which correspond the geochemical features observed in the leucite-bearing and leucite-free lavas, respectively. In fact, the distinct melting degrees of S2 and S3 required to generate the related magma-types emphasized these geochemical differences in the modelled melts (in particular for the Ba/Th and Sr/Y ratios), reproducing what observed in leucite-bearing (higher Ba/Th and Sr/Y) and leucite-free lavas.

The isotopic composition of the Arasbaran ultrapotassic magmas is characterized by the least radiogenic Sr and most radiogenic Nd values with respect to previously published data from the area (Lahrud - Shafaii Moghadam et al., 2018; Salavat Range - Soltanmohammadi et al., 2021, Moghan - Amraee et al., 2019). At a regional scale, analogies and differences can be highlighted between the subduction-related igneous rocks of NW Iran and Central-Eastern Pontides sectors of the Alpine-Himalayan belt. The similarity is represented by the less radiogenic values showed by ultrapotassic leucite-bearing rocks with respect to shoshonitic leucite-free rocks in both sectors. The difference is a general displacement toward more radiogenic values of both rock types in the Eastern Pontides sector with respect to NW Iran. This is in excellent agreement with the general isotopic trend of the Cenozoic ultrapotassic (lamproitic) magmatism along the Alpine-Himalayan belt identified by Casalini et al. (2022), probably indicating that the same sedimentary end-members (i.e., HC and LC sediments) are involved in a similar subduction environment, but at decreasing proportion with respect the to the ambient mantle from W to E. Using the same components, the Pb isotope systematics also allows to reproduce leucite-bearing rocks as a mixing between the inferred subducted oceanic crust and HC-sediment partial melt and leucite-free rocks with Low-Carbonate sediment partial melt, the latter showing comparatively higher radiogenic Pb values (Fig. 10a). Coherently, the Pb isotopic values confirm that the metasomatic agents of the leucite-bearing rocks are characterized by a lower sediment contribution with respect to those of leucite-free rocks.

Similar results can be obtained using elemental ratios such as Ba/La and Nd isotopic composition, confirming the reliability of the model and the source heterogeneity that characterizes the mantle section of the Arasbaran area (Fig.10b). Other geochemical features of leucite-bearing rocks, such as the high Sr/Y (up to 300) and Eu/Eu* (1.05-1.15) are compatible with the involvement of marine carbonate sediment as metasomatic component of their mantle source (Nath et al., 1992; Nagarajan et al., 2011).

Geochronological K-Ar data indicate a nearly coeval generation of the Arasbaran leucite-bearing (39.4-39.6 +/- 1.0 Ma) and -free (41.9 +/- 1.1 Ma) magmatism in the Middle-Late Eocene, in agreement with previous data on hypabyssal rocks from the same area (42.7– 38.4 Ma, Alberti et al., 1976). The significant variability of the magmatic products occurred over a limited area in this short time-span indicate that this event represents an important step in the magmatic evolution of the Ahar-Arasbaran area. This is also confirmed by the intermediate age (40.0 +/- 1.1 Ma) showed by the *Marallu* rocks, which show petrographic, geochemical and isotopic evidence of mixing between older leucite-free and younger leucite-bearing rocks, with the former predominating over the latter. The spatio-temporal relationships of these different magmatic episodes suggest that during Middle Eocene magmatism in the Arasbaran area slightly migrated northwestward, becoming progressively more SiO_2-undersaturated (Fig. 13). This transition is at the opposite with respect to what observed in most circum-Mediterranean occurrences, where a clear temporal succession from initially ultrapotassic, then shoshonitic and finally high-K calc-alkaline magmatism was interpreted as the progressive involvement of host mantle rocks (sub-alkaline end-member) over the metasomatic veins (strongly alkaline end-member) during source melting (Avanzinelli et al., 2009; Conticelli et al., 2011). This model is constrained by the different liquidus temperatures of the alkaline (lower) and sub-alkaline (higher) end-members and their contribution to the primary melts at growing mantle melting degrees in response to isotherm relaxation following the Neo-Tethyan slab roll-back in the mature subduction geodynamics (Bianchini et al., 2008; Avanzinelli et al., 2009; Conticelli et al., 2009a; 2009b). The elemental and isotopic features of ultrapotassic and shoshonitic rocks of the circum-Mediterranean invariably show the involvement of a significant proportion (up to 65 vol% for Tuscan lamproite, Conticelli et al., 2007) of sedimentary (terrigenous or pelagic in nature) melt component in their mantle source (Conticelli et al., 2007; 2009a; 2010; Avanzinelli et al., 2008; 2009), able to create net veined metasomatic domains that probably acted as exclusive source for ultrapotassic magmas. In this sector of the Neothetyan subduction, a significantly lower contribution of the sedimentary component to the metasomatic agents of the Arasbaran magmas doesn't suggests the creation of a net veined mantle source, but rather a more diffused metasomatism of the peridotitic mantle wedge. The metasomatic domains should have the flavor of carbonate-rich late subducted sediment relatively close to the trench (S2) fading into a more decided carbonate-poor signature outward (S3), progressively overprinting the contribution from the altered oceanic crust to the mantle wedge (S1).

This sector of the Alpine-Himalayan belt, is characterized since the Cretaceous onward, by a northeastward subduction of the Neotethys oceanic slab underneath the southern margin of the Eurasia plate, followed by continental collision starting from the Oligocene in northwestern Iran with a progressive SW migration of deformation and topography (Agard et al., 2011; Aghazadeh et al., 2011). In this geodynamic scenario, The Middle Eocene Arasbaran magmatism should represent a subduction-related event, triggered by slab retreat and roll-back (Fig. 14; Raibiee et al., 2019 and references therein). The slab roll-back and retreat caused lithospheric extension in NW Iran (Shafaii Moghadam et al., 2018 and references therein) leading to asthenospheric up-welling that caused heating and lithosphere erosion through the melting of the metasomatised mantle wedge, the so called "magmatic flare-up" that was particularly intense during Eocene (Verdel et al., 2011). In this framework, the melting of leucite-bearing (S2) and -free (S3) sources occurred slightly diachronous and zonally arranged (Fig. 14a) probably both for the late arrival of high carbonate sediments at depth in concomitance with incipient slab steepening and roll back (e.g., Conticelli et al., 2015; (Ammannati et al., 2016)) . The higher melting degree of S3 with respect to S2 source predicted by the model should be explained by the isotherms geometry in the mantle wedge generated in response to the slab retreat geodynamic trigger (e.g., Frezzotti et al., 2009) as well as by the higher proportion of metasomatic lower solidus component in the mantle source. In this scenario an eastward dipping polarity of the subduction plane broadly fits with the observed distribution in space and time of the associated magmatism, with the S2 source located relatively closer to the subducted slab with respect to the S3 source (Fig. 14b). The Eocene Arasbaran melting sequence from shoshonitic to ultrapotassic parallels the time-dependent geochemical variation observed from Late Cretaceous in Central Anatolia (Gülmez et al., 2016) through Paleocene in the eastern Pontides (Eyuboglu et al., 2011) occurrences, and from other eastern sectors of the Alpine-Himalayan belt such as the Neapolitan district of the Roman province (Cioni et al., 2008, and references therein; Conticelli et al., 2011) and at Stromboli in the Aeolian Arc (Ellam et al., 1988; Peccerillo, 2001, 2005; Alagna et al., 2010; Conticelli et al., 2011).

The Arasbaran leucite-bearing rocks are very similar to plagioleucicites, a rare volcanic product worldwide, that at a regional scale can be compared with some Paleocene occurrences from Eastern Everek Hanları (Altherr et al., 2008)) and Southern Pontides (Amasya, Tüysüz, 1996, Ankara, Çapan, 1984). These magmatic products are more common in other sectors of the Alpine-Himalayan belt, such as the Roman volcanic province in central-southern Italy (Peccerillo, 2005 and references therein, Avanzinelli et al., 2008; 2018; Conticelli et al., 2011; 2015). In particular, the Arasbaran rocks show intermediate geochemical composition between the Paleocene Anatolian plagioleucitites and those from the Roman (Neapolitan district) province (Supplementary Fig. 3). The generation of the Neapolitan plagioleucitites was interpreted as the result of partial melting of previously metasomatized mantle furher enriched by the addition of carbonate sediments melts (Avanzinelli et al., 2018). A similar genetic model is proposed for the Arasbaran leucite-bearing rocks, but with a different metasomatic agent characterized by a lower sediment/altered oceanic crust ratio. This is consistent with the observed differences in the isotopic and trace element composition of the NW Iran, Anatolian and Italian plagioleucitites (Fig. 10).

4. Conclusions

The Middle Eocene K-rich magmatism of the Arasbaran area in NW Iran vary from shoshonitic to ultrapotassic affinity, the latter representing a relatively rare occurrence in this sector of the Alpine-Himalayan belt. This magmatic event is related to the melting of mantle sources variously metasomatised by different sedimentary and mafic components during the Neo-Tethys subduction under the Eurasian plate, triggered by slab roll-back and tearing after the Late Cretaceous-Early Eocene Arabian-Eurasian continental collision. The geochemical features of ultrapotassic leucite-bearing magmas are compatible with the involvement of a low (4-5%) HC-sedimentary contribution to a mantel source previously metasomatized by AOC-derived components. On the other hand, a higher (7-8%) LC-sedimentary partial melt component (added to a similar AOC-modified mantle wedge) is required to generate the shoshonitic leucite-free magmas. The almost coeval eruption of both magma types indicate a common geodynamic trigger, which produced an earlier relatively high-melting degree event of the S2 source, to generate the leu-free shoshonites, and a later low degree melts of the S3, to generate the leucite-bearing ultrapotassic rocks the latter occurring at lower temperature being closer to the subducted slab and characterized by a lesser amount of a lower solidus domains. The relative distance from the slab of the two metasomatic domains is probably due to the late arrival of HC- with respect to LC-sediment to the trench due to the evolution of the subduction system toward the continental collision. This would have produced the observed distribution of the Arasbaran lavas, with the ultrapotassic magmas mainly located to the NW and shoshonitic magmas in the SE part of the area. The similarities in the nature of the metasomatic agents and in the geodynamic evolution with the Mediterranean subduction-related magmatism suggest commonalities along the whole Alpine-Himalayan belt, whereas the distinctly lower sedimentary contribution to the mantle sources of the Arasbaran magmas confirm the decreasing W-E trend observed along these subduction systems.

Acknowledgements

We thank Renzo Tassinari and Paolo Di Giuseppe for lab assistance. This study was supported by the Iran National Science Foundation (INSF) grant # 4012817 issued to Merhaji Aghazadeh, the Payam-e-Noor

University, and MUR funding through PRIN grants 20158A9CBM and 2015EC9PJ5 issued to S. Conticelli and R. Avanzinelli, respectively.

Author contributions Statement

MA and SC Conceived the research; MA and ZB made the field work and the sampling; CN, MA, EB, and ZB made the mineralogical and petrographic work; CN and GB made the XRF and ICP-MS analyses; EB and MC made the Sr, Nd, and Pb isotope purifications; EB, MC, RA, and SA made the isotope measurements; CN, MA, and EB wrote the manuscript; all the authors discussed the data and reviewed the manuscript.

References:

Agard, P., Omrani, J., Jolivet, L., Whitechurch, H., Vrielynck, B., Spakman, W., Monie, P., Meyer, B., Wortel, R. , 2011. Zagros orogeny: a subduction-dominated process. Geol. Mag., 148, 692 - 725. https://doi.org/10.1017/S001675681100046X

Aghazadeh, M., Castro, A., Omran, N.R., Emami, M.H., Moinvaziri, H., Badrzadeh, Z., 2010. The gabbro (shoshonitic)–monzonite–granodiorite association of Khankandi pluton, Alborz Mountains, NW Iran. J. Asian Earth Sci. 38, 199–219. https://doi.org/https://doi.org/10.1016/j.jseaes.2010.01.002

Aghazadeh, M., Castro, A., Badrzadeh, Z., Vogt, K., 2011. Post-collisional polycyclic plutonism from the Zagros hinterland: the Shaivar Dagh plutonic complex, Alborz belt, Iran. Geol. Mag. 148, 980–1008. https://doi.org/10.1017/S0016756811000380

Agostini, S., Di Giuseppe, P., Manetti, P., Savaşçın, M.Y., Conticelli, S., 2022. Geochemical and isotopic (Sr-Nd-Pb) signature of crustal contamination in Na-alkali basaltic magmas of South-East Turkey. Ital. J. Geosci. 141, 363–384. https://doi.org/10.3301/IJG.2022.21

Akal, C., 2008. K-richterite-olivine-phlogopite-diopside-sanidine lamproites from the Afyon Volcanic Province, Turkey. Geol. Mag.145, 570-575. https://doi.org/10.1017/S0016756808004536

Alagna, K.E., Peccerillo, A., Martin, S., Donati, C., 2010. Tertiary to present evolution of magmatism in Italy.. J. Virtual Explor. 36, 18. https://doi.org/10.3809/jvirtex.2010.00233

Alberti, A.A., Comin-Chiaramonti, P., Sinigoi, S., Nicoletti, M., Petrucciani, C., 1980. Neogene and quaternary volcanism in Eastern Azerbaijan (Iran): some K-Ar age determinations and geodynamic implications. Geol. Rundschau 69, 216–225. https://doi.org/10.1007/BF01869034

Allen, M., Armstrong, H., 2008. Arabia–Eurasia collision and the forcing of mid-Cenozoic global cooling, Palaeogeogr. Palaeoclimatol. Palaeoecol. 265, 52-58, https://doi.org/10.1016/j.palaeo.2008.04.021.

Altherr, R., Topuz, G., Siebel, W., Şen, C., Meyer, H.-P., Satır, M., Lahaye, Y., 2008. Geochemical and Sr–Nd–Pb isotopic characteristics of Paleocene plagioleucitites from the Eastern Pontides (NE Turkey). Lithos 105, 149–161. https://doi.org/https://doi.org/10.1016/j.lithos.2008.03.001

Ammannati, E., Jacob, D.E., Avanzinelli, R., Foley, S.F., Conticelli, S., 2016. Low Ni olivine in silica-undersaturated ultrapotassic igneous rocks as evidence for carbonate metasomatism in the mantle. Earth Planet. Sci. Lett. 444, 64–74. https://doi.org/https://doi.org/10.1016/j.epsl.2016.03.039

Amraee, A., Zareisahamieh, R., Moayyed, M., Ahmadikhalaji, A., Azimzadeh, A., Santos, J.F., 2019b. Peshtasar basalts: An example of post-collision basalts in sedimentary basin of Moghan, NW Iran. J. Earth Syst. Sci. 128, 1–22. https://doi.org/10.1007/s12040-019-1083-z

Avanzinelli, R., Boari, E., Conticelli, S., Francalanci, L., Guarnieri, L., Perini, G., Petrone, C., Tommasini, S., Ulivi, M., 2005. High precision Sr, Nd, and Pb isotopic analyses using the new generation Thermal Ionisation Mass Spectrometer ThermoFinnigan Triton-Ti®. Period. di Mineral. 74, 147–166.

Avanzinelli, R., Casalini, M., Elliott, T., Conticelli, S., 2018. Carbon fluxes from subducted carbonates revealed by uranium excess at Mount Vesuvius, Italy. Geology 46, 259–262. https://doi.org/10.1130/G39766.1

Avanzinelli, R., Bianchini, G., Tiepolo, M., Jasim, A., Natali, C., Braschi, E., Dallai, L., Beccaluva, L., Conticelli, S., 2020. Subduction-related hybridization of the lithospheric mantle revealed by trace element and Sr-Nd-Pb isotopic data in composite xenoliths from Tallante (Betic Cordillera, Spain). Lithos 352–353, 105316. https://doi.org/10.1016/j.lithos.2019.105316

Avanzinelli, R., Lustrino, M., Mattei, M., Melluso, L., Conticelli, S., 2009. Potassic and ultrapotassic magmatism in the circum-Tyrrhenian region: Significance of carbonated pelitic vs. pelitic sediment recycling at destructive plate margins. Lithos 113:213–227. https://doi.org/10.1016/j.lithos.2009.03.029

Avanzinelli, R., Elliott, T., Tommasini, S., Conticelli, S., 2008. Constraints on the Genesis of Potassium-rich Italian Volcanic Rocks from U/Th Disequilibrium. J Petrol 49, 195–223. https://doi.org/10.1093/petrology/egm076

Barling, J., Goldstein, S.L., 1990. Extreme isotopic variations in Heard Island lavas and the nature of mantle reservoirs. Nature 348, 59–62. https://doi.org/10.1038/348059a0

Beccaluva, L., Bianchini, G., Coltorti, M., Siena, F., Verde, M., 2005. Cenozoic tectono-magmatic evolution of the central-western Mediterranean: migration of an arc-interarc basin system and variations in the mode of subduction. In Finetti I. (ed) *Crop Project – Deep Seismic exploration of the Central Mediterranean and Italy. pp. 623-640.*

Beccaluva, L., Bianchini, G., Natali, C., Siena, F., 2011. Geodynamic control on orogenic and anorogenic magmatic phases in Sardinia and Southern Spain: Inferences for the Cenozoic evolution of the western Mediterranean. Lithos 123. https://doi.org/10.1016/j.lithos.2011.01.007

Beccaluva, L., Bianchini, G., Mameli, P., Natali, C., 2013. Miocene shoshonite volcanism in Sardinia: Implications for magma sources and geodynamic evolution of the central-western Mediterranean. Lithos 180–181. https://doi.org/10.1016/j.lithos.2013.08.006

Bianchini, G., Beccaluva, L., Siena, F., 2008. Post-collisional and intraplate Cenozoic volcanism in the rifted Apennines/Adriatic domain. Lithos 101, 125–140. https://doi.org/https://doi.org/10.1016/j.lithos.2007.07.011

Bianchini, G., Braga, R., Langone, A., Natali, C., Tiepolo, M., 2015. Metasedimentary and igneous xenoliths from Tallante (Betic Cordillera, Spain): Inferences on crust-mantle interactions and clues for post-collisional volcanism magma sources. Lithos 220–223, 191–199. https://doi.org/10.1016/j.lithos.2015.02.011

Boari, E., Avanzinelli, R., Melluso, L., Giordano, G., Mattei, M., De Benedetti, A., Morra, V., Conticelli, S., 2009. Isotope geochemistry (Sr–Nd–Pb) and petrogenesis of leucite-bearing volcanic rocks from "Colli Albani" volcano, Roman Magmatic Province, Central Italy: inferences on volcano evolution and magma genesis. Bull Volcanol 71, 977–1005. https://doi.org/10.1007/s00445-009-0278-6

Bohrson, W.A., Spera, F.J., Heinonen, J.S., Brown, G., Scruggs, M., Adams, J., Takach, M., Zeff, G., Suikkanen, E. 2020. Diagnosing open-system magmatic processes using the Magma Chamber Simulator (MCS): part I—major elements and phase equilibria. Contrib. to Mineral. Petrol. 175, 104. https://doi.org/10.1007/s00410-020-01722-z

Bragagni A, Mastroianni F, Münker C, Conticelli, S., Avanzinelli, R., 2022 A carbon-rich lithospheric mantle as a source for the large CO2 emissions of Etna volcano (Italy). Geology 50, 486–490. https://doi.org/10.1130/G49510.1

Carter, L., Skora, S., Blundy, J., De Hoog, J., Elliott, T., 2015. An Experimental Study of Trace Element Fluxes from Subducted Oceanic Crust. J. Petrol. 56, 1585–1606. https://doi.org/10.1093/petrology/egv046

Casalini, M., Avanzinelli, R., Tommasini, S., Natali, C., Bianchini, G., Prelević, D., Mattei, M., Conticelli, S., 2022. Petrogenesis of Mediterranean lamproites and associated rocks: The role of overprinted metasomatic events in the post-collisional lithospheric upper mantle. Geol Soc London, Spec Publ 513, 271–296. https://doi.org/10.1144/SP513-2021-36

Çapan, U.Z., 1984. Ankara melanjı içindeki zeolitli alkali bazaltik volkanizmanın karakteri ve yaşı hakkında. Türkiye Jeoloji Kurumu 38. Bilimsel ve Teknik Kurultayı, Bildiri özetleri: 121–123.

Castro, A., Aghazadeh, M., Badrzadeh, Z., Chichorro, M., 2013. Late Eocene-Oligocene post-collisional monzonitic intrusions from the Alborz magmatic belt, NW Iran. An example of monzonite magma generation from a metasomatized mantle source. Lithos 180–181, 109–127. https://doi.org/10.1016/j.lithos.2013.08.003

Chase, C.G., 1981. Oceanic island Pb: Two-stage histories and mantle evolution. Earth Planet. Sci. Lett. 52, 277–284. https://doi.org/https://doi.org/10.1016/0012-821X(81)90182-5

Chauvel, C., Hofmann, A., Vidal, P., 1992. HIMU-EM: the French Polynesian connection. Earth Planet. Sci. Lett. 110, 99–119. https://doi.org/10.1016/0012-821X(92)90042-T
Cioni, R., D'Oriano, C., Bertagnini, A., 2008. Fingerprinting ash deposits of small scale eruptions by their physical and textural features. J. Volcanol. Geotherm. Res 177, 277–287. https://doi.org/https://doi.org/10.1016/j.jvolgeores.2008.06.003
Çoban, H., Flower, M., 2007. Late Pliocene lamproites from Bucak, Isparta (southwestern Turkey): Implications for mantle 'wedge' evolution during Africa-Anatolian plate convergence. J Asian Earth Sci 29, 160–176. https://doi.org/10.1016/j.jseaes.2006.06.006
Çoban, H., Flower, M.F.J., 2006. Mineral phase compositions in silica-undersaturated 'leucite' lamproites from the Bucak area, Isparta, SW Turkey. Lithos 89, 275–299. https://doi.org/https://doi.org/10.1016/j.lithos.2005.12.006
Comin-Chiaramonti P, Ruberti, E., Cundari, A., De Min, A., Gittins, J., Gomes, C., Gwalani, l., 2009 Genesis of Analcime and Nepheline-Potassium Feldspar-Kalsilite Intergrowths : A Review. Acta Vulcanol. 21 123-132.
Comin-Chiaramonti, P., Meriani, S., Mosca, R., Sinigoi, S., 1979. On the occurrence of analcime in the northeastern Azerbaijan volcanics (northwestern Iran). Lithos 12, 187–198. https://doi.org/https://doi.org/10.1016/0024-4937(79)90003-3
Condie, K.C., 2001. Mantle Plumes and their Record in Earth History. Cambridge University Press, Cambridge. https://doi.org/10.1017/CBO9780511810589
Conte, A.M., Perinelli, C., Bianchini, G., Natali, C., Martorelli, E., Chiocci, F.L., 2016. New insights on the petrology of submarine volcanics from the Western Pontine Archipelago (Tyrrhenian Sea, Italy). J. Volcanol. Geotherm. Res. 327. https://doi.org/10.1016/j.jvolgeores.2016.08.005
Conticelli, S., Peccerillo, A., 1992. Petrology and geochemistry of potassic and ultrapotassic volcanism in central Italy: petrogenesis and inferences on the evolution of the mantle sources. Lithos 28, 221–240. https://doi.org/https://doi.org/10.1016/0024-4937(92)90008-M
Conticelli, S., Francalanci, L., Manetti, P., Cioni, R., Sbrana, A., 1997. Petrology and geochemistry of the ultrapotassic rocks from the Sabatini Volcanic District, central Italy: the role of evolutionary processes in the genesis of variably enriched alkaline magmas. J Volcanol Geotherm Res 75, 107–136. https://doi.org/https://doi.org/10.1016/S0377-0273(96)00062-5
Conticelli, S., D'Antonio, M., Pinarelli, L., Civetta, L., 2002. Source contamination and mantle heterogeneity in the genesis of Italian potassic and ultrapotassic volcanic rocks: Sr–Nd–Pb isotope data from Roman Province and Southern Tuscany. Mineral. Petrol. 74, 189–222. https://doi.org/10.1007/s007100200004
Conticelli, S., Carlson, R., Widom, E., Serri, G., 2007. Chemical and isotopic composition (Os, Pb, Nd, and Sr) of Neogene to Quaternary calc-alkalic, shoshonitic, and ultrapotassic mafic rocks from the Italian peninsula: Inferences on the nature of their mantle sources. Spec Pap Geol Soc Am 418:171–202. https://doi.org/10.1130/2007.2418(09)
Conticelli, S., Marchionni, S., Rosa, D. Giordano, G., Boari, E., Avanzinelli, R., 2009a. Shoshonite and sub-alkaline magmas from an ultrapotassic volcano: Sr–Nd–Pb isotope data on the Roccamonfina volcanic rocks, Roman Magmatic Province, Southern Italy. Contrib. to Mineral. Petrol. 157, 41–63. https://doi.org/10.1007/s00410-008-0319-8
Conticelli, S., Guarnieri, L., Farinelli, A., Mattei, M., Avanzinelli, R., Bianchini, G., Boari, E., Tommasini, S., Tiepolo, M., Prelević, D., Venturelli, G., 2009b. Trace elements and Sr–Nd–Pb isotopes of K-rich, shoshonitic, and calc-alkaline magmatism of the Western Mediterranean Region: Genesis of ultrapotassic to calc-alkaline magmatic associations in a post-collisional geodynamic setting. Lithos 107, 68–92. https://doi.org/10.1016/j.lithos.2008.07.016Conticelli, S., Laurenzi, M., Giordano, G., Mattei, M., Avanzinelli, R., Melluso, L., Tommasini, S., Boari, E., Cifelli, F., Perini, G., 2010. Leucite-bearing (kamafugitic/leucititic) and -free (lamproitic) ultrapotassic rocks and associated shoshonites from Italy: Constraints on petrogenesis and geodynamics. J. Virtual Explor. 36. https://doi.org/10.3809/jvirtex.2010.00251
Conticelli, S., Avanzinelli, R., Marchionni, S., Tommasini, S., Melluso, L., 2011. Sr-Nd-Pb isotopes from the Radicofani Volcano, Central Italy: constraints on heterogeneities in a veined mantle responsible for the shift from ultrapotassic shoshonite to basaltic andesite magmas in a post-collisional setting. Mineral. Petrol. 103, 123–148. https://doi.org/10.1007/s00710-011-0161-y

Conticelli, S., Avanzinelli, R., Ammannati, E., Casalini, M., 2015. The role of carbon from recycled sediments in the origin of ultrapotassic igneous rocks in the Central Mediterranean. Lithos 232, 174–196. https://doi.org/https://doi.org/10.1016/j.lithos.2015.07.002
Dallai, L., Bianchini, G., Avanzinelli, R., Natali, C., Conticelli, S., 2019. Heavy oxygen recycled into the lithospheric mantle. Sci Rep 9, 8793. https://doi.org/10.1038/s41598-019-45031-3
Dallai, L., Bianchini, G., Avanzinelli, R., Deloule, E., Natali, C., Gaeta, M., Cavallo, A., Conticelli, S., 2022. Quartz-bearing rhyolitic melts in the Earth's mantle. Nat Commun 13, 7765. https://doi.org/10.1038/s41467-022-35382-3
Didon, J., Gemain, Y. M., 1976, Le Sabalan, Volcan Plio-quaternair de l"Azerbaidjan oriental (Iran); étude géologique et pétrographique de l"edifice et de son environnement régional. Thése de 3éme Cycle, Univ. Grenoble, 304 p.
Di Giuseppe, P., Agostini, S., Manetti, P., Savaşçın, M., Conticelli, S., 2018. Sub-lithospheric origin of Na-alkaline and calc-alkaline magmas in a post-collisional tectonic regime: Sr-Nd-Pb isotopes in recent monogenetic volcanism of Cappadocia, Central Turkey. Lithos 316–317, 304–322. https://doi.org/https://doi.org/10.1016/j.lithos.2018.07.018
Di Giuseppe, P., Agostini, S., Di Vincenzo, G., Manetti, P., Savaşçın, M., Conticelli, S., 2021. From subduction to strike slip-related volcanism: insights from Sr, Nd, and Pb isotopes and geochronology of lavas from Sivas–Malatya region, Central Eastern Anatolia. Int J Earth Sci 110, 849–874. https://doi.org/10.1007/s00531-021-01995-0
Dilek, Y., Altunkaynak, Ş., 2007. Cenozoic crustal evolution and mantle dynamics of post-collisional magmatism in western Anatolia. *Int. Geol. Rev. 49*, 431-453. https://doi.org/10.2747/0020-6814.49.5.431
Dilek, Y., Imamverdiyev, N., Altunkaynak, Ş., 2010. Geochemistry and tectonics of Cenozoic volcanism in the Lesser Caucasus (Azerbaijan) and the peri-Arabian region: collision-induced mantle dynamics and its magmatic fingerprint. Int. Geol. Rev. 52, 536–578. https://doi.org/10.1080/00206810903360422
Doglioni, C., Agostini, A., Crespi, M., Innocenti, F., Manetti P., Riguzzi, F., Savasci, Y., 2002. On the extension in western Anatolia and the Aegean sea. J. Virtual Explor. 8. https://doi.org/doi:10.3809/jvirtex.2002.00049
Ellam, R.M., Menzies, M.A., Hawkesworth, C.J., Leeman, W., Rosi, M., Serri, G., 1988. The transition from calc-alkaline to potassic orogenic magmatism in the Aeolian Islands, Southern Italy. Bull. Volcanol. 50, 386–398. https://doi.org/10.1007/BF01050638
Elliott, T., 2003. Tracers of the Slab. Inside the subduction factory, Geophys. Monogr. Ser. https://doi.org/doi:10.1029/138GM03
Elliott, T., Plank, T., Zindler, A., White, W., Bourdon, B., 1997. Element transport from slab to volcanic front at the Mariana arc. J. Geophys. Res. 102, 14,991-15,019. https://doi.org/10.1029/97JB00788
Eyuboglu, Y., 2010. Late Cretaceous high-K volcanism in the eastern Pontide orogenic belt: implications for the geodynamic evolution of NE Turkey. Int. Geol. Rev. 52, 142–186. https://doi.org/10.1080/00206810902757164
Eyuboglu, Y., Chung, S.-L., Santosh, M., Dudas, F., Akaryalı, E., 2011. Transition from shoshonitic to adakitic magmatism in the eastern Pontides, NE Turkey: Implications for slab window melting. Gondwana Res, 19, 413–429. https://doi.org/10.1016/j.gr.2010.07.006
Foley, S., 1992. Vein-plus-wall-rock melting mechanisms in the lithosphere and the origin of potassic alkaline magmas. Lithos 28, 435–453. https://doi.org/10.1016/0024-4937(92)90018-T
Foley, S.F., Venturelli, G., Green, D.H., Toscani, L. 1987. The ultrapotassic rocks: Characteristics, classification, and constraints for petrogenetic models. Earth-Science Rev. 24, 81–134. https://doi.org/https://doi.org/10.1016/0012-8252(87)90001-8
Francalanci, L., Innocenti, F., Manetti, P., Savasçin, M.Y., 2000. Neogene alkaline volcanism of the Afyon-Isparta area, Turkey: petrogenesis and geodynamic implications. Mineral Petrol 70, 285–312. https://doi.org/10.1007/s007100070007
Freda, C., Gaeta, M., Palladino, D.M., Trigila, R., 1997. The Villa Senni Eruption (Alban Hills, central Italy): the role of H2O and CO2 on the magma chamber evolution and on the eruptive scenario. J Volcanol Geotherm Res 78, 103–120. https://doi.org/https://doi.org/10.1016/S0377-0273(97)00007-3
Frezzotti, M.L., Peccerillo, A.,, Panza G., 2009. Carbonate metasomatism and CO2 lithosphere–asthenosphere degassing beneath the Western Mediterranean: An integrated model arising from petrological and

geophysical data. Chem. Geol. 262, 108–120. https://doi.org/https://doi.org/10.1016/j.chemgeo.2009.02.015

Gaeta, M., Fabrizio, G., Cavarretta, G., 2000. F-phlogopites in the Alban Hills Volcanic District (Central Italy): indications regarding the role of volatiles in magmatic crystallisation. J. Volcanol. Geoth. Res. 99, 179–193. https://doi.org/10.1016/ S0377-0273(00)00172-4

Grosjean, M., Moritz, R., Rezeau, H., Hovakimyan, S., Ulianov, A., Chiaradia, M., Melkonyan, R., 2022, Arabia-Eurasia convergence and collision control on Cenozoic juvenile K-rich magmatism in the South Armenian block, Lesser Caucasus. Earth-Sci. Rev. 226, 103949. https://doi.org/10.1016/j.earscirev.2022.103949.

Gülmez, F., Genç, Ş.C., Prelević, D., Tüysüz, O., Karacik, Z., Roden, M., Billor, Z., 2016. Ultrapotassic Volcanism from the Waning Stage of the Neotethyan Subduction: a Key Study from the Izmir–Ankara–Erzincan Suture Belt, Central Northern Turkey. J Petrol 57, 561–593. https://doi.org/10.1093/petrology/egw02

Heinonen, J.S., Bohrson, W.A., Spera, F.J., Brown, G.A., Scruggs, M., Adams, J., 2020. Diagnosing open-system magmatic processes using the Magma Chamber Simulator (MCS): part II—trace elements and isotopes. Contrib. to Mineral. Petrol. 175, 105. https://doi.org/10.1007/s00410-020-01718 -9

Hart, S.R., 1984. A large-scale isotope anomaly in the Southern Hemisphere mantle. Nature 309, 753–757. https://doi.org/10.1038/309753a0

Hart, S.R., 1988. Heterogeneous mantle domains: signatures, genesis and mixing chronologies. Earth Planet. Sci. Lett. 90, 273–296. https://doi.org/https://doi.org/10.1016/0012-821X(88)90131-8

Hastie, A., Kerr, A., Pearce, J., Mitchell, S., 2007. Classification of Altered Volcanic Island Arc Rocks using Immobile Trace Elements: Development of the Th Co Discrimination Diagram. J. Petrol. 48, 2341–2357. https://doi.org/10.1093/petrology/egm062

Hauff, F., Hoernle, K., Schmidt, A., 2003. Sr-Nd-Pb composition of Mesozoic Pacific oceanic crust (Site 1149 and 801, ODP Leg 185): Implications for alteration of ocean crust and the input into the Izu-Bonin-Mariana subduction system. Geochemistry, Geophys. Geosystems 4. https://doi.org/10.1029/2002GC000421

Hofmann, A.W., White, W.M., 1982. Mantle plumes from ancient oceanic crust. Earth Planet. Sci. Lett. 57, 421–436. https://doi.org/10.1016/0012-821X(82)90161-3

Innocenti, F., Agostini, S., Di Vincenzo, G., Doglioni, C., Manetti, P., Savaşçin, M., Tonarini, S., 2005. Neogene and Quaternary volcanism in Western Anatolia: Magma sources and geodynamic evolution. Mar Geol 221, 397–421. https://doi.org/https://doi.org/10.1016/j.margeo.2005.03.016

Le Maitre, R.W.L., Streckeisen, A., Zanettin, B., Bas, M.J.L., Bonin, B., Bateman, P., 2002. Igneous Rocks: A Classification and Glossary of Terms: Recommendations of the International Union of Geological Sciences Subcommission on the Systematics of Igneous Rocks. Cambridge University Press.

Li, H., Hermann, J., Zhang, L., 2022. Melting of subducted slab dictates trace element recycling in global arcs. Sci Adv 8:eabh2166. https://doi.org/10.1126/sciadv.abh2166

Lloyd, F.E., Arima, M., Edgar, A.D., 1985. Partial melting of a phlogopite-clinopyroxenite nodule from south-west Uganda: an experimental study bearing on the origin of highly potassic continental rift volcanics. Contrib. to Mineral. Petrol. 91, 321–329. https://doi.org/10.1007/BF00374688

Luhr, J.F. and Kyser, T.K., 1989. Primary igneous analcime: The Colima minettes. *Am. Mineral*. **74**, 216-223.

Lustrino, M., Wilson, M., 2007. The circum-Mediterranean anorogenic Cenozoic igneous province. Earth-Science Rev 81:1–65. https://doi.org/https://doi.org/10.1016/j.earscirev.2006.09.002

Lustrino, M., Fedele, L., Agostini, S., Prelević, D., Salari, G., 2019. Leucitites within and around the Mediterranean area. Lithos 324-325, 216-233. https://doi.org/10.1016/j.lithos.2018.11.007.

McQuarrie, N. and van Hinsbergen, D.J., 2013. Retrodeforming the Arabia-Eurasia collision zone: Age of collision versus magnitude of continental subduction. Geology, 41, 315-318. https://doi.org/10.1130/G33591.1

Mattioli, M., Lustrino, M., Ronca, S., Bianchini, G., 2012. Alpine subduction imprint in Apennine volcaniclastic rocks. Geochemical–petrographic constraints and geodynamic implications from Early Oligocene Aveto-Petrignacola Formation (N Italy). Lithos 134–135, 201–220. https://doi.org/https://doi.org/10.1016/j.lithos.2011.12.017

McCulloch, M.T., Gamble, J.A., 1991. Geochemical and geodynamical constraints on subduction zone magmatism. Earth Planet. Sci. Lett. 102, 358–374. https://doi.org/10.1016/0012-821X(91)90029-H

Mitchell, R.H., 1995. Melting Experiments on a Sanidine Phlogopite Lamproite at 4–7 GPa and their Bearing on the Sources of Lamproitic Magmas. J. Petrol. 36, 1455–1474. https://doi.org/10.1093/petrology/36.5.1455

Moayyed, M., Moazzen, M., Calagari, A., Jahangiri, A., Modjarrad, M., 2008. Geochemistry and petrogenesis of lamprophyric dykes and the associated rocks from Eslamy peninsula, NW Iran: Implications for deep-mantle metasomatism. Chemie der Erde - Geochemistry 68, 141–154. https://doi.org/10.1016/j.chemer.2006.04.002

Nagarajan, R., Madhavaraju, J., Armstrong-Altrin, J.S., Nagendra, R., 2011. Geochemistry of Neoproterozoic limestones of the Shahabad Formation, Bhima Basin, Karnataka, southern India. Geosci. J. 15, 9–25. https://doi.org/10.1007/s12303-011-0005-0

Nakamura, Y., Tatsumoto, M., 1988. Pb, Nd, and Sr isotopic evidence for a multicomponent source for rocks of Cook-Austral Islands and heterogeneities of mantle plumes. Geochim. Cosmochim. Acta 52, 2909–2924. https://doi.org/https://doi.org/10.1016/0016-7037(88)90157-3

Nath, B. N., Roelandts, I., Sudhakar, M., & Plüger, W.L., 1992. Rare earth element patterns of the Central Indian Basin sediments related to their lithology. *Geophys. Res. Lett. 19*, 1197-1200. https://doi.org/10.1029/92GL01243

Nobre Silva, I. G., Weis, D., and Scoates, J. S., 2010. Effects of acid leaching on the Sr-Nd-Hf isotopic compositions of ocean island basalts, *Geochem. Geophys. Geosyst.*, 11, Q09011, https://doi.org/10.1029/2010GC003176.

Palacz, Z.A., Saunder, A.D., 1986. Coupled trace element and isotope enrichment in the Cook-Austral-Samoa Islands, Southwest Pacific. Earth Planet. Sci. Lett. 79, 270–280. https://doi.org/https://doi.org/10.1016/0012-821X(86)90185-8

Pearce, J., 1982. Trace Element Characteristics of Lavas from Destructive Plate Boundaries, in: Orogenic Andesites. pp. 525–548.

Peccerillo, A., 2001. Geochemical similarities between the Vesuvius, Phlegraean Fields and Stromboli Volcanoes: petrogenetic, geodynamic and volcanological implications. Mineral. Petrol. 73, 93–105. https://doi.org/10.1007/s007100170012

Peccerillo, A., 2005. Plio-Quaternary Volcanism in Italy. Springer Berlin, Heidelberg. 365 pp. https://doi.org/10.1007/3-540-29092-3

Peccerillo, A., Taylor, S.R., 1976. Geochemistry of Eocene calc-alkaline volcanic rocks from the Kastamonu area, Northern Turkey. Contrib. to Mineral. Petrol. 58, 63–81. https://doi.org/10.1007/BF00384745

Peccerillo, A., Poli, G,. Serri, G., 1988. Petrogenesis of orenditic and kamafugitic rocks from central Italy. Can Mineral 26, 45–65.

Plank, T., Langmuir, C.H., 1998. The chemical composition of subducting sediment and its consequences for the crust and mantle. Chem. Geol. 145, 325–394. https://doi.org/https://doi.org/10.1016/S0009-2541(97)00150-2.

Prelević, D., Foley, S.F., 2007. Accretion of arc-oceanic lithospheric mantle in the Mediterranean: Evidence from extremely high-Mg olivines and Cr-rich spinel inclusions in lamproites. Earth Planet Sci Lett 256, 120–135. https://doi.org/https://doi.org/10.1016/j.epsl.2007.01.018

Prelević, D., Foley, S., Cvetković, V., Romer, R., 2004. The analcime problem and its impact on the geochemistry of ultrapotassic rocks from Serbia. Mineral. Mag. - Min. MAG 68, 633–648. https://doi.org/10.1180/0026461046840209

Prelević, D., Foley, S., Romer, R., Cvetkovic, V., Downes, H., 2005. Tertiary Ultrapotassic Volcanism in Serbia: Constraints on Petrogenesis and Mantle Source Characteristics. J Petrol. 46, 1443–1487. https://doi.org/10.1093/petrology/egi022

Prelević, D., Foley, S.F., Romer, R., Conticelli, S., 2008 Mediterranean Tertiary lamproites derived from multiple source components in postcollisional geodynamics. Geochim. Cosmochim. Acta 72, 2125–2156. https://doi.org/https://doi.org/10.1016/j.gca.2008.01.029

Prelević, D., Akal, C., Romer, R., Foley, S., 2010 Lamproites as indicators of accretion and/or shallow subduction in the assembly of south-western Anatolia, Turkey. Terra Nov 22:443–452. https://doi.org/10.1111/j.1365-3121.2010.00963.x

Prelević, D., Akal, C., Foley, S.F., Stracke, A., Van Den Bogaard, P., 2012. Ultrapotassic Mafic Rocks as Geochemical Proxies for Post-collisional Dynamics of Orogenic Lithospheric Mantle: the Case of Southwestern Anatolia, Turkey. J Petrol 53, 1019–1055. https://doi.org/10.1093/petrology/egs008

Prelević, D., Akal, C., Romer, R.L., Mertz-Kraus, R., Helvacı, C., 2015. Magmatic Response to Slab Tearing: Constraints from the Afyon Alkaline Volcanic Complex, Western Turkey. J Petrol 56, 527–562. https://doi.org/10.1093/petrology/egv008

Rabiee, A., Rossetti, F., Tecce, F., Asahara, Y., Azizi, H., Glodny, J., Lucci, F., Nozaem, R., Opitz, J., Selby, D., 2019. Multiphase magma intrusion, ore-enhancement and hydrothermal carbonatisation in the Siah-Kamar porphyry Mo deposit, Urumieh-Dokhtar magmatic zone, NW Iran. Ore Geol. Rev. 110, 102930. https://doi.org/https://doi.org/10.1016/j.oregeorev.2019.05.016

Rustioni, G., Audetat, A., Keppler, H., 2021. The composition of subduction zone fluids and the origin of the trace element enrichment in arc magmas. Contrib. to Mineral. Petrol. 176, 51. https://doi.org/10.1007/s00410-021-01810-8

Saccani, E., Allahyari, K., Beccaluva, L., Bianchini, G., 2013. Geochemistry and petrology of the Kermanshah ophiolites (Iran): Implication for the interaction between passive rifting, oceanic accretion, and OIB-type components in the Southern Neo-Tethys Ocean. Gondwana Res. 24, 392–411. https://doi.org/https://doi.org/10.1016/j.gr.2012.10.009

Saccani, E., 2015. A new method of discriminating different types of post-Archean ophiolitic basalts and their tectonic significance using Th-Nb and Ce-Dy-Yb systematics. Geosci. Front. 6, 481–501. https://doi.org/https://doi.org/10.1016/j.gsf.2014.03.006

Sengor, A.M.C., Yilmaz, Y., 1981. Tethyan evolution of Turkey: A plate tectonic approach. Tectonophysics 75, 181–190. https://doi.org/10.1016/0040-1951(81)90275-4

Shafaii Moghadam, H., Ghorbani, G., Khedr, M., Fazlnia, N., Chiaradia, M., Eyuboglu, Y., Santosh, M., Galindo, C., López-Martínez, M., Gourgaud, A., Arai, S., 2014a. Late Miocene K-rich volcanism in the Eslamieh Peninsula (Saray), NW Iran: Implications for geodynamic evolution of the Turkish–Iranian High Plateau. Gondwana Res. 26, 1028–1050. https://doi.org/10.1016/j.gr.2013.09.015

Shafaii Moghadam, H., Zaki Khedr, M., Chiaradia, M., Stern, R.J., Bakhshizad, F., Arai, S., Ottley, C.J., Tamura, A., 2014b. Supra-subduction zone magmatism of the Neyriz ophiolite, Iran: constraints from geochemistry and Sr-Nd-Pb isotopes. Int. Geol. Rev. 56, 1395–1412. https://doi.org/10.1080/00206814.2014.942391

Shafaii Moghadam, H., Griffin, W.L., Kirchenbaur, M., Garbe-Schönberg, D., Khedr, M.Z., Kimura, J.I., Stern, R.J., Ghorbani, G., Murphy, R., O'Reilly, S.Y., Arai, S., Maghdour-Mashhour, R., 2018. Roll-back, extension and mantle upwelling triggered eocene potassic magmatism in NW Iran. J. Petrol. 59, 1417–1465. https://doi.org/10.1093/petrology/egy067

Shaw, D., 1970. Trace element fractionation during anatexis. Geochim. Cosmochim. Acta 34, 237–243. https://doi.org/10.1016/0016-7037(70)90009-8

Skora, S., Blundy, J.D., Brooker, R.A., Green, E.C.R., de Hoog, J.C.M., Connolly, J.A.D., 2015. Hydrous Phase Relations and Trace Element Partitioning Behaviour in Calcareous Sediments at Subduction-Zone Conditions. J. Petrol. 56, 953–980. https://doi.org/10.1093/petrology/egv024

Soltanmohammadi, A., Grégoire, M., Ceuleneer, G., Benoit, M., Bédard, L., Gouy, S., Rabinowicz, M., 2021. Origin of Antecrysts in Igneous Rocks from the Salavat Range (NW Iran): an Explanation for the Geochemical Signature of Potassic Alkaline Rocks. J Petrol 62, egab031. https://doi.org/10.1093/petrology/egab031

Soltanmohammadi, A., Grégoire1, M., Rabinowicz, M., Gerbault, M., Ceuleneer, G., Rahgoshay, M., Bystricky, M., Benoit, M., 2018. Transport of volatile-rich melt from the mantle transition zone via compaction pockets: Implications for mantle metasomatism and the origin of Alkaline Lavas in the Turkish-Iranian plateau. J. Petrol. 59, 2273–2310. https://doi.org/10.1093/petrology/egy097

Stampfli, G.M., 2000. Tethyan oceans. Geol. Soc. London, Spec. Publ. 173, 1 LP – 23. https://doi.org/10.1144/GSL.SP.2000.173.01.01

Stolz, A.J., Jochum, K.P., Spettel, B., Hofmann, A.W., 1996. Fluid- and melt-related enrichment in the subarc mantle: Evidence from Nb/Ta variations in island-arc basalts. Geology 24, 587–590. https://doi.org/10.1130/0091-7613(1996)024

Tatsumi, Y., Hamilton, D.L., Nesbitt, R.W., 1986. Chemical characteristics of fluid phase released from a subducted lithosphere and origin of arc magmas: Evidence from high-pressure experiments and natural

rocks. J. Volcanol. Geotherm. Res. 29, 293–309. https://doi.org/https://doi.org/10.1016/0377-0273(86)90049-1
Thomsen, T.B., Schmidt, M.W., 2008. Melting of carbonated pelites at 2.5–5.0 GPa, silicate–carbonatite liquid immiscibility, and potassium–carbon metasomatism of the mantle. Earth Planet. Sci. Lett. 267, 17–31. https://doi.org/https://doi.org/10.1016/j.epsl.2007.11.027
Todt, W., Cliff, R.A., Hanser, A., Hofmann, A.W., 1996. Evaluation of a 202Pb–205Pb Double Spike for High - Precision Lead Isotope Analysis.*, in: Earth Processes: Reading the Isotopic Code, Geophysical Monograph Series. pp. 429–437. https://doi.org/https://doi.org/10.1029/GM095p0429
Tommasini, S., Avanzinelli, R., Conticelli, S., 2011. The Th/La and Sm/La conundrum of the Tethyan realm lamproites. Earth Planet Sci Lett 301:469–478. https://doi.org/10.1016/j.epsl.2010.11.023
Tüysüz, O., 1996. Geology of Amasya and surroundings. In: 11th Pteroleum Congress of Turkey, Proceedings Ankara, pp. 32–48.
Verdel, C., Wernicke, B. P., Hassanzadeh, J., Guest, B., 2011. A Paleogene extensional arc flare-up in Iran. *Tectonics* 30, TC3008. https://doi.org/10.1029/2010TC002809
Weaver, B.L., 1991. Trace element evidence for the origin of ocean-island basalts. Geol. 19, 123EP – 123. https://doi.org/10.1130/0091-7613(1991)019<0123:TEEFTO>2.3.CO;2
Wilson, M., Bianchini, G., 1999. Tertiary-Quaternary magmatism within the Mediterranean and surrounding regions. Geol. Soc. London, Spec. Publ. 156, 141 LP – 168. https://doi.org/10.1144/GSL.SP.1999.156.01.09
Woodhead, J., Eggins, S., Gamble, J., 1993. High field strength and transition element systematics in island arc and back-arc basin basalts: Evidence for multi-phase melt extraction and a depleted mantle wedge. Earth Planet. Sci. Lett. 114, 491–504. https://doi.org/https://doi.org/10.1016/0012-821X(93)90078-N
Zanchetta, S., Berra, F., Zanchi, A., Bergomi, M., Caridroit, M., Nicora, M., Heidarzadeh, G., 2013. The record of the Late Palaeozoic active margin of the Palaeotethys in NE Iran: Constraints on the Cimmerian orogeny. Gondwana Res. 24, 1237–1266. https://doi.org/10.1016/j.gr.2013.02.013
Zindler, A., Hart, S., 1986. Chemical Geodynamics. Annu. Rev. Earth Planet. Sci. 14, 493. https://doi.org/10.1146/annurev.ea.14.050186.002425

Table captions:

Table 1 – Bulk rock major and trace elements composition of Eocene Arasbaran igneous rocks obtained by x-ray fluorescence (XRF). Rock type (Lc-bearing and Lc-free), classification, sampling locality and geographical coordinates are also reported. Lc = leucite; Bas. Tr-And.= Basaltic Trachy-Andesite, Tr-And. = Trachy-Andesite; Ph-Trachyte = Phonolitic Trachyte.

Table 2 – Bulk rock trace (incompatible and REE) elements composition of representative Eocene Arasbaran igneous rocks obtained by inductively coupled plasma mass spectrometry (ICP-MS). Sample characteristics and abbreviations as in Table 1.

Table 3 – Sr, Nd and Pb isotope composition of selected Arasbaran igneous rocks. Both measured and initial values are reported. Sample characteristics and abbreviations as in Table 1.

Figure Captions:

Figure 1 – (a) Location of the study area and present distribution of Eocene magmatic rocks across

southwest Asia (modified from Allen and Armstrong, 2008); (b) Sampling locations of leucite-bearing (Majid Abad, Quarah Su, Moshiran - red symbols) and leucite-free (south Moshiran, Marallu, Tullun, Moradlu - blue symbols) igneous rocks from the Arasbaran area (NW Iran). The geological features are taken from the Geological map 1:100,000 published by Geological Survey of Iran (GSI).

Figure 2 – Petrographic features of leucite-bearing rocks from the WNW part of the Arasbaran area (NW Iran). Lavas from Majid Abad section are characterized by porphyritic to megaporhyritic analcimized leucite (a) and by plagioclase and clinopyroxene phenocrysts in a microcrystalline groundmass (b). Pillow lavas from Quarah Su outcrop show altered plagioclase phenocrysts in a microcrystalline to glassy groundmass (c), whereas columnar jointing lavas contain large clinopyroxene phenocrysts surrounded by abundant foids (d). Lavas from Moshiran show petrographic similarities with those from Majid Abad, and are characterized by leucite (deeply analcimized) crystals up to centrimetric in size (e), and the presence of abundant plagioclase phenocrysts (f). Pictures b, d, e, f are taken by optical microscopy in plane polarized light, picture c in crossed polarized light.

Figure 3 – Petrographic features and leucite-free rocks from the ESE part of the Arasbaran area (NW Iran). Lavas from Marallu outcrop show abundant glomeroporhyritic textures with clinopyroxene phenocrysts, often containing glass (a), and by sieve textured plagioclase and clinopyroxene in biotite-rich matrix (b). Samples from South Moshiran and Tullun outcrops share the same petrographic features, characterized by the presence of olivine, clinopyroxene and plagioclase phenocrysts in a microcrystalline (c) to glassy (d) matrix. Dikes from Moradlu are characterized by mafic to felsic compositions, with the former showing variously iddingsitised olivine, plagioclase and clinopyroxene phenocrysts in a fine-grained olocrystalline matrix composed of the same mineral paragenesis (e), and the latter by the presence of big alkali-feldspars and biotite phenocrysts (f). Pictures b, d, e, f are taken by optical microscopy in plane polarized light, picture c in crossed polarized light.

Figure 4 – (a) TAS (Le Maitre et al., 2002) and (b) K_2O *vs* SiO_2 (Peccerillo and Taylor, 1976) classification diagrams of leucite-bearing and leucite-free igneous rocks from Arasbaran area (NW Iran). B = basalt, BA = basaltic andesite , A= andesite, D = dacite, K-Tr-B = potassic trachybasalt, S = shoshonite, L = latite, Tr = trachyte, Bs/T = basanite/tephrite, Ph-T = phonolitic tephrite, T-Ph = tephritic phonolite, Ph = phonolite, CA = calcalkaline series, HK-CA = high-K calcalkaline series, SHO = shoshonite series.

Figure 5 – Δq *vs* K_2O (Peccerillo and Manetti, 1985) diagrams showing the different SiO_2-saturation conditions of leucite-bearing and leucite-free igneous rocks from Arasbaran area (NW Iran). Symbols as in figure 4.

Figure 6 – Major element versus MgO (wt%) bivariate diagrams of leucite-bearing and leucite-free igneous rocks from Arasbaran area (NW Iran). Symbols as in figure 4.

Figure 7 – Primordial Mantle **(**PM)-normalized incompatible element patterns of leucite-bearing (a) and leucite-free (b) igneous rocks from Arasbaran area (NW Iran). The distribution of nearly coeval leucite-bearing (c) and leucite-free (d) rocks from NW Iran (Lahrud – Shafaii Moghadam et al., 2018; Moghan – Amraee et al., 2019) and from Eastern Pontides (Altherr et al., 2008; Eyuboglu et al., 2011) are also reported for comparison. Symbols as in figure 4.

Figure 8 – Trace element discrimination diagrams for leucite-bearing and leucite-free igneous rocks from Arasbaran area (NW Iran). a) Ce/Yb *vs* Ta/Yb (Pearce, 1982), b) Th *vs* Co (Hastie et al., 2007) for altered rocks and c) N-MORB normalized Th *vs* Nb (Saccani, 2015).

Figure 9 – Initial Sr-Nd isotope ratios of leucite-bearing and leucite-free igneous rocks from Arasbaran area (NW Iran). The distribution of nearly coeval leucite-bearing and leucite-free rocks from NW Iran (Lahrud – Shafaii Moghadam et al., 2018; Moghan – Amraee et al., 2019) and from Eastern Pontides (Altherr et al., 2008; Eyuboglu et al., 2011) are also reported for comparison. S1 is the composition of the mantle wedge (MW; Sr = 22 ppm, $^{87}Sr/^{86}Sr$ = 0.70298, Nd = 0.3 ppm, $^{143}Nd/^{144}Nd$ = 0.51299) after the first metasomatic events obtained by the addition of 6% of slab partial melts (Sr = 630 ppm, $^{87}Sr/^{86}Sr$ = 0.70393, Nd = 3.0 ppm, $^{143}Nd/^{144}Nd$ = 0.51273) of Zagros Neotethyan MORB ophiolites as AOC (Saccani et al., 2013; Shafaii Moghadam et al., 2014b). The blue and red mixing lines represents the second metasomatic events characterized by the addition of low-carbonate (LC) and high-carbonate (HC) sediment melts to the S1 mantle source, respectively. The composition of AOC partial melts and those of HC (Apennine marl SD48 – Avanzinelli et al., 2018; Sr = 519 ppm, $^{87}Sr/^{86}Sr$ = 0.70822, Nd = 2.8 ppm, $^{143}Nd/^{144}Nd$ = 0.512163) and LC (Apennine marl SD11 – Avanzinelli et al., 2018; Sr = 355 ppm, $^{87}Sr/^{86}Sr$ = 0.71121, Nd = 22 ppm, $^{143}Nd/^{144}Nd$ = 0.51234) sediments partial melts were obtained using bulk/melt ratios from the experimental work of Carter et al., 2015 (AOC) and Skora et al., 2015 (HC and LC) at temperatures between 900 and 1000 °C. Dashed lines represents tie lines linking the same proportions of HC and LC sediment melt component. Symbols as in figure 4.

Figure 10 – a) Initial Pb isotope ratios ($^{207}Pb/^{204}Pb$ *vs* $^{206}Pb/^{204}Pb$) and b) Ba/La *vs* $^{143}Nd/^{144}Nd$ of leucite-bearing and leucite-free igneous rocks from Arasbaran area (NW Iran). The distribution of nearly

coeval leucite-bearing and leucite-free rocks from NW Iran (Lahrud – Shafaii Moghadam et al., 2018; Moghan – Amraee et al., 2019) and from Eastern Pontides (Altherr et al., 2008; Eyuboglu et al., 2011) are also reported for comparison. Grey and white solid lines represent the mixing trends between the average of subducted oceanic crust, represented by Neyriz (Shafaii Moghadam et al., 2014b) and Kermanshash (Saccani et al., 2013) Neotethyan ophiolites (Ba/La = 5-10, $^{143}Nd/^{144}Nd$ = 0.51277-0.51299), a high-carbonate (HC) sediment (Apennine marl SD48 – Avanzinelli et al., 2015; Ba/La = 230, $^{143}Nd/^{144}Nd$ = 0.512163) and a low-carbonate sediment (Mariana pelagic clay 801- Plank and Langmuir, 1998; Ba/La = 4.4, $^{143}Nd/^{144}Nd$ = 0.512134) partial melts. Bulk/melt ratios are taken from the experimental work of Skora et al., 2015 for HC and LC sediments at temperatures of 850-900°C. The Northern Hemisphere Reference Line (NHRL) is from Hart (1984). Symbols as in figure 4.

Figure 11 – Ba/Th vs. $^{87}Sr/^{86}Sr_{(i)}$ (a) and vs. $(La/Sm)_N$ (b) showing the distribution of leucite-bearing and -free lavas from the Arasbaran area. The composition of worldwide arc magmas, as well as the fields of Mariana arc (representative of AOC predominant fluid metasomatism) and of Neapolitan district of the Roman province (Vesuvius, representative of predominant carbonate melt metasomatism) are shown for comparison. Data from Elliot et al., 1997 and Avanzinelli et al., 2008.

Figure 12 – Non-modal partial melting model for the leucite-bearing (a) and -free (b) Arasbaran magmas. The red field represents the compositional variation of magmas produced by S2 and S3 mantle sources metasomatised by sediment partial melts produced at 900-1000°C (Skora et al.,. 2015). Partition coefficient from the GERM database (https://kdd.earthref.org/KdD) and from LaTourrette et al. (1995). End-member lithologies and compositions as in Fig. 9. See text for further details.

Figure 13 – Δq *vs* age (Ma) distribution of leucite-bearing and leucite-free igneous rocks from Arasbaran area (NW Iran). Age analytical errors (Table 3) are expressed by error bars.

Figure 14 – Geodynamic sketch depicting the generation of the leucite-bearing and leucite-free magmas in the Arasbaran area (Ardabil Province, NW Iran). During late Cretaceous the subducting Neo-tethyan plate brought first at the depth of melting (around 3 GPa, Shafai Moghadam et al., 2018) LC-sediment (a), which were followed by the late arrival of HC-sediments at similar melting conditions (e.g., Skora et al., 2015) due to slab verticalization and retreat at a more mature stage of subduction (e.g., Conticelli et al., 2015), with the creation of two distinct metasomatic domains (S3 and S2) in the mantle wedge (b). In the Eocene, slab roll-back and retreat recalling

asthenospheric up-welling and heat flow to the overlying mantle wedge. Melting of the mantle metasomatised domains that produced the Arasbaran volcanism started from and was more effective on mantle domains at a higher distance from the colder subducting plate, i.e., from the S3 source, progressively involving sectors of mantle wedge located closer to the Neothetyan slab that suffered a lower thermal perturbation (c).

Supplementary Table captions:

Supplementary Table 1 – Method accuracy and reproducibility for Sr-Nd (TIMS) and Pb (MC-ICP-MS) measurements.

Supplementary figure captions:

Supplementary Figure 1 – Representative field photographs of 6 sampling localities of the Eocene Arasbaran igneous rocks: a) *Majid Abad*, b) *south Moshiran,* c) *Gheshlagh,* d) *Moradlu,* e) *Moshiran,* f) *Marallu,.*

Supplementary Figure 2 – Major element variation over MgO (wt%) and fractional crystallization trends for leucite-bearing (FC1) and -free (FC2) Arasbaran rocks modelled by MCS software (Bohrson et al., 2020). Symbols as in Fig. 4. * = corrected compositions for the most mafic and potassic leucite-bearing sample (M31, M36, M39) See text for further details on modelling.

Supplementary Figure 3 – Classification diagrams for ultrapotassic rocks (after Foley, 1987) showing the least differentiated leucite-bearing samples (yellow symbols) together with their corrected composition for clinopyroxene accumulation and analcime substitution over leucite (red symbols). The composition of ultrapotassic rocks from the Roman province (squares) and the fields of those from the Neapolitan district (dashed) and Anatolian plagioleucitites (dark gray) are also reported for comparison (data from Conticelli et al., 2015 and Altherr et al., 2008).

Figure 1 Click here to access/download;Figure;Fig 1_2ab_2023_mod.pdf

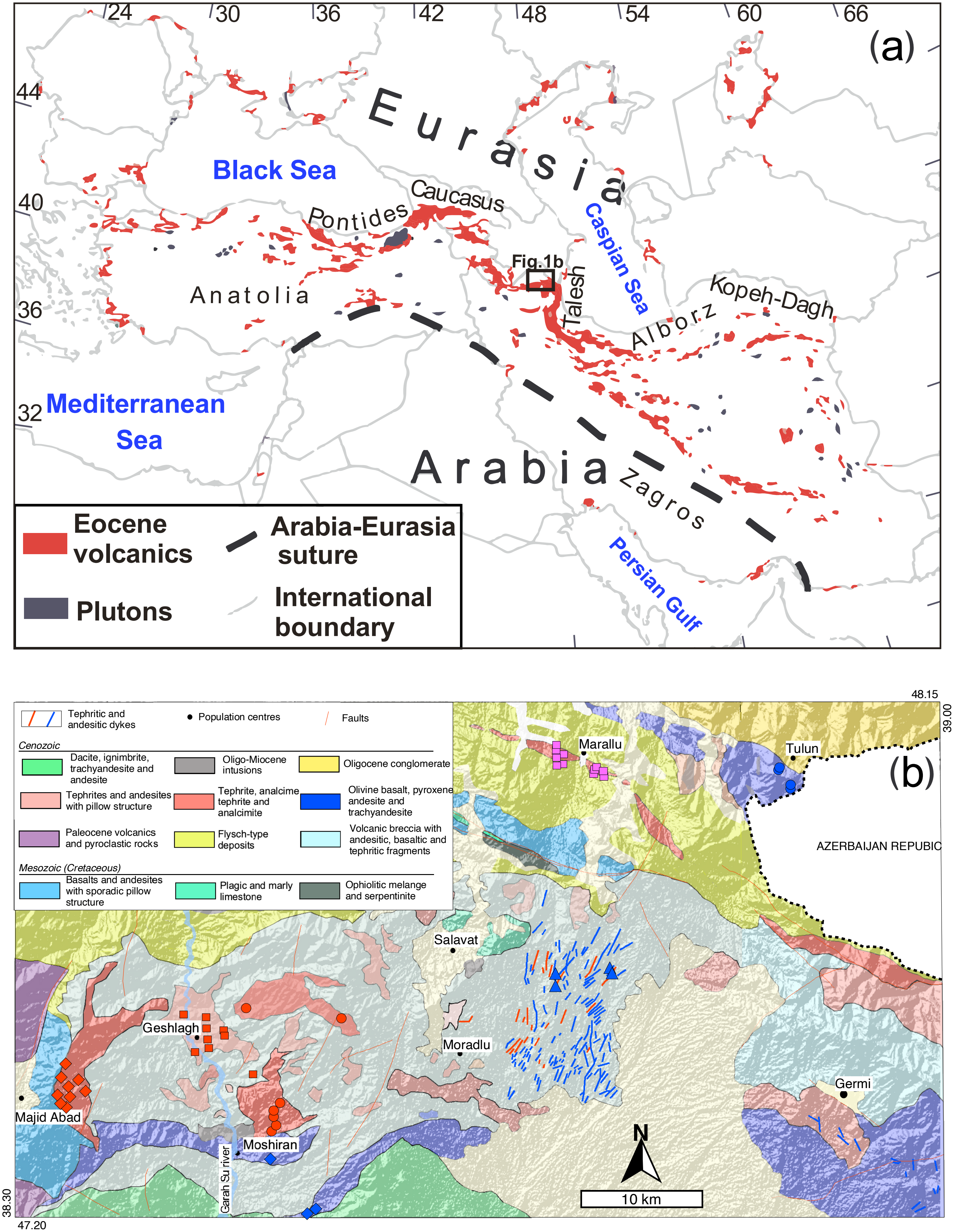

Figure 2

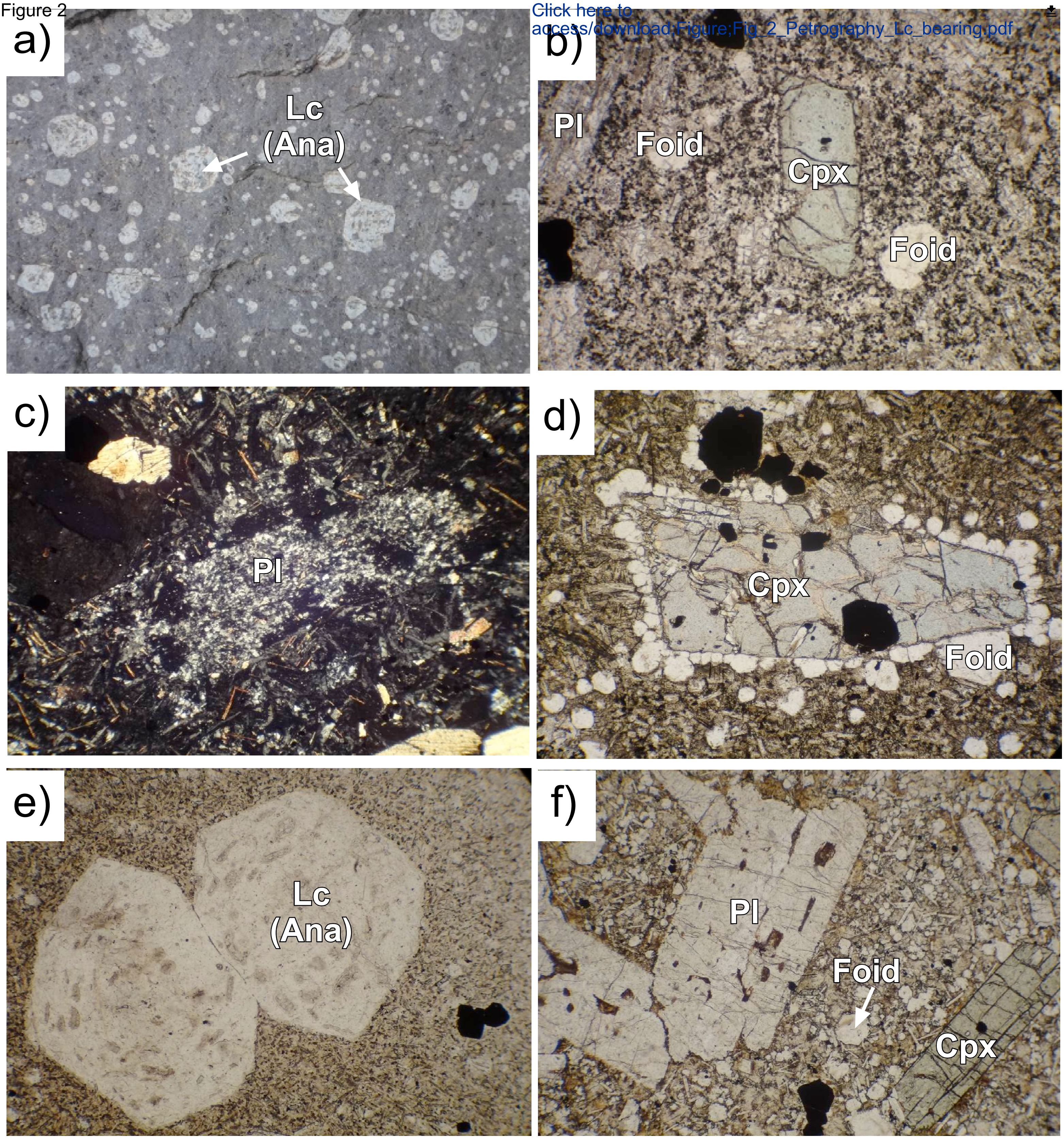

Figure 3

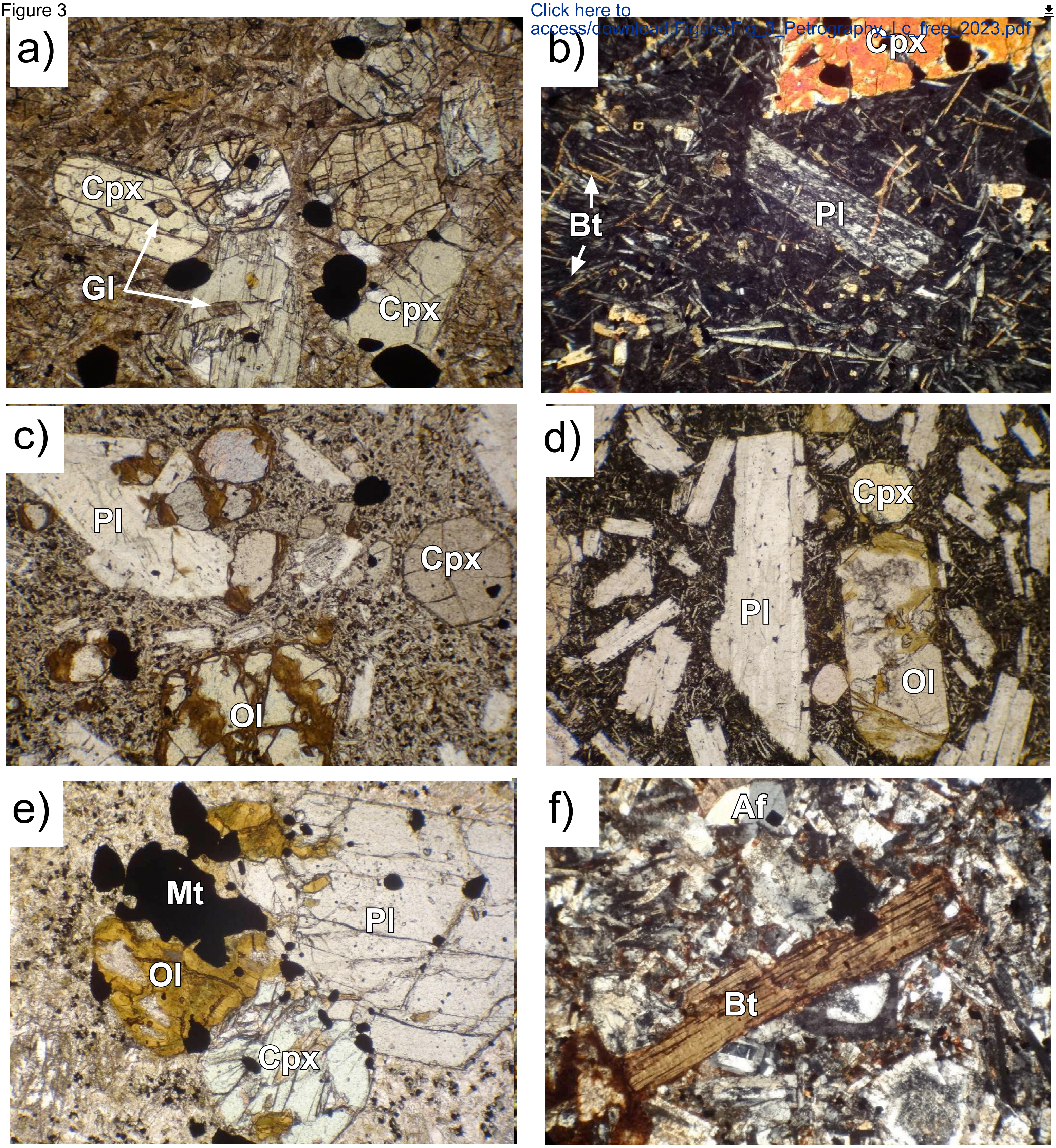

Figure 4

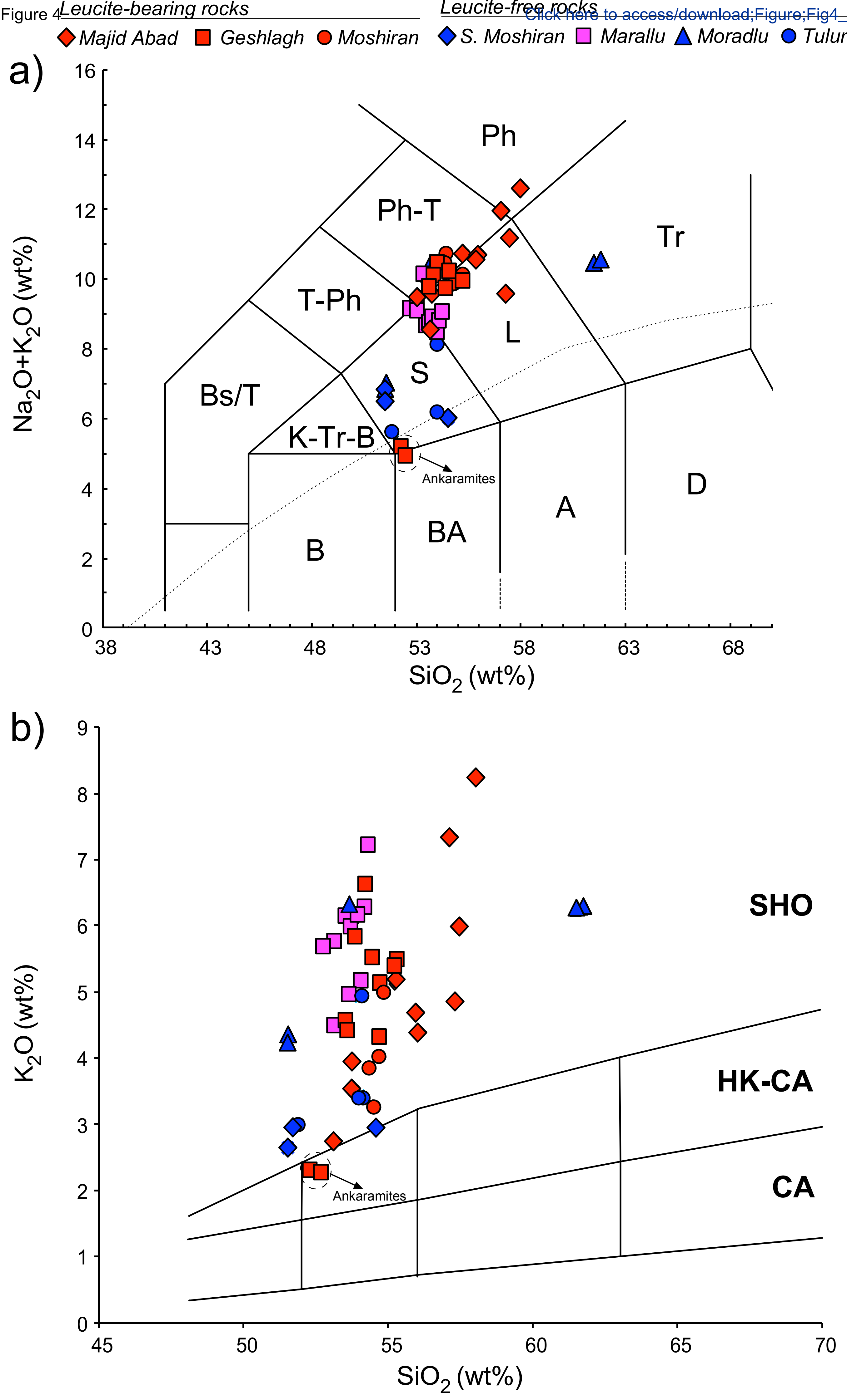
Leucite-bearing rocks
Majid Abad
Geshlagh
Moshiran
Leucite-free rocks
S. Moshiran
Marallu
Moradlu
Tulun
a)
Ph
Ph-T
T-Ph
Bs/T
S
K-Tr-B
Tr
L
B
BA
A
D
Ankaramites
Na_2O+K_2O (wt%)
SiO_2 (wt%)
b)
SHO
HK-CA
CA
Ankaramites
K_2O (wt%)
SiO_2 (wt%)

Figure 5

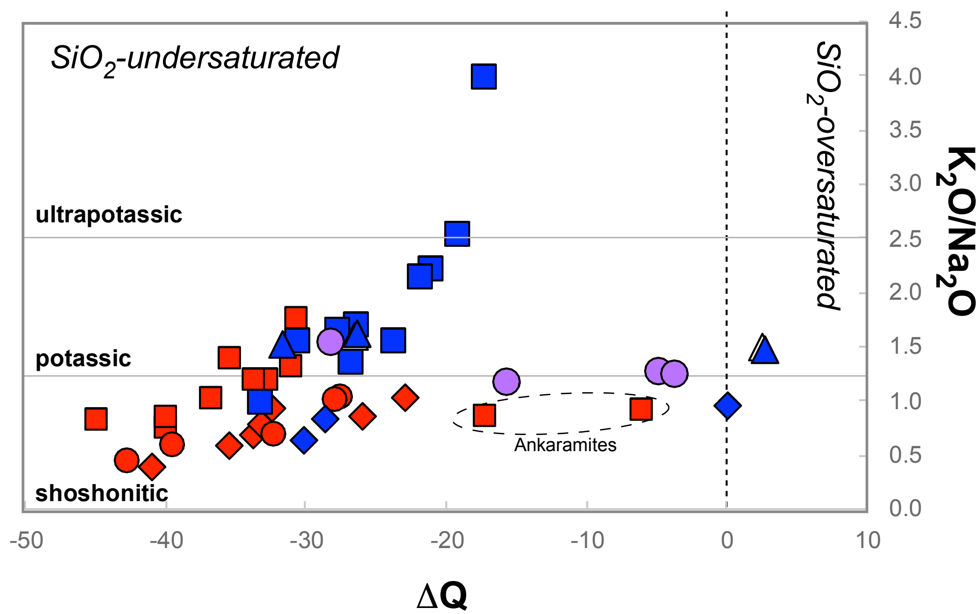
SiO2-undersaturated
SiO2-oversaturated
ultrapotassic
potassic
shoshonitic
Ankaramites
-50
-40
-30
-20
-10
0
10
ΔQ
0.0
0.5
1.0
1.5
2.0
2.5
3.0
3.5
4.0
4.5
K2O/Na2O

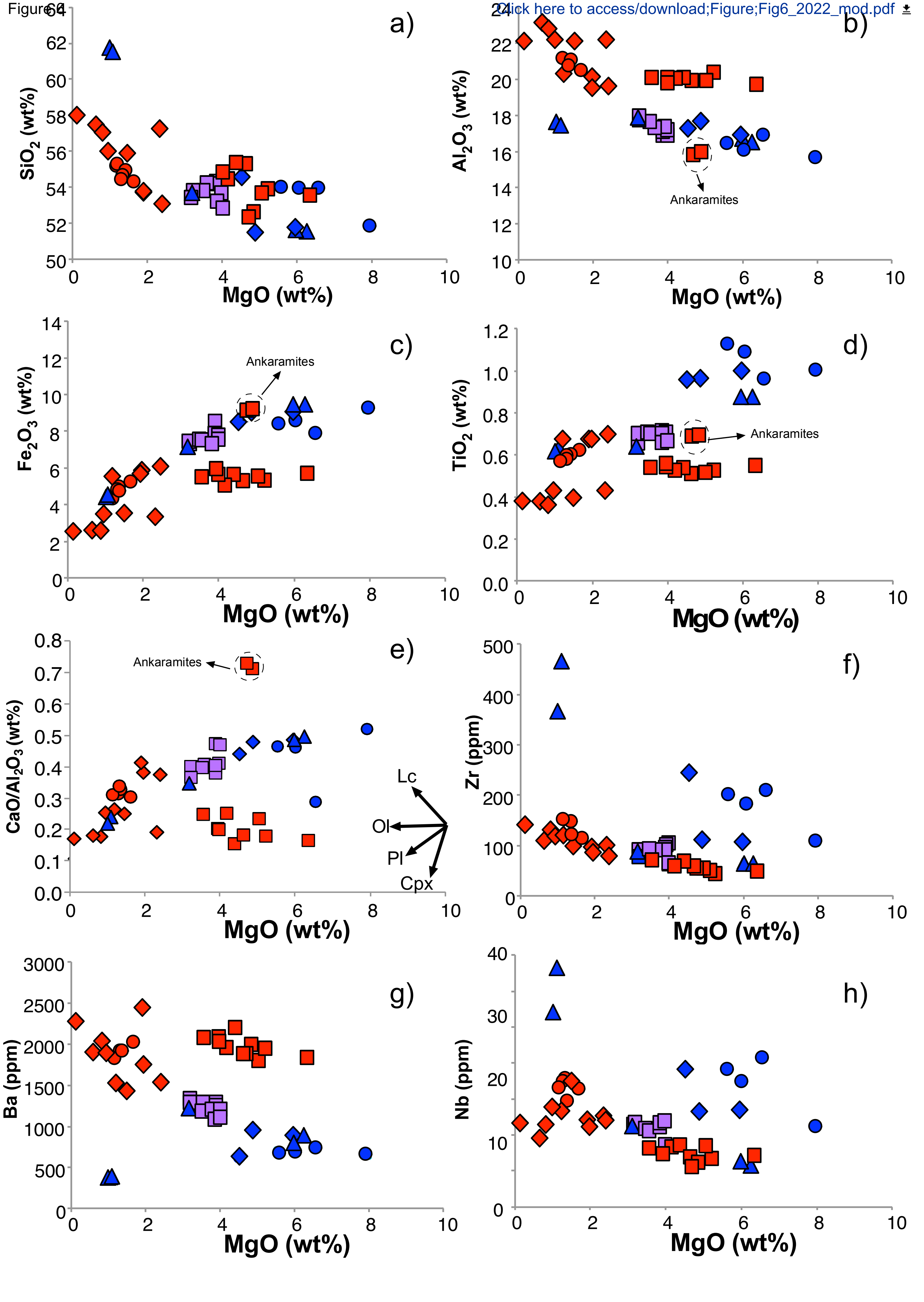
a)
SiO_2 (wt%)
MgO (wt%)
b)
Al_2O_3 (wt%)
Ankaramites
MgO (wt%)
c)
Fe_2O_3 (wt%)
Ankaramites
MgO (wt%)
d)
TiO_2 (wt%)
Ankaramites
MgO (wt%)
e)
CaO/Al_2O_3 (wt%)
Ankaramites
Lc
Ol
Pl
Cpx
MgO (wt%)
f)
Zr (ppm)
MgO (wt%)
g)
Ba (ppm)
MgO (wt%)
h)
Nb (ppm)
MgO (wt%)

Figure 7

Click here to access/download;Figure;Fig7_2022_mod.pdf

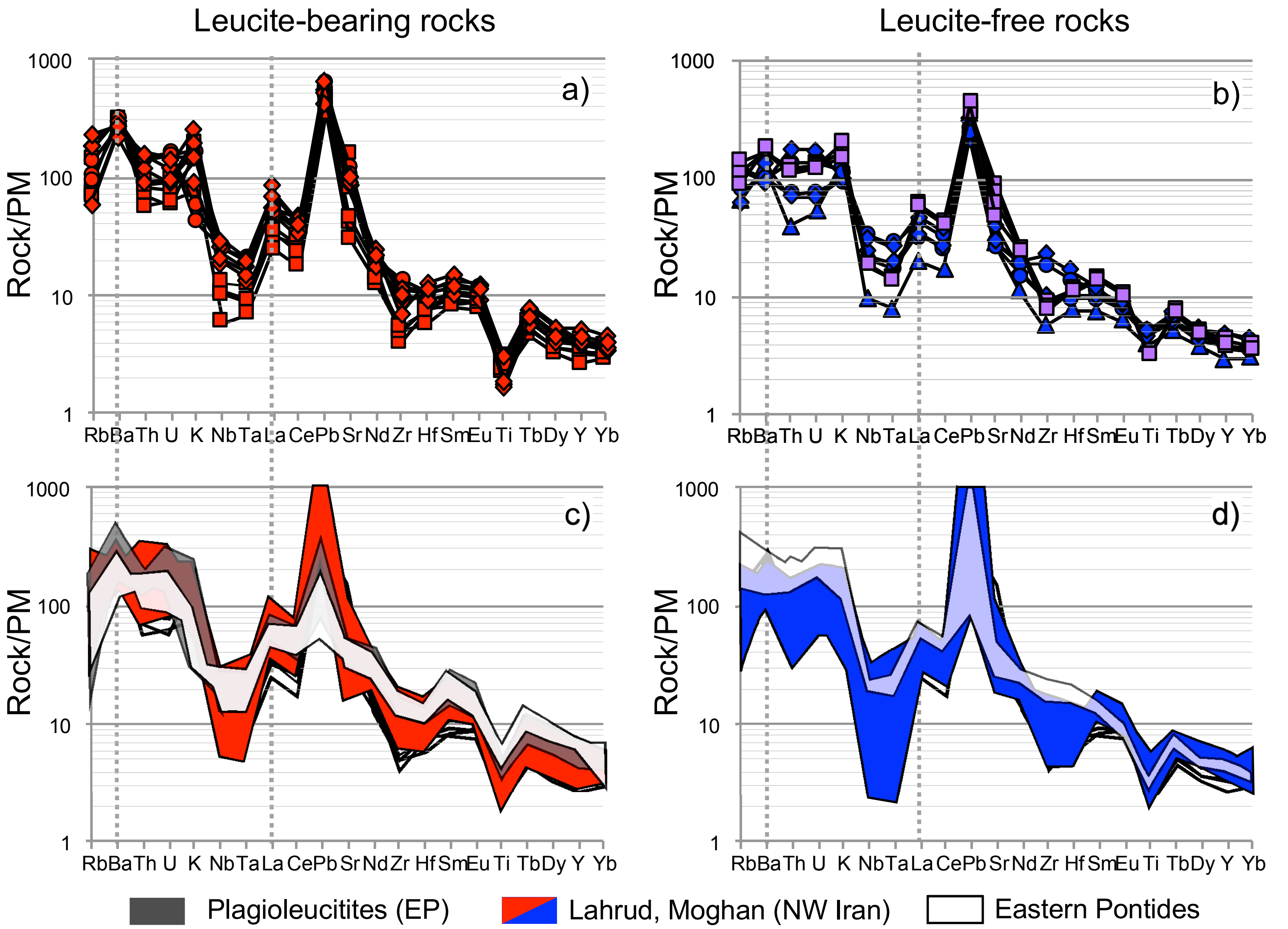

Figure 8

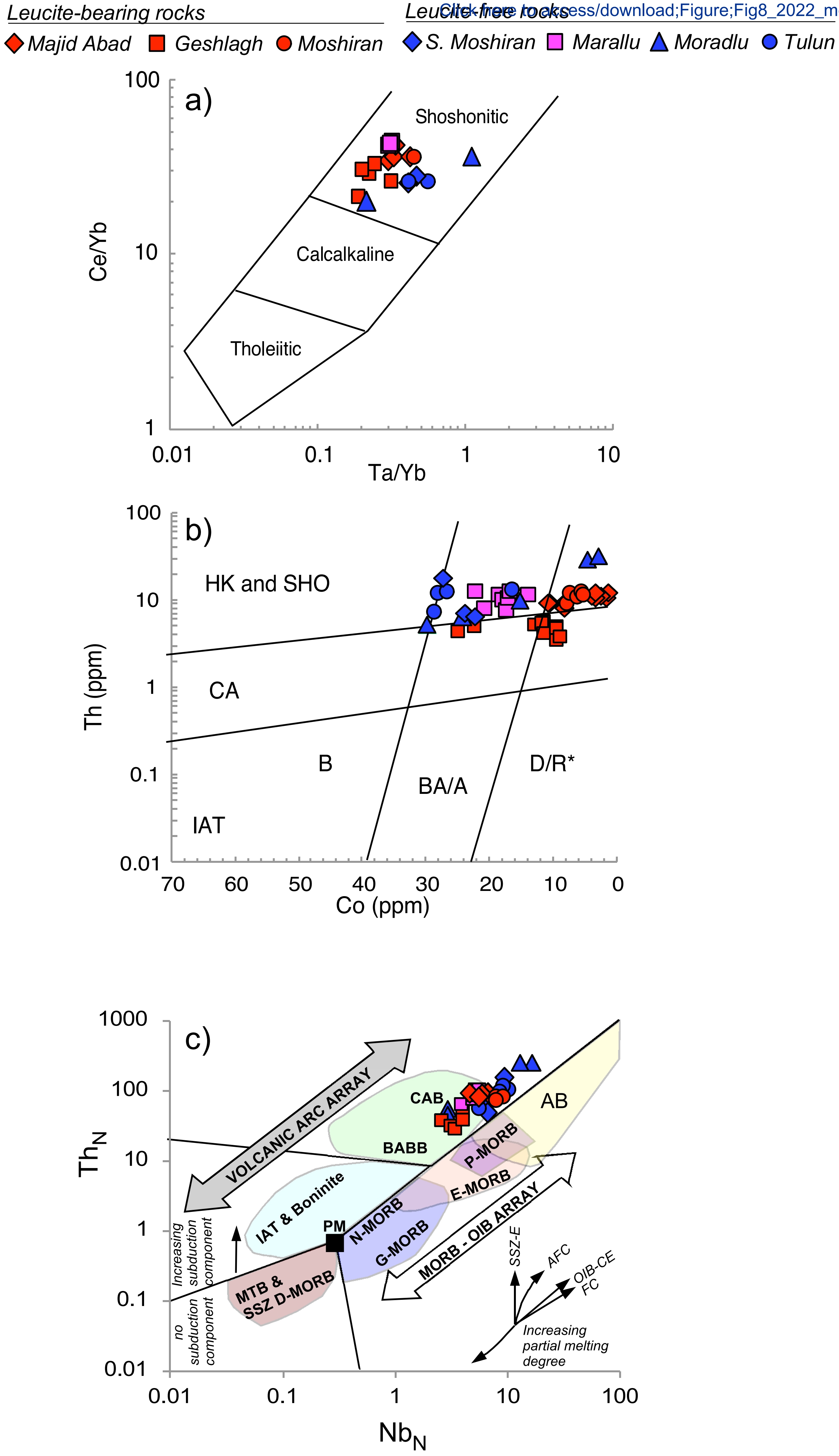

Leucite-bearing rocks
Majid Abad
Geshlagh
Moshiran
Leucite-free rocks
S. Moshiran
Marallu
Moradlu
Tulun
a)
Shoshonitic
Calcalkaline
Tholeiitic
Ce/Yb
Ta/Yb
100
10
1
0.01
0.1
1
10
b)
HK and SHO
CA
B
BA/A
D/R*
IAT
Th (ppm)
Co (ppm)
100
10
1
0.1
0.01
70
60
50
40
30
20
10
0
c)
VOLCANIC ARC ARRAY
CAB
BABB
AB
P-MORB
E-MORB
IAT & Boninite
PM
N-MORB
G-MORB
MTB &
SSZ D-MORB
MORB - OIB ARRAY
Increasing subduction component
no subduction component
SSZ-E
AFC
OIB-CE
FC
Increasing partial melting degree
Th_N
Nb_N
1000
100
10
1
0.1
0.01
0.01
0.1
1
10
100

Figure 9

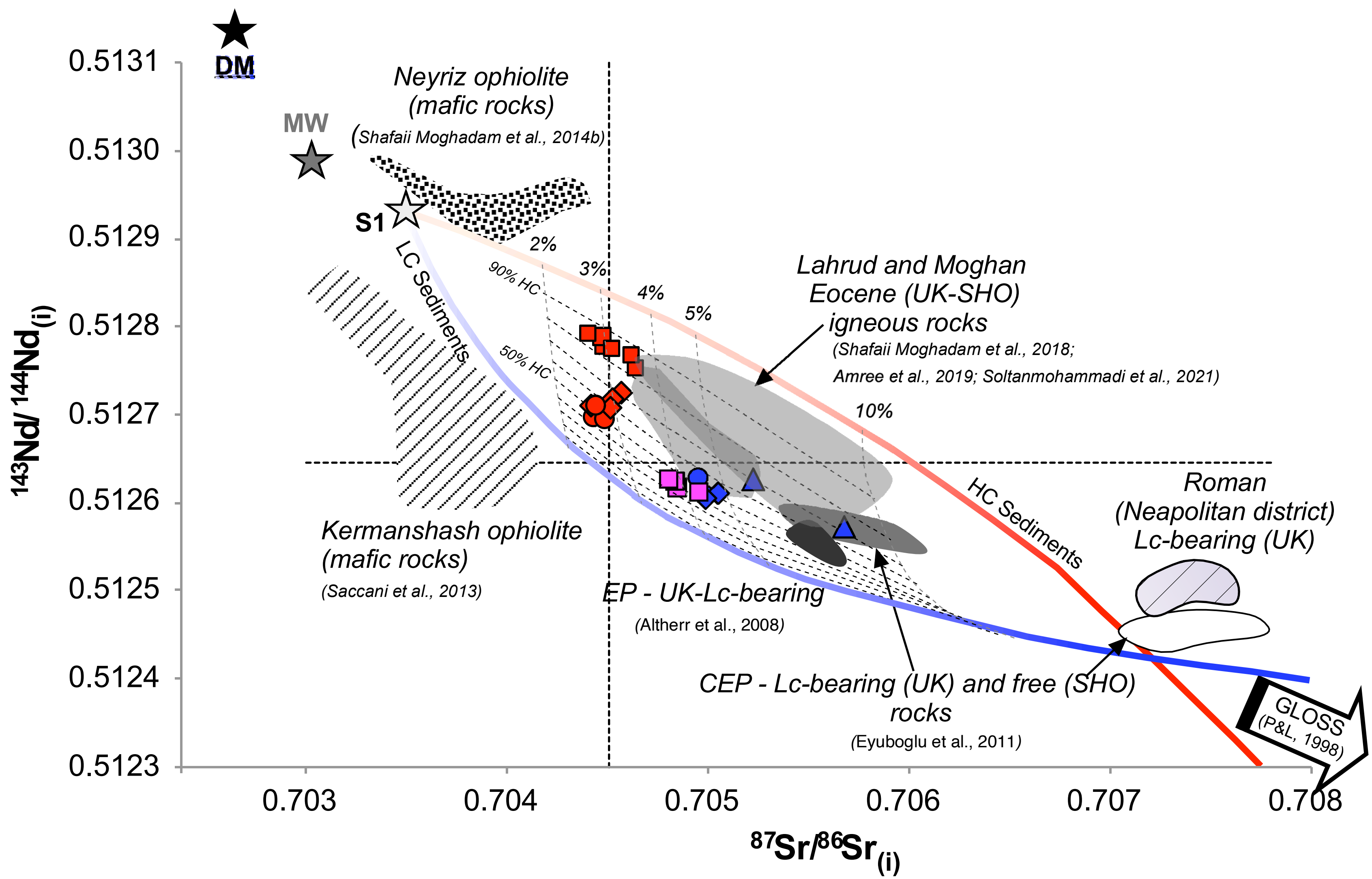

DM
MW
S1
0.5131
0.5130
0.5129
0.5128
0.5127
0.5126
0.5125
0.5124
0.5123
143Nd/144Nd(i)
0.703
0.704
0.705
0.706
0.707
0.708
87Sr/86Sr(i)
Neyriz ophiolite
(mafic rocks)
(Shafaii Moghadam et al., 2014b)
LC Sediments
90% HC
50% HC
2%
3%
4%
5%
10%
Lahrud and Moghan
Eocene (UK-SHO)
igneous rocks
(Shafaii Moghadam et al., 2018;
Amree et al., 2019; Soltanmohammadi et al., 2021)
HC Sediments
Kermanshash ophiolite
(mafic rocks)
(Saccani et al., 2013)
EP - UK-Lc-bearing
(Altherr et al., 2008)
Roman
(Neapolitan district)
Lc-bearing (UK)
CEP - Lc-bearing (UK) and free (SHO)
rocks
(Eyuboglu et al., 2011)
GLOSS
(P&L, 1998)

Figure 10

Click here to access/download;Figure;Fig10_2022_mod.pdf

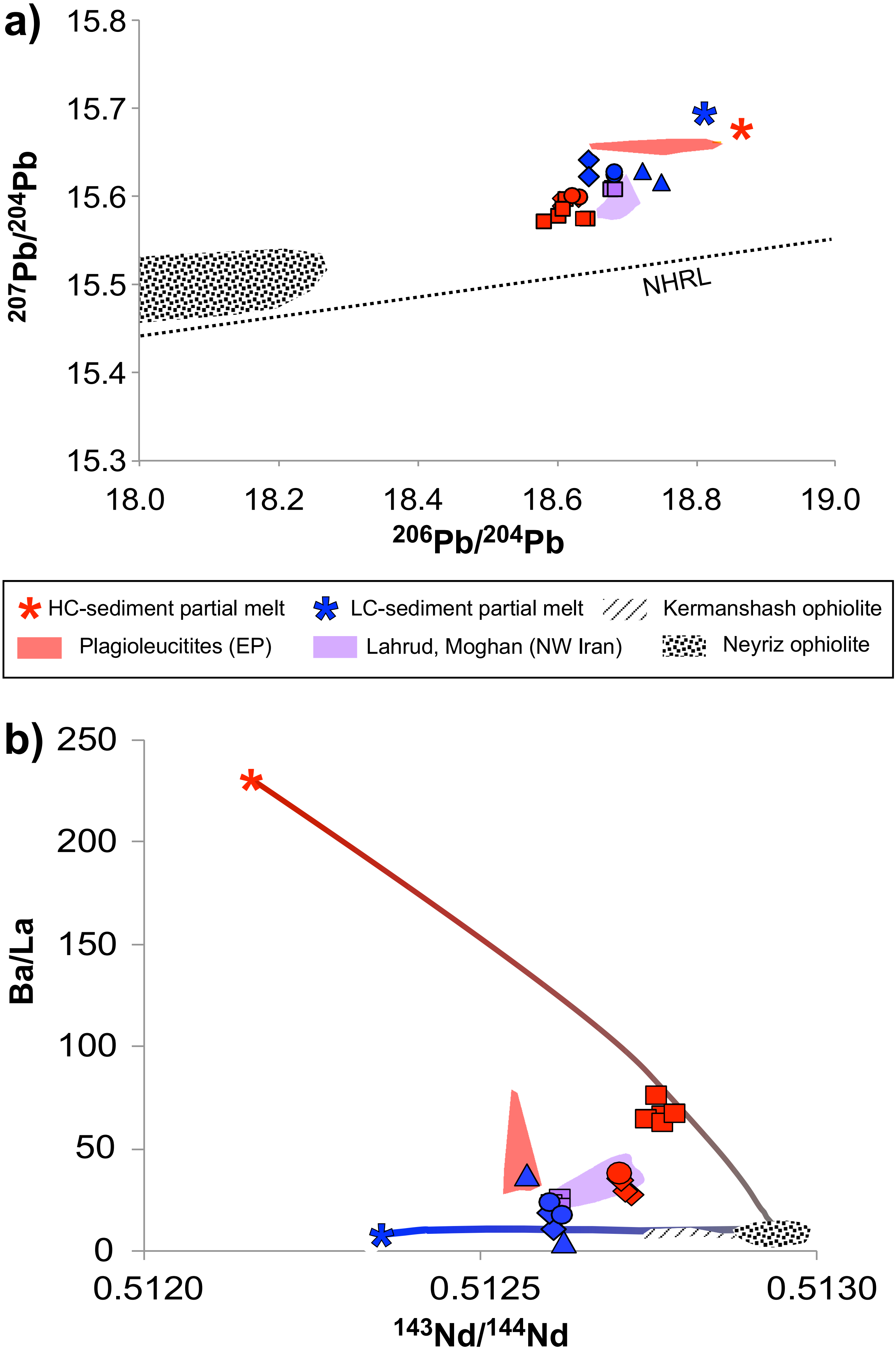

Figure 11

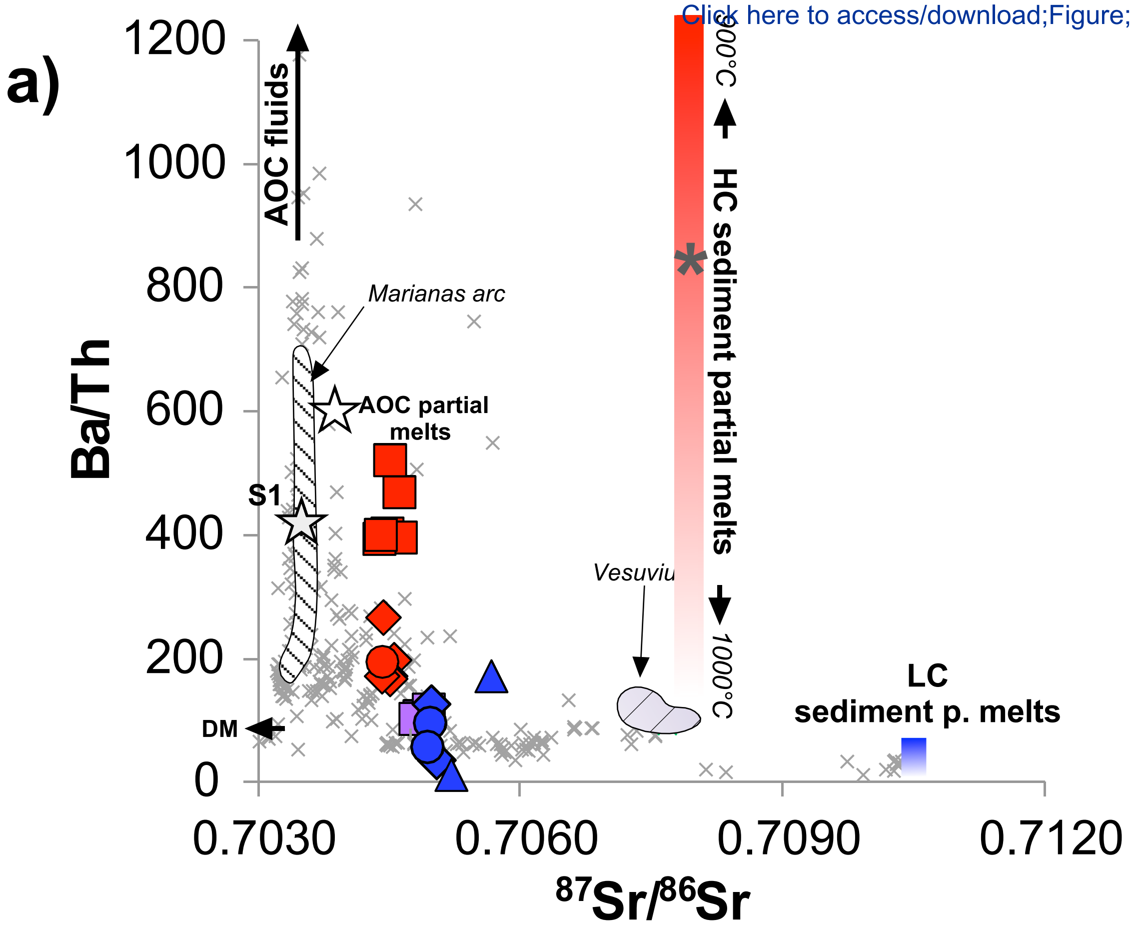
a)
Ba/Th
1200
1000
800
600
400
200
0
0.7030
0.7060
0.7090
0.7120
$^{87}Sr/^{86}Sr$
AOC fluids
Marianas arc
AOC partial melts
S1
DM
Vesuviu
900°C
HC sediment partial melts
1000°C
LC sediment p. melts

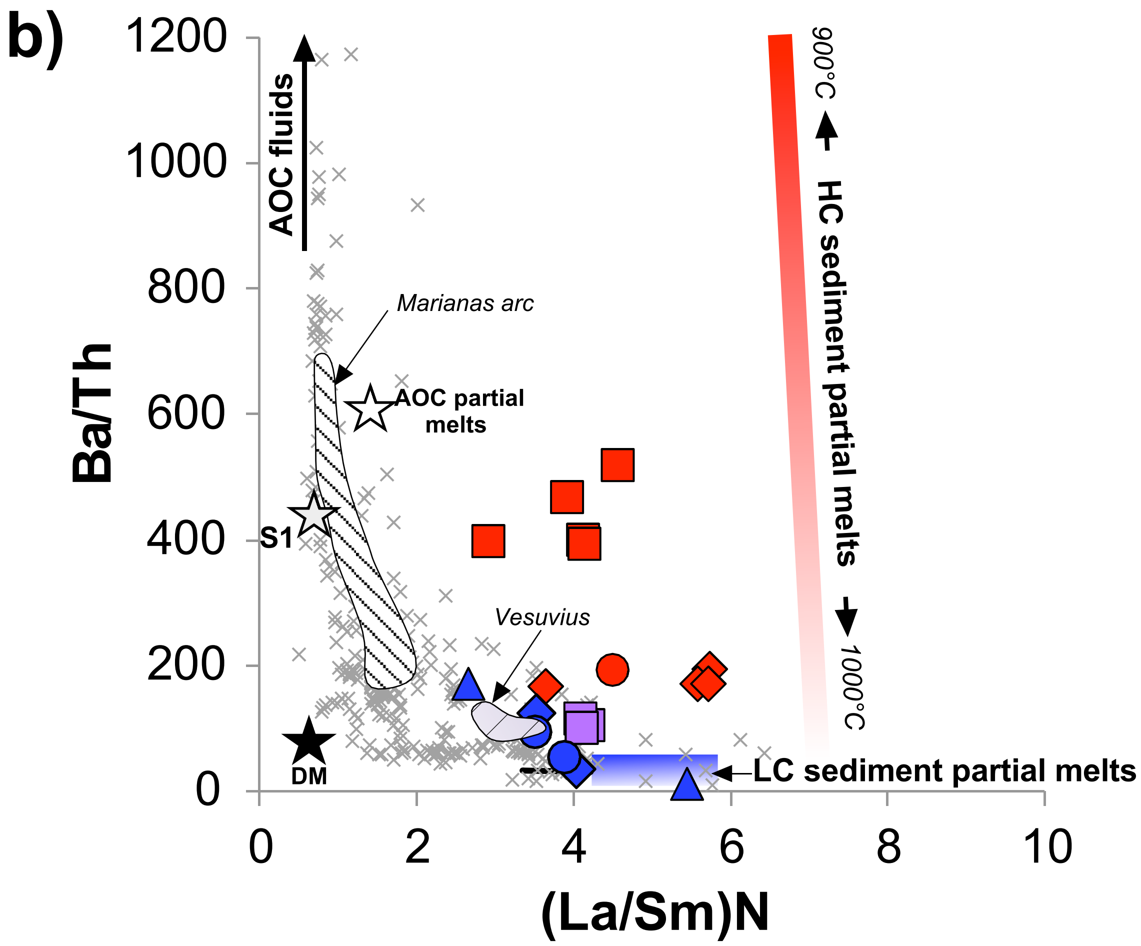
b)
Ba/Th
1200
1000
800
600
400
200
0
0
2
4
6
8
10
(La/Sm)N
AOC fluids
Marianas arc
AOC partial melts
S1
DM
Vesuvius
900°C
HC sediment partial melts
1000°C
LC sediment partial melts

Figure 12

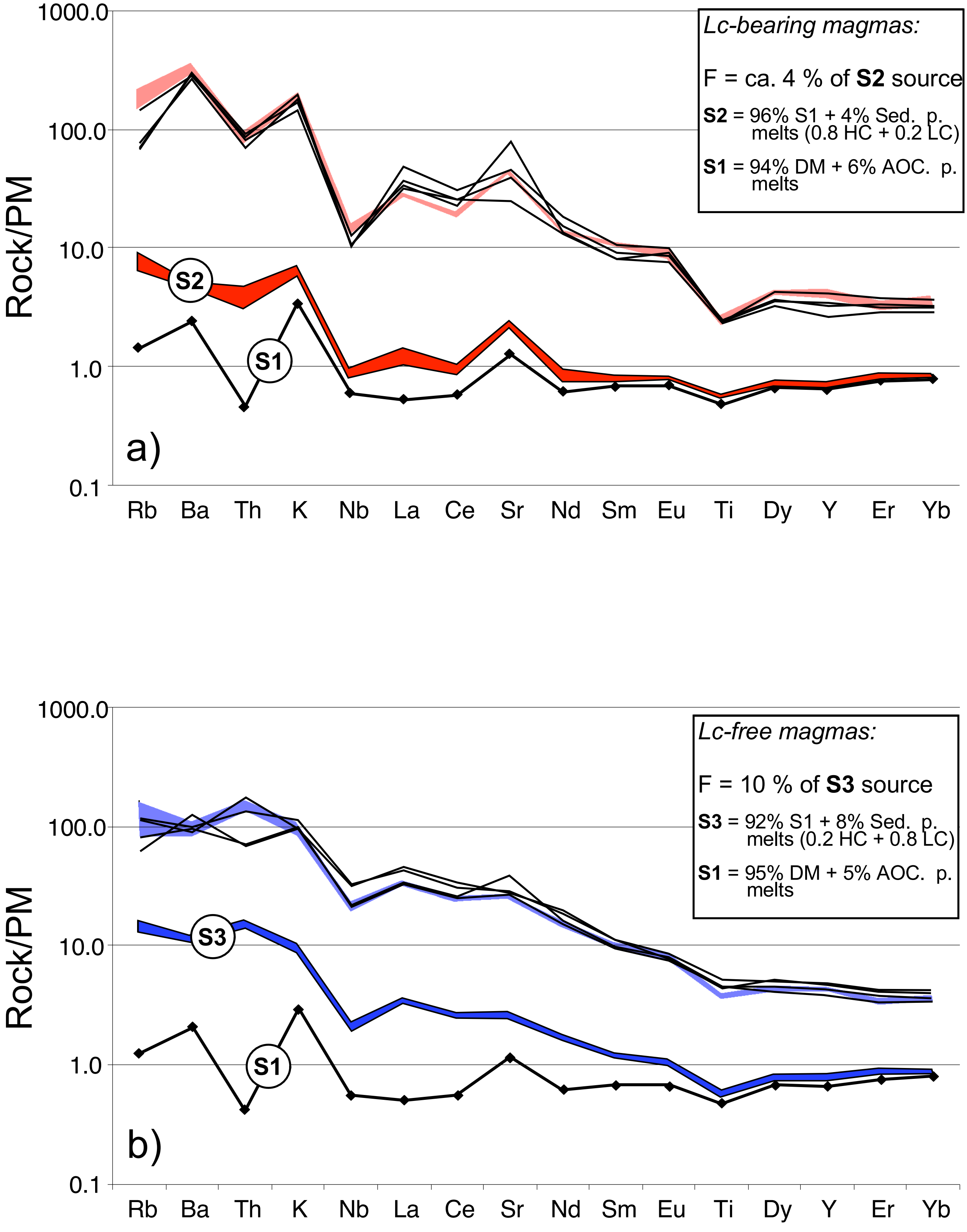

Rock/PM
1000.0
100.0
10.0
1.0
0.1
Lc-bearing magmas:
F = ca. 4 % of **S2** source
S2 = 96% S1 + 4% Sed. p. melts (0.8 HC + 0.2 LC)
S1 = 94% DM + 6% AOC. p. melts
S2
S1
a)
Rb Ba Th K Nb La Ce Sr Nd Sm Eu Ti Dy Y Er Yb
Rock/PM
1000.0
100.0
10.0
1.0
0.1
Lc-free magmas:
F = 10 % of **S3** source
S3 = 92% S1 + 8% Sed. p. melts (0.2 HC + 0.8 LC)
S1 = 95% DM + 5% AOC. p. melts
S3
S1
b)
Rb Ba Th K Nb La Ce Sr Nd Sm Eu Ti Dy Y Er Yb

Figure 13

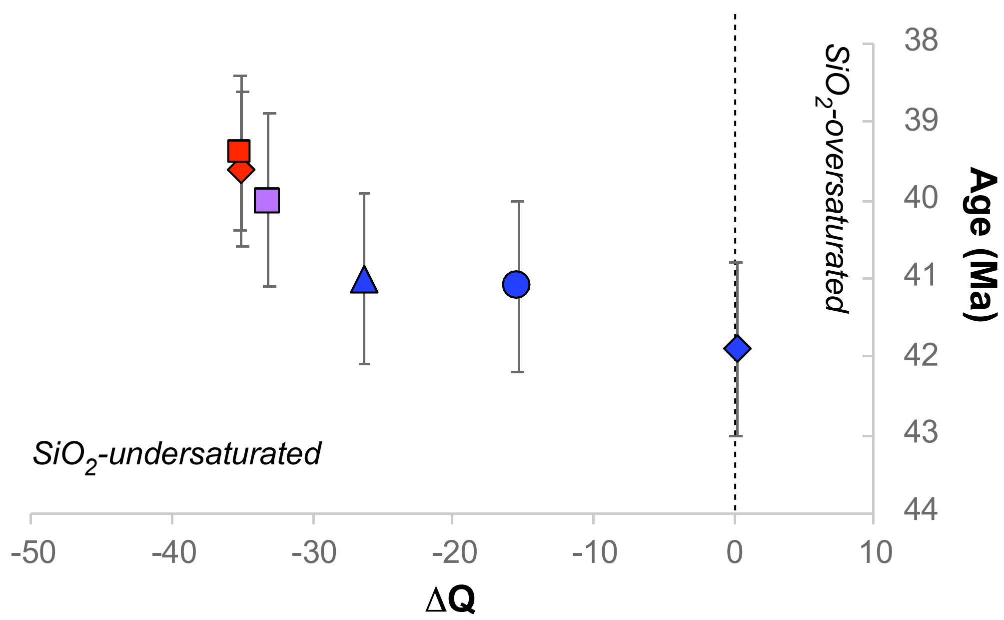

SiO2-oversaturated
SiO2-undersaturated
38
39
40
41
42
43
44
Age (Ma)
-50
-40
-30
-20
-10
0
10
ΔQ

Figure 14

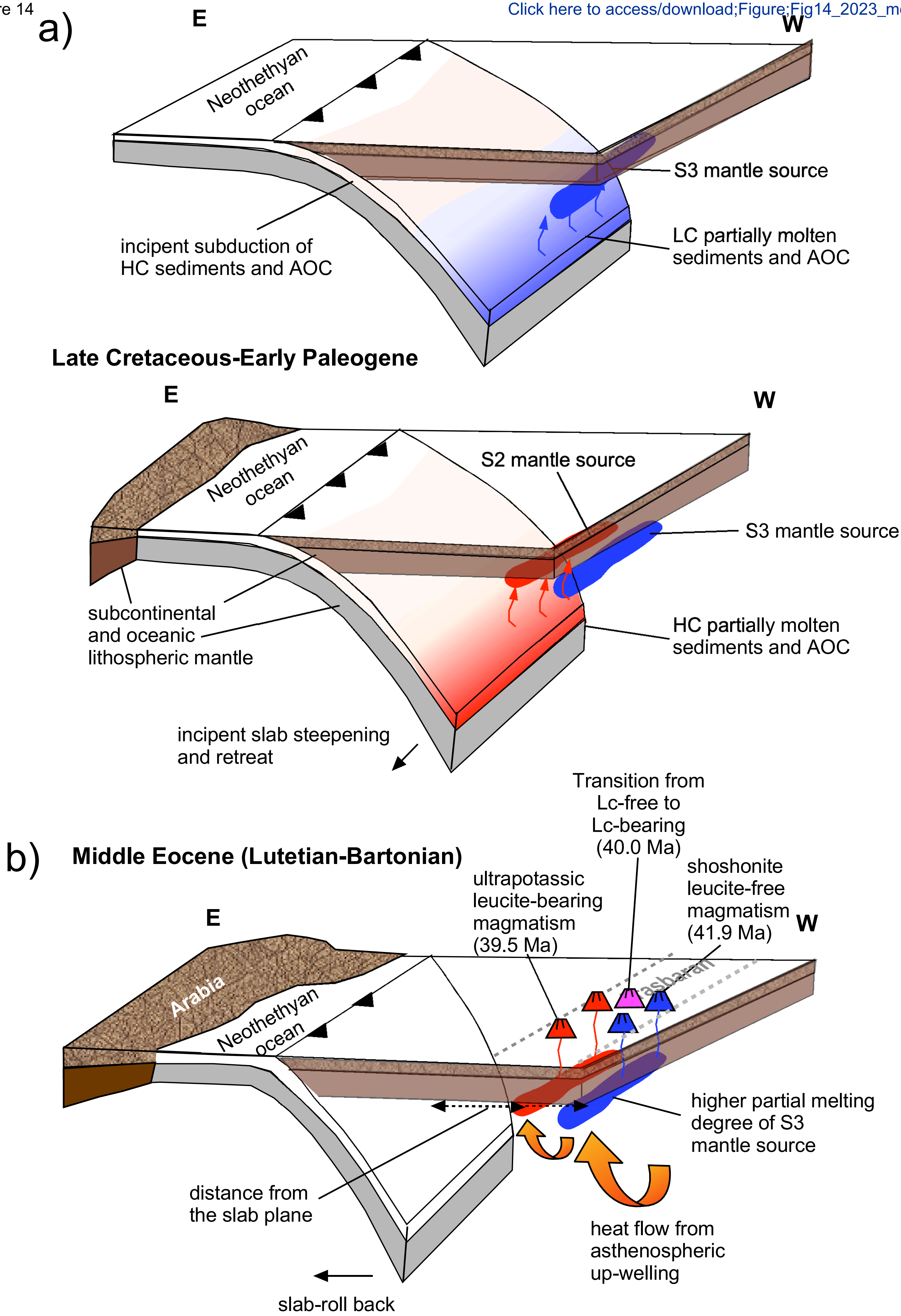

a)
E
W
Neothethyan ocean
S3 mantle source
incipient subduction of HC sediments and AOC
LC partially molten sediments and AOC
Late Cretaceous-Early Paleogene
E
W
Neothethyan ocean
S2 mantle source
S3 mantle source
subcontinental and oceanic lithospheric mantle
HC partially molten sediments and AOC
incipient slab steepening and retreat
b)
Middle Eocene (Lutetian-Bartonian)
Transition from Lc-free to Lc-bearing (40.0 Ma)
ultrapotassic leucite-bearing magmatism (39.5 Ma)
shoshonite leucite-free magmatism (41.9 Ma)
E
W
Arabia
Neothethyan ocean
higher partial melting degree of S3 mantle source
distance from the slab plane
heat flow from asthenospheric up-welling
slab-roll back

Table 1

Sample	M-03	M-04	M-05	M-06	M-07	M-08	M-09	M-10	M-11	M-12	M-13	M-14	M-15	M-16
Lithology	Lava	Lava	Lava	Lava	Lava	Lava	Lava	Lava	Lava	Lava	Lava	Lava	Dike	Dike
Rock-type	**Lc-free**	**Lc-free**	**Lc-free**	**Lc-free**	**Lc-free**	**Lc-free**	**Lc-free**	**Lc-free**	**Lc-free**	**Lc-free**	**Lc-free**	**Lc-free**		
Classification	Tr-And.	Tr-And.	Tr-And.	Tr-And.	Tr-And.	Tr-And.	Tr-And.	Tr-And.	Tr-And.	Tr-And.	Tr-And.	Tr-And.	Trachite	Bas. Tr-And.
Locality	Marallu	Marallu	Marallu	Marallu	Marallu	Marallu	Marallu	Marallu	Marallu	Marallu	Marallu	Marallu	Moradlu	Moradlu
Latitude	38.9459051	38.9459954	38.9465935	38.9457806	38.9459436	38.9561972	38.9562259	38.9579623	38.9585147	38.9599503	38.9605733	38.9584426	38.8028251	38.8028341
Longitude	47.8794081	47.8794002	47.8788937	47.8811681	47.8814978	47.8373524	47.8372843	47.8358998	47.8361526	47.8360252	47.8367078	47.8394844	47.8705157	47.8705161
SiO_2 (wt%)	52.22	52.62	52.78	52.09	52.80	51.15	47.41	51.81	51.40	51.94	51.95	52.10	59.96	60.16
TiO_2	0.67	0.69	0.68	0.69	0.69	0.66	0.60	0.64	0.64	0.68	0.63	0.68	0.61	0.60
Al_2O_3	17.33	16.90	16.86	16.76	16.65	17.92	13.72	16.40	16.44	16.55	17.20	17.14	16.96	17.10
Fe_2O_3	7.22	7.54	7.27	7.49	7.37	6.70	9.29	7.02	7.31	8.30	7.05	7.29	4.27	4.27
MnO	0.19	0.19	0.19	0.19	0.19	0.15	0.18	0.19	0.18	0.19	0.18	0.18	0.11	0.11
MgO	3.16	3.81	3.52	3.88	3.79	3.79	5.85	3.80	3.92	3.83	3.15	3.43	1.08	1.00
CaO	6.90	6.66	6.82	6.87	6.28	7.51	10.32	7.76	7.69	6.68	6.29	6.80	4.08	3.75
Na_2O	2.68	3.23	2.41	3.58	1.76	3.85	6.60	3.30	3.35	4.45	3.87	2.72	4.05	4.13
K_2O	5.94	5.03	6.11	4.81	7.01	4.59	1.85	5.62	5.54	4.41	5.96	5.83	6.09	6.10
P_2O_5	0.75	0.73	0.74	0.76	0.69	0.55	0.79	0.99	0.91	0.72	0.88	0.76	0.32	0.32
LOI	2.94	2.62	2.63	2.88	2.77	3.14	3.39	2.48	2.60	2.24	2.85	3.08	2.48	2.45
Sum	100.0	100.0	100.0	100.0	100.0	100.0	100.0	100.0	100.0	100.0	100.0	100.0	100.0	100.0
Ba (ppm)	1311	1185	1275	1202	1279	1135	1913	1067	1082	1241	1212	1192	368	371
Ce	77	73	86	82	86	60	54	81	74	86	88	84	131	131
Co	17	18	17	22	18	18	25	21	17	17	14	17	3	5
Cr	47	38	44	41	37	26	114	48	49	53	48	35	17	27
Cu	169	165	163	164	164	130	156	180	178	155	168	174	32	32
La	54	62	57	49	55	33	32	50	47	61	57	55	87	86
Nb	13	13	12	13	12	7	7	13	10	13	13	12	38	31
Ni	14	12	14	11	15	7	7	17	13	8	11	13	6	5
Pb	25	28	23	27	21	17	26	23	24	31	26	25	38	30
Rb	111	85	102	80	129	93	76	96	78	64	91	104	208	176
Sc	15	14	13	15	14	13	23	15	14	16	13	14	8	8
Sr	1667	1886	1984	1625	1827	2489	607	1140	931	975	965	1311	325	261
Th	10	11	10	12	10	5	7	8	7	12	11	10	30	29
V	209	200	209	196	209	205	266	211	229	220	193	212	44	44
Y	21	22	21	21	20	19	14	23	18	20	19	20	27	21
Zn	64	72	64	70	67	56	70	53	55	80	61	69	47	46
Zr	89	97	90	101	94	55	44	89	65	85	75	91	464	364

Sample	M-17	M-18	M-20	M-21	M-22	M-23	M-24	M-25	M-26	M-27	M-28	M-29	M-30	M-31
Lithology	Dike	Dike	Dike	Lava	Lava	Lava	Lava	Lava	Lava	Lava	Lava	Lava	Lava	Columnar lava flow
Rock-type				**Lc-bearing**	**Lc-bearing**	**Lc-bearing**	**Lc-bearing**	**Lc-bearing**	**Lc-bearing**	**Lc-bearing**	**Lc-bearing**	**Lc-bearing**	**Lc-bearing**	**Lc-bearing**
Classification	Bas. Tr-And.	Tr-And.	Ph-Trachite	Tr-And.	Tr-And.	Tr-And.	Tr-And.	Tr-And.	Tr-And.	Tr-And.	Tr-And.	Tr-And.	Tr-And.	Tr-And.
Locality	Moradlu	Moradlu	Moradlu	Majid Abad	Majid Abad	Majid Abad	Majid Abad	Majid Abad	Majid Abad	Majid Abad	Majid Abad	Majid Abad	Majid Abad	Gheshlagh
Latitude	38.8030825	38.8030823	38.7991213	38.7158643	38.7143556	38.7168686	38.7150633	38.7154252	38.7201523	38.7220457	38.7230337	38.7220588	38.7136686	38.7448248
Longitude	47.8699389	47.8699504	47.8214028	47.3709702	47.3680568	47.3672082	47.3678157	47.3681841	47.3661205	47.3647223	47.369321	47.3689668	47.4012808	47.4958826
SiO_2 (wt%)	49.75	49.73	52.26	54.78	53.00	51.41	55.72	51.89	54.98	50.98	54.59	53.48	54.12	51.09
TiO_2	0.84	0.84	0.62	0.35	0.65	0.64	0.36	0.65	0.36	0.67	0.41	0.41	0.38	0.52
Al_2O_3	15.93	16.08	17.39	21.88	19.55	18.71	21.31	19.46	22.18	18.88	21.18	21.22	21.42	18.80
Fe_2O_3	9.02	8.97	6.89	2.47	5.30	5.62	2.46	5.40	2.53	5.85	3.19	3.32	3.38	5.36
MnO	0.16	0.16	0.18	0.15	0.18	0.18	0.15	0.21	0.14	0.21	0.15	0.14	0.11	0.17
MgO	6.05	5.77	3.10	0.80	1.16	1.88	0.13	1.86	0.61	2.32	2.23	0.92	1.43	6.08
CaO	7.88	7.79	6.05	3.85	5.13	7.17	3.65	8.00	4.03	7.06	4.05	5.40	5.37	3.04
Na_2O	2.54	2.57	4.01	4.43	5.32	5.80	4.20	4.48	4.99	6.51	4.51	5.99	5.70	5.25
K_2O	4.08	4.19	6.13	7.04	4.98	3.39	7.91	3.82	5.72	2.62	4.62	4.18	4.52	4.31
P_2O_5	0.34	0.36	0.77	0.19	0.64	0.87	0.16	0.83	0.14	0.93	0.37	0.42	0.36	0.82
LOI	3.40	3.53	2.60	4.05	4.09	4.32	3.96	3.40	4.32	3.97	4.69	4.53	3.21	4.56
Sum	100.0	100.0	100.0	100.0	100.0	100.0	100.0	100.0	100.0	100.0	100.0	100.0	100.0	100.0
Ba (ppm)	873	822	1217	2042	1527	1749	2281	2443	1906	1538	5019	1886	1427	1832
Ce	38	43	88	89	95	90	96	86	91	95	78	77	91	59
Co	30	24	15	2	8	8	1	11	3	11	3	4	4	9
Cr	72	67	44	10	16	30	9	26	9	28	12	17	10	12
Cu	100	103	160	41	50	116	80	75	54	95	58	109	30	181
La	24	23	58	74	54	53	62	54	65	43	56	55	37	28
Nb	7	7	12	13	15	13	13	14	11	14	14	16	20	8
Ni	19	19	10	0	2	3	1	6	bdl	1	2	bdl	bdl	2
Pb	15	15	28	35	33	33	31	29	37	30	35	47	36	33
Rb	60	60	105	94	118	62	115	66	134	56	69	155	47	49
Sc	19	18	13	3	6	10	4	11	3	8	4	4	5	8
Sr	604	498	1139	1653	1030	1773	1685	2018	2099	1931	3689	2176	1875	751
Th	5	6	10	10	9	8	12	9	11	9	10	11	12	3
V	239	241	182	84	192	234	88	243	83	247	100	108	43	171
Y	18	17	19	20	26	21	22	23	16	20	13	14	12	15
Zn	54	55	60	52	63	77	49	67	53	76	54	60	49	55
Zr	63	64	85	131	120	83	142	93	110	78	98	116	99	46

M-32	**M-33**	**M-34**	**M-35**	**M-36**	**M-37**	**M-38**	**M-39**	**M-40**	**M-41**	**M-42**	**M-43**	**M-44**	**M-45**
Pillow	Pillow	Pillow	Pillow	Columnar lava flow	Columnar lava flow	Pillow	Columnar lava flow	Pillow	Pillow	Columnar lava flow	Lava	Lava	Pillow
Lc-bearing	**Lc-bearing**	**Lc-bearing**	**Lc-bearing**	**Lc-bearing**	**Lc-bearing**	**Lc-bearing**	**Lc-bearing**	**Lc-bearing**	**Lc-bearing**	**Lc-bearing**	**Lc-bearing**	**Lc-bearing**	**Lc-bearing**
Tr-And.	Tr-And.	Tr-And.	Tr-And.	Tr-And.	Tr-And.	Tr-And.	Tr-And.	Ankaramite	Ankaramite	Tr-And.	Tr-And.	Tr-And.	Tr-And.
Gheshlagh	Gheshlagh	Gheshlagh	Gheshlagh	Gheshlagh	Gheshlagh	Gheshlagh	Gheshlagh	Gheshlagh	Gheshlagh	Gheshlagh	Moshiran	Moshiran	Moshiran
38.7451281	38.7562069	38.7556365	38.7627018	38.7604231	38.7570949	38.760427	38.7600865	38.7478394	38.7467993	38.7458287	38.7302594	38.7711075	38.7195846
47.4977109	47.4885812	47.488711	47.503813	47.5054594	47.5098191	47.5211901	47.5219376	47.5090922	47.5088601	47.5087456	47.5466533	47.6325006	47.5299777
49.45	51.91	50.92	52.75	51.56	51.91	52.58	51.13	50.34	49.81	51.53	50.38	51.80	52.14
0.51	0.53	0.51	0.51	0.50	0.50	0.48	0.49	0.65	0.65	0.51	0.60	0.59	0.52
17.90	18.77	18.56	19.17	19.54	19.09	18.91	19.04	15.26	15.04	19.07	17.19	19.12	19.10
5.80	5.61	5.89	5.36	5.01	4.80	5.05	5.22	8.61	8.63	5.11	6.39	4.99	5.44
0.16	0.16	0.16	0.15	0.17	0.16	0.14	0.16	0.19	0.19	0.16	0.17	0.18	0.17
3.28	3.77	3.55	4.22	5.02	4.00	4.43	4.83	4.67	4.50	3.41	3.53	1.93	3.82
5.61	3.78	4.07	2.91	3.47	4.80	3.42	4.41	10.87	10.97	4.73	5.81	6.44	3.80
5.64	5.54	5.47	4.39	4.05	4.00	4.36	5.03	2.51	2.75	3.61	3.61	7.18	4.85
4.26	4.09	4.14	5.21	5.56	5.26	5.12	4.22	2.19	2.17	6.28	5.25	1.68	4.87
0.70	0.74	0.70	0.68	0.87	0.81	0.67	0.80	0.43	0.44	0.70	0.76	0.65	0.63
6.70	5.11	6.02	4.65	4.25	4.67	4.84	4.67	4.28	4.85	4.90	6.30	5.42	4.66
100.0	100.0	100.0	100.0	100.0	100.0	100.0	100.0	100.0	100.0	100.0	100.0	100.0	100.0
1919	2011	2226	2191	1927	1950	1875	1806	1961	1890	2061	1673	2235	2097
62	58	49	60	69	60	58	58	47	42	60	55	83	58
11	13	14	12	9	10	11	10	23	25	12	12	8	12
9	12	10	7	10	14	10	13	43	49	10	22	19	13
183	180	179	187	189	202	198	196	187	185	187	217	152	152
26	31	31	33	31	41	25	36	30	34	43	34	43	33
8	8	8	10	8	9	8	9	7	6	9	11	17	10
1	2	2	3	5	4	4	3	17	15	6	7	bdl	2
36	35	33	35	32	32	26	33	24	23	31	28	42	31
56	48	53	55	95	55	59	30	52	50	56	72	64	42
8	7	7	6	7	7	7	7	18	17	7	10	7	6
962	835	827	767	957	1383	629	1043	3257	3034	2327	1225	2540	1677
5	5	5	5	4	5	4	5	5	4	6	4	10	5
171	166	167	168	170	162	155	173	325	317	170	245	144	151
15	15	15	18	13	16	15	16	16	16	17	19	15	15
68	68	69	63	56	54	57	55	72	72	52	58	83	65
59	57	59	67	44	58	55	53	55	52	70	73	97	60

M-46	**M-47**	**M-48**	**M-49**	**M-51**	**M-52**	**M-53**	**M-54**	**M-55**	**M-56**	**M-57**	**M-58**	**M-59**	**M-60**
Lava	Lava	Lava	Lava	Lava	Lava	Lava	Lava	Lava	Lava	Lava	Lava	Lava	Lava
Lc-bearing	**Lc-bearing**	**Lc-bearing**	**Lc-bearing**	**Lc-bearing**	**Lc-bearing**	**Lc-bearing**	**Lc-free**	**Lc-free**	**Lc-free**	**Lc-free**	**Lc-free**	**Lc-free**	**Lc-free**
Tr-And.	Tr-And.	Tr-And.	Tr-And.	Tr-And.	Tr-And.	Tr-And.	Bas. Tr-And.	Bas. Tr-And.	Bas. Tr-And.	Bas. Tr-And.	Bas. Tr-And.	Bas. Tr-And.	Bas. Tr-And.
Moshiran	Moshiran	Moshiran	Moshiran	Moshiran	Moshiran	Moshiran	S. Moshiran	S. Moshiran	S. Moshiran	Tullun	Tullun	Tullun	Tullun
38.7797263	38.7118642	38.7021909	38.7028287	38.7051955	38.69866	38.69027	38.6691001	38.6396829	38.6402442	38.9262968	38.9263349	38.9671141	38.9671135
47.543613	47.5748866	47.5743325	47.5776898	47.579856	47.5747002	47.5649496	47.5565741	47.6023064	47.6009711	48.0575946	48.0576737	47.9867806	47.9868037
51.99	52.05	52.34	52.75	53.00	52.32	52.18	54.26	50.68	50.54	52.30	51.10	53.05	53.11
0.62	0.59	0.56	0.58	0.55	0.57	0.60	0.95	0.95	0.98	0.93	0.99	1.07	1.11
19.35	19.29	19.91	20.16	20.38	19.94	19.73	17.19	17.41	16.58	16.41	15.46	15.81	16.15
5.39	5.03	4.67	4.55	4.12	4.73	5.10	8.43	8.88	8.91	7.65	9.10	8.46	8.26
0.20	0.18	0.18	0.19	0.17	0.19	0.19	0.15	0.18	0.17	0.12	0.17	0.14	0.16
1.66	1.22	1.27	1.34	1.13	1.29	1.59	4.50	4.80	5.84	6.36	7.82	5.93	5.49
5.95	7.60	6.20	6.55	6.28	6.69	5.94	7.59	8.35	8.07	4.66	7.98	7.24	7.47
7.87	7.24	7.17	4.65	4.83	5.55	6.37	3.04	4.02	3.48	3.11	2.57	2.70	2.73
1.87	1.22	3.14	4.82	4.91	3.85	3.70	2.93	2.61	2.87	4.78	2.95	3.37	3.33
0.72	0.60	0.67	0.61	0.62	0.61	0.64	0.35	0.51	0.52	0.49	0.37	0.48	0.45
4.37	4.97	3.88	3.80	4.02	4.26	3.96	0.62	1.62	2.02	3.20	1.50	1.75	1.74
100.0	100.0	100.0	100.0	100.0	100.0	100.0	100.0	100.0	100.0	100.0	100.0	100.0	100.0
2002	1956	1922	1918	1830	1926	2029	635	951	894	748	664	691	698
92	85	96	90	89	93	87	83	62	64	92	65	73	76
9	8	6	6	7	7	6	28	22	24	17	29	28	27
19	38	19	22	16	16	24	47	128	206	44	267	158	151
153	147	150	162	166	159	155	64	66	74	100	83	90	92
45	51	50	56	50	61	53	61	35	49	58	29	52	41
18	20	20	17	19	20	19	22	15	15	24	13	20	22
bdl	bdl	bdl	4	3	1	bdl	12	25	47	19	80	60	55
43	46	42	36	36	40	42	22	20	21	25	17	17	18
96	74	118	93	100	115	57	89	58	47	124	66	84	84
6	7	7	8	6	6	7	17	15	16	13	20	17	17
2309	2323	2248	2069	1991	2616	2149	594	1090	831	625	569	581	607
10	13	12	11	10	11	11	18	6	7	13	7	12	12
162	159	145	157	139	163	164	188	215	208	160	209	182	188
16	17	20	21	22	22	20	29	25	23	27	20	25	27
89	89	79	73	62	80	80	71	76	75	69	77	71	75
95	121	123	127	149	147	113	244	110	108	211	108	183	203

Table 2

Click here to access/download;Table;Table 2.pdf

Sample	M-04	M-06	M-12	M-14	M-15	M-17	M-21	M-26	M-27	M-29	M-32	M-33	M-36	M-38	M-40	M-44	M-45	M-47	M-51	M-54	M-56	M-58	M-60
Lithology	Lava	Lava	Lava	Lava	Dike	Dike	Lava	Lava	Lava	Lava	Pillow	Pillow	Columnar lava flow	Pillow	Pillow	Lava	Pillow	Lava	Lava	Lava	Lava	Lava	Lava
Rock-type	Lc-free	Lc-free	Lc-free	Lc-free			Lc-bearing	Lc-bearing	Lc-bearing	Lc-bearing	Lc-bearing	Lc-bearing	Lc-bearing	Lc-bearing	Lc-bearing	Lc-bearing	Lc-bearing	Lc-bearing	Lc-bearing	Lc-free	Lc-free	Lc-free	Lc-free
Classification	Tr-And.	Tr-And.	Tr-And.	Tr-And.	Trachite	Bas. Tr-And.	Tr-And.	Tr-And.	Tr-And.	Tr-And.	Tr-And.	Tr-And.	Tr-And.	Tr-And.	Ankaramite	Tr-And.	Tr-And.	Tr-And.	Tr-And.	Bas. Tr-And.	Bas. Tr-And.	Bas. Tr-And.	Bas. Tr-And.
Locality	Marallu	Marallu	Marallu	Marallu	Moradlu	Moradlu	Majid Abad	Majid Abad	Majid Abad	Majid Abad	Gheshlagh	Gheshlagh	Gheshlagh	Gheshlagh	Gheshlagh	Moshiran	Moshiran	Moshiran	Moshiran	S. Moshiran	S. Moshiran	Tulun	Tulun
Rb (ppm)	71.8	71.3	55.2	88.1	156	41.3	102.6	119.0	37.0	144.1	56.5	44.2	91.2	48.6	44.6	58.5	42.7	63.6	87.4	73.3	39.4	51.6	74.3
Sr	1747	1547	913	1314	262	520	1802	1914	1594	2152	848	701	957	518	2932	2217	1594	1820	1736	477	666	466	509
Y	17.9	19.6	17.9	16.9	16.2	13.5	23.4	17.2	18.3	20.1	15.8	14.8	18.7	12.0	15.2	19.0	15.8	18.5	18.1	22.0	18.9	17.2	21.7
Zr	140	143	139	147	430	85	152	127	154	168	92	99	94	97	65	152	99	149	149	216	126	123	191
Nb	13.4	13.3	13.2	13.5	58.4	6.8	16.2	13.4	14.6	20.8	7.2	7.6	7.3	7.5	4.2	18.2	9.0	18.0	18.4	22.5	15.9	15.0	23.4
La	40.0	41.3	39.1	39.3	36.1	13.7	52.9	38.8	37.3	48.4	27.4	25.7	33.2	21.5	16.8	35.5	23.2	36.5	35.6	31.7	23.7	23.0	29.7
Ce	74.9	77.1	73.1	75.4	76.8	29.8	74.5	61.3	78.3	69.8	46.4	45.6	55.1	45.8	30.7	61.9	40.4	63.5	63.8	60.8	46.0	44.3	55.4
Pr	8.22	8.56	8.09	8.16	6.99	3.44	8.81	6.62	8.11	8.24	5.35	5.15	6.28	4.47	3.87	6.95	4.67	7.07	6.83	6.75	5.31	5.11	6.37
Nd	32.9	33.9	32.5	32.6	24.7	14.8	32.7	24.6	33.5	30.2	21.4	20.6	24.7	18.0	17.1	27.6	18.6	27.6	27.1	26.7	21.9	20.8	25.5
Sm	6.17	6.49	6.15	6.22	4.28	3.33	5.94	4.48	6.59	5.47	4.15	4.02	4.69	3.54	3.72	5.22	3.62	5.14	5.10	5.07	4.35	4.22	4.93
Eu	1.72	1.80	1.71	1.73	0.69	1.04	2.09	1.55	2.02	1.88	1.49	1.45	1.69	1.27	1.47	1.98	1.53	1.84	1.90	1.30	1.36	1.26	1.44
Gd	5.66	5.94	5.61	5.65	4.10	3.27	5.73	4.38	6.16	5.16	3.97	3.88	4.59	3.46	3.85	5.79	3.96	5.58	5.68	5.56	4.78	4.37	5.34
Tb	0.78	0.82	0.78	0.78	0.61	0.54	0.81	0.61	0.86	0.73	0.58	0.56	0.66	0.50	0.55	0.75	0.55	0.72	0.72	0.77	0.68	0.64	0.75
Dy	3.54	3.80	3.60	3.52	3.02	2.82	3.78	2.91	3.93	3.38	2.79	2.72	3.13	2.40	2.74	3.32	2.63	3.25	3.23	3.83	3.32	3.02	3.70
Ho	0.70	0.75	0.70	0.70	0.65	0.59	0.77	0.59	0.76	0.68	0.58	0.56	0.64	0.49	0.54	0.67	0.54	0.65	0.65	0.79	0.69	0.62	0.76
Er	1.88	2.01	1.91	1.87	1.92	1.58	2.15	1.67	2.00	1.91	1.63	1.60	1.80	1.39	1.46	1.83	1.51	1.83	1.81	2.18	1.87	1.67	2.12
Tm	0.30	0.33	0.31	0.30	0.35	0.26	0.37	0.28	0.31	0.32	0.27	0.27	0.30	0.23	0.26	0.32	0.28	0.32	0.32	0.38	0.35	0.30	0.37
Yb	1.77	1.89	1.76	1.74	2.12	1.48	2.18	1.70	1.84	1.95	1.66	1.61	1.82	1.42	1.45	1.82	1.56	1.82	1.78	2.19	1.81	1.68	2.06
Lu	0.27	0.29	0.28	0.26	0.34	0.23	0.34	0.26	0.28	0.31	0.26	0.25	0.28	0.22	0.22	0.28	0.25	0.29	0.28	0.35	0.27	0.26	0.32
Hf	3.40	3.48	3.46	3.58	9.71	2.38	3.33	2.82	3.86	3.46	2.30	2.43	2.33	2.42	1.75	3.30	2.32	3.18	3.14	4.98	3.03	2.90	4.12
Ta	0.58	0.58	0.56	0.58	2.34	0.32	0.67	0.55	0.62	0.82	0.36	0.37	0.37	0.36	0.28	0.82	0.50	0.81	0.80	1.04	0.75	0.70	1.07
Th	10.0	10.6	9.7	9.6	20.6	3.4	13.1	10.0	7.6	13.5	6.8	6.8	7.3	6.0	4.8	12.2	7.8	12.2	12.1	14.9	5.8	6.1	11.4
U	2.69	2.73	2.58	2.70	6.09	1.10	2.50	1.86	2.01	3.04	2.49	1.66	1.92	1.20	1.32	3.37	2.02	3.43	3.18	3.56	1.43	1.54	2.81

Sample	M-04	M-06	M-12	M-14	M-15	M-17	M-21	M-25	M-26	M-27	M-29	M-32
Lithology	Lava	Lava	Lava	Lava	Dike	Dike	Lava	Lava	Lava	Lava	Lava	Pillow
Petrography	Lc-free	Lc-free	Lc-free	Lc-free			Lc-bearing	Lc-bearing	Lc-bearing	Lc-bearing	Lc-bearing	Lc-bearing
Rock-type	Tr-And.	Tr-And.	Tr-And.	Tr-And.	Trachite	Bas. Tr-And.	Tr-And.	Tr-And.	Tr-And.	Tr-And.	Tr-And.	Tr-And.
Locality	Marallu	Marallu	Marallu	Marallu	Moradlu	Moradlu	Majid Abad	Majid Abad	Majid Abad	Majid Abad	Majid Abad	Gheshlagh
Age (Ma)	40.0	40.0	***40.0***	40.0	41.0	***41.0***	39.6	***39.6***	39.6	39.6	39.6	40
err	1.1	1.1	***1.1***	1.1	1.1	***1.1***	1.0	***1.0***	1.0	1.0	1.0	1.1
Rb (ppm)	72	71	55	88	156	41	103	*66	119	37	144	56
Sr	1747	1547	913	1314	262	520	1802	*2018	1914	1594	2152	848
$^{87}Sr/^{86}Sr$	0.704926	0.704920	0.704920	0.705089	0.706297	0.705836	0.704662	0.704492	0.704627	0.704560	0.704535	0.704574
2se	0.000008	0.000007	0.000007	0.000006	0.000007	0.000007	0.000007	0.000007	0.000007	0.000007	0.000007	0.000007
$(^{87}Sr/^{86}Sr)i$	0.704852	0.704840	0.704812	0.704959	0.705217	0.705669	0.704569	0.704438	0.704522	0.704513	0.704418	0.704479
2se*	0.000010	0.000010	0.000011	0.000012	0.000082	0.000015	0.000010	0.000008	0.000010	0.000007	0.000011	0.000010
Nd (ppm)	33	34	33	33	25	15	33	nd	25	33	30	21
Sm	6.2	6.5	6.1	6.2	4.3	3.3	5.9	nd	4.5	6.6	5.5	4.2
$^{143}Nd/^{144}Nd$	0.512643	0.512652	0.512653	0.512640	0.512655	0.512609	0.512754	0.512737	0.512747	0.512738	0.512738	0.512818
2se	0.000005	0.000006	0.000005	0.000004	0.000005	0.000007	0.000005	0.000005	0.000005	0.000005	0.000006	0.000008
$(^{143}Nd/^{144}Nd)i$	0.512614	0.512622	0.512623	0.512610	0.512627	0.512572	0.512725	nc	0.512718	0.512707	0.512709	0.512787
2se*	0.000005	0.000007	0.000005	0.000004	0.000005	0.000007	0.000005	nc	0.000005	0.000005	0.000006	0.000008
Pb* (ppm)	28	27	31	25	38	15	35	29	37	30	46.5	35.8
U	2.69	2.73	2.58	2.70	6.09	1.10	2.50	nd	1.86	2.01	3.04	2.49
Th	10.0	10.6	9.7	9.6	20.6	3.4	13.1	*9.2	10.0	7.6	13.5	6.8
$^{206}Pb/^{204}Pb$	18.717	18.717	18.717	18.720	18.770	18.772	18.630	18.633	18.634	18.637	18.628	18.667
2se	0.002	0.002	0.003	0.002	0.002	0.003	0.002	0.002	0.002	0.002	0.003	0.002
$^{208}Pb/^{204}Pb$	38.844	38.842	38.861	38.838	38.893	38.896	38.735	38.723	38.747	38.738	38.707	38.691
2se	0.004	0.005	0.006	0.005	0.003	0.007	0.003	0.005	0.004	0.004	0.006	0.005
$^{207}Pb/^{204}Pb$	15.609	15.608	15.609	15.607	15.630	15.617	15.598	15.596	15.600	15.598	15.591	15.574
2se	0.002	0.002	0.003	0.002	0.001	0.003	0.001	0.002	0.002	0.002	0.003	0.002
$(^{206}Pb/^{204}Pb)i$	18.679	18.676	18.683	18.676	18.704	18.743	18.601	nc	18.613	18.611	18.602	18.639
2se*	0.011	0.012	0.010	0.012	0.014	0.011	0.010	nc	0.010	0.010	0.010	0.011
$(^{208}Pb/^{204}Pb)i$	15.608	15.606	15.607	15.605	15.627	15.616	15.596	nc	15.599	15.597	15.590	15.573
2se*	0.010	0.010	0.010	0.010	0.010	0.010	0.010	nc	0.010	0.010	0.010	0.010
$(^{207}Pb/^{204}Pb)i$	38.796	38.792	38.819	38.786	38.819	38.867	38.685	nc	38.712	38.705	38.669	38.666
2se*	0.032	0.031	0.032	0.030	0.033	0.031	0.031	nc	0.032	0.029	0.031	0.030

Sample	M-33	M-36	M-38	M-39	M-40	M-44	M-45	M-47	M-51	M-54	M-56	M-58	M-60
Lithology	Pillow	Columnar lava flow	Pillow	Columnar lava flow	Pillow	Lava	Pillow	Lava	Lava	Lava	Lava		
Petrography	Lc-bearing	Lc-bearing	Lc-bearing	Lc-bearing	Lc-bearing	Lc-bearing	Lc-bearing	Lc-bearing	Lc-bearing	Lc-free	Lc-free	Lc-free	Lc-free
Rock-type	Tr-And.	Tr-And.	Tr-And.	Tr-And.	Ankaramite	Tr-And.	Tr-And.	Tr-And.	Tr-And.	Bas. Tr-And.	Bas. Tr-And.	Bas. Tr-And.	Bas. Tr-And.
Locality	Gheshlagh	Gheshlagh	Gheshlagh	Gheshlagh	Gheshlagh	Moshiran	Moshiran	Moshiran	Moshiran	S.Moshiran	S.Moshiran	Tulun	Tulun
Age (Ma)	40	***39.4***	40	39.4	***24.4***	40	40	40	40	***41.9***	41.9	***41.1***	41.1
err	1.1	***1.0***	1.1	1.0	***0.7***	1.1	1.1	1.1	1.1	***1.1***	1.1	***1.1***	1.1
Rb (ppm)	44	91	49	*30	45	59	43	64	87	73	39	52	74
Sr	701	957	518	*1043	2932	2217	1594	1820	1736	477	666	466	509
$^{87}Sr/^{86}Sr$	0.704578	0.704684	0.704769	0.704437	0.704434	0.704517	0.704681	0.704476	0.704522	0.705305	0.705089	0.705173	0.705179
2se	0.000007	0.000008	0.000007	0.000007	0.000007	0.000007	0.000006	0.000006	0.000007	0.000007	0.000008	0.000007	0.000007
$(^{87}Sr/^{86}Sr)i$	0.704483	0.704521	0.704615	0.704390	0.704407	0.704476	0.704640	0.704424	0.704439	0.705045	0.704991	0.704977	0.704946
2se*	0.000010	0.000015	0.000014	0.000008	0.000007	0.000007	0.000007	0.000007	0.000010	0.000020	0.000011	0.000016	0.000018
Nd (ppm)	21	25	18	nd	17	28	19	28	27	27	22	21	26
Sm	4.0	4.7	3.5	nd	3.7	5.2	3.6	5.1	5.1	5.1	4.4	4.2	4.9
$^{143}Nd/^{144}Nd$	0.512807	0.512804	0.512797	0.512793	0.512826	0.512725	0.512782	0.512728	0.512740	0.512642	0.512638	0.512640	0.512658
2se	0.000005	0.000007	0.000006	0.000004	0.000005	0.000003	0.000006	0.000007	0.000012	0.000006	0.000006	0.000006	0.000005
$(^{143}Nd/^{144}Nd)i$	0.512776	0.512774	0.512765	nc	0.512791	0.512695	0.512751	0.512698	0.512710	0.512611	0.512605	0.512607	0.512627
2se*	0.000005	0.000007	0.000006	nc	0.000005	0.000003	0.000006	0.000007	0.000012	0.000006	0.000006	0.000006	0.000006
Pb* (ppm)	34.9	31.8	26.2	33	24	42	31	46	36	22	21	17	18
U	1.66	1.92	1.20	nd	1.32	3.37	2.02	3.43	3.18	3.56	1.43	1.54	2.81
Th	6.8	7.3	6.0	*4.6	4.8	12.2	7.8	12.2	12.1	14.9	5.8	6.1	11.4
$^{206}Pb/^{204}Pb$	18.621	18.669	18.599	18.620	18.628	18.660	18.637	18.650	18.664	18.707	18.670	18.717	18.739
2se	0.002	0.003	0.001	0.002	0.003	0.003	0.002	0.004	0.003	0.001	0.002	0.002	0.002
$^{208}Pb/^{204}Pb$	38.691	38.710	38.663	38.632	38.742	38.761	38.744	38.758	38.749	38.868	38.780	38.835	38.857
2se	0.003	0.007	0.002	0.003	0.006	0.007	0.004	0.009	0.007	0.003	0.004	0.004	0.005
$^{207}Pb/^{204}Pb$	15.576	15.573	15.571	15.558	15.584	15.597	15.596	15.601	15.597	15.643	15.622	15.626	15.627
2se	0.001	0.003	0.001	0.001	0.002	0.003	0.002	0.003	0.003	0.001	0.001	0.002	0.002
$(^{206}Pb/^{204}Pb)i$	18.602	18.645	18.581	nc	18.607	18.628	18.611	18.621	18.629	18.639	18.641	18.681	18.676
2se*	0.010	0.010	0.010	nc	0.010	0.011	0.011	0.011	0.011	0.013	0.010	0.011	0.014
$(^{208}Pb/^{204}Pb)i$	15.575	15.572	15.570	nc	15.584	15.596	15.595	15.599	15.596	15.639	15.620	15.624	15.624
2se*	0.010	0.009	0.010	nc	0.010	0.010	0.010	0.010	0.010	0.010	0.010	0.010	0.010
$(^{207}Pb/^{204}Pb)i$	38.666	38.680	38.633	nc	38.716	38.722	38.711	38.724	38.705	38.775	38.742	38.787	38.773
2se*	0.030	0.031	0.031	nc	0.030	0.032	0.032	0.031	0.031	0.034	0.030	0.031	0.032

Inital values are calculated on the basis of the age of the different suites of rocks measured on selected representative samples (highlited in bold). Age propagated error (2se*) are obtained by Montecarlo simulation. * data by XRF

Supplementary Table 1

Click here to access/download
Supplementary material/Appendix (Files for online publication only)
Supplementary table 1.pdf

Supplementary Figure 1

Supplementary Figure 2

Supplementary Figure 3

Click here to access/download
Supplementary material/Appendix (Files for online publication only)
Supplementary Figure 3_2022_mod.pdf

Declaration of interests

☒The authors declare that they have no known competing financial interests or personal relationships that could have appeared to influence the work reported in this paper.

☐The authors declare the following financial interests/personal relationships which may be considered as potential competing interests: